IOWA STATE UNIVERSITY
Digital Repository

2012

Formation and tidal synchronization of sdB stars in binaries an asteroseismic investigation using Kepler Observations

Herbert William Pablo
Iowa State University

Follow this and additional works at: http://lib.dr.iastate.edu/etd

Part of the Astrophysics and Astronomy Commons

Formation and tidal synchronization of sdB stars in binaries

an asteroseismic investigation using *Kepler* Observations

by

Herbert William Pablo

A dissertation submitted to the graduate faculty

in partial fulfillment of the requirements for the degree of

DOCTOR OF PHILOSOPHY

Major: Astrophysics

Program of Study Committee:

Steven D. Kawaler, Major Professor

Charles Kerton

Gene Takle

Edward Yu

Massimo Marengo

Iowa State University

Ames, Iowa

2012

TABLE OF CONTENTS

LIST OF TABLES

LIST OF FIGURES

viii

Dedication

To my parents, who always told me that I could do anything I wanted. They always made sure I believed in myself and I wouldn't be where I am today without their love and support. To my siblings, who showed me that the things which are most important to accomplishing your goals are hardwork and determination.

Acknowledgements

There are many people who made this work possible, but I would specifically like to my advisor for his advice and support. I would also like to thank my committee for taking time out of their busy schedules to review my thesis, and also for most likely being the only 5 people to ever read my thesis in it's entirety. In addition, I would like to thank the people of KASC working group 11 for giving me useful feedback on my papers. I would also like to thank Dr. Mike McCollough. While the work I did with him is not in my thesis, he provided me a new perspective on astronomy and life I could not have gotten from anyone else. Finally I would like to thank all my friends and colleagues who provided useful discussions and support throughout the years. I would specifically like to acknowledge Josh Cardenzana, Arun Madhavan, Sarah Willis, Riley Smith, and Andy Baran.

Abstract

Subdwarf B (sdB) stars are low mass (0.5 $M_\odot$) helium burning stars with thin hydrogen envelopes and T_{eff} 22000–40000 K. Many of these stars are found in binary systems. One common proposed formation mechanism is common envelope (CE) ejection, where the companion spirals deep into the star's envelope ejecting the outer layers and forming a close binary system. In this dissertation, we use short cadence (t_{int}=58.86 s) *Kepler* photometric time–series data to study three close sdB binaries with P ≈ 10 hours and g-mode pulsations. Asteroseismic analysis finds that each system has a constant period spacing of $\Delta P \approx 250$ s consistent with single sdB stars. This analysis also shows the presence of rotational multiplets which we used to find the rotation period. In all three cases the binary system is far from tidal synchronization with a rotation period an order of magnitude longer than the orbital period. These observations agree with predictions using the Zahn formulation of tidal evolution which predicts a synchronization time longer than the sdB lifetime (10^8 yr). We use this synchronization time to backtrack the sdB's rotation history and find its initial rotation period as it is first exiting the CE. This is one of the only observationally based constraints that has been placed on CE evolution. Preliminary investigations of single sdB stars show similar rotation periods, indicating that the rotation period may be independent of the formation channel.

CHAPTER 1. OVERVIEW OF EVIDENCE FOR STELLAR INTERACTION

1.1 Introduction

It is often said that astronomy is the oldest of the sciences. This is only natural since the sky has been around longer than humans have roamed the Earth. At first glance, the sky consists of pinpoints of light that move in regular identifiable patterns, but further study has brought about a multitude of increasingly difficult questions. We persist with this study as it gives us our only chance of truly understanding the Universe in which we live.

The building blocks of virtually all large astronomical structures are stars. The wide variety in the appearance of the observed stars depends largely on three variables: mass, age and companionship. With them we can derive a complete picture of the star and its evolution. This information is often difficult to obtain. Stellar observations, even over the entire course of human history, are essentially snapshots in the life spans of all but the most rapidly evolving stars. For this reason, we infer much of a star's life cycle by piecing it together from stellar observations at various evolutionary stages. The limitations of this method indicate that there are many areas where our knowledge is lacking.

A pertinent example of this is close binary star systems. In such systems, it is often not possible to deal with each star independently because of the profound impact each can have on its companion. Despite these complexities, binary systems are extremely valuable because they provide us with a method for determining the mass of each component. Though difficult to obtain, mass is a necessary quantity because it determines the evolutionary path for single stars.

Since stars are aptly described as giant balls of hydrogen (with some helium and a sprinkling of heavy metals), we can describe this evolution as consisting of three stages: gravitational contraction and formation, core hydrogen burning (main-sequence), and core hydrogen depletion (post main-sequence). After hydrogen core exhaustion the final evolutionary phases occur relatively swiftly meaning examples in nature are rare. During this phase a star will swell 10-100 times its original size. When this occurs in the presence of a close companion the complexity is increased since the interaction between these components can cause each star's mass to change.

One class of stars which is thought to be formed as a result of this binary evolution is subdwarf B (sdB) stars. These evolved, core helium burning stars, which are the focus of this dissertation, are small ($R \approx 0.2\ R_{\odot}$) and hot (T_{eff}) > 22000 K) with very thin hydrogen envelopes (see section 1.3 for more details). There are many theories on how sdB stars form, but their intial state and how they evolve after formation remains somewhat of a mystery. Since these stars are often found in binaries and they are often known to pulsate, we have considerably more information at our disposal than in many other single or binary star systems. Therefore, answering questions on their origin and evolution is promising. Recently, space-based photometric observations have made this information more accessible, affording us the rare opportunity to study this genre of star in rich detail. The information we obtain should also be useful in the study of other binary systems.

1.2   Hertzsprung-Russell Diagram

Since a major portion of this dissertation focuses on evolution of evolved stars, I would be remiss not to introduce the Hertzsprung-Russell diagram. This diagram plots stars in the spectral type (analogous to temperature) vs. luminosity (electromagnetic energy per unit time) plane (Russell, 1914). The plotted points show distinct patterns (see Figure 1.1) which, as later determined, are related to the evolutionary state of the star. The most prominent feature is a diagonal band known as the "main sequence". Stars located along this line burn hydrogen

in their core. Since this process is the longest of a star's active life, the majority of observed stars are situated there. Once the star expends the hydrogen in its core, the core contracts and hydrogen burning begins in a shell around the core. This causes the envelope to expand, the luminosity to increase and the temperature to decrease. The star's motion on the H-R diagram is above the main sequence and to the right (redder) creating a "Red giant". Stars with sufficient mass will continue along this path until conditions are ripe for core helium ignition. Once this occurs, the stars lie along a "horizontal branch" just above the main sequence. Remnant cores which are no longer burning are called white dwarfs whose small radii places them well below the main sequence.
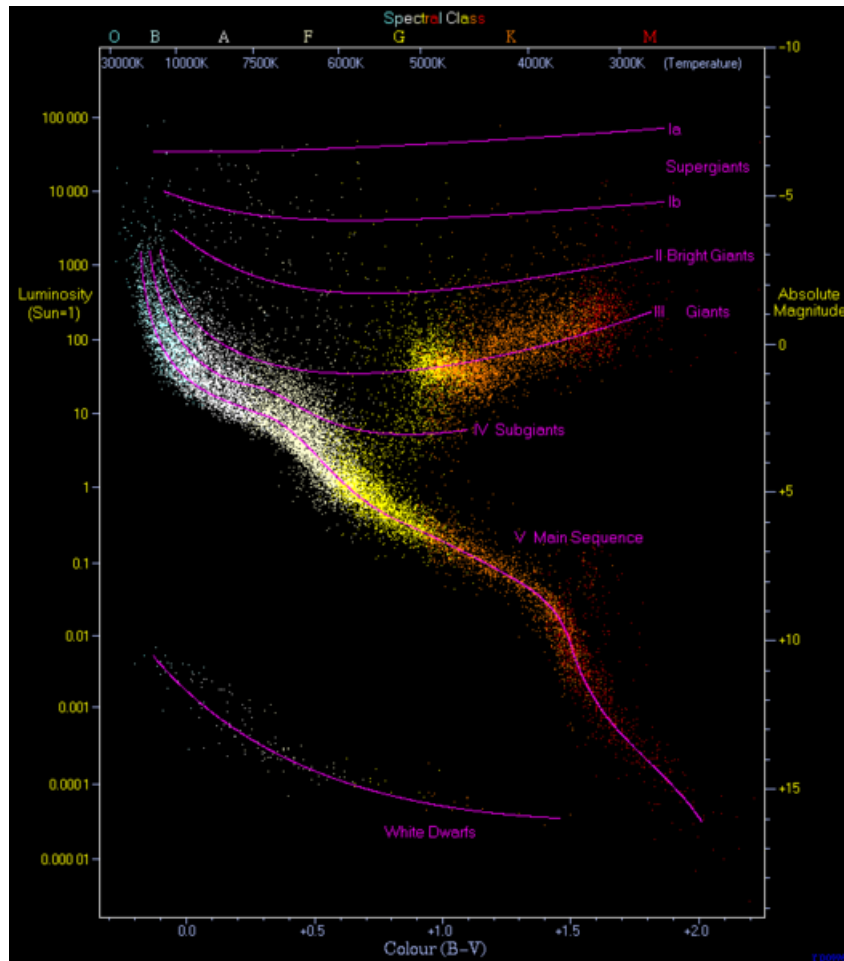
Figure 1.1   This H-R diagram is made using 22000 stars from Hipparcos Catalogue. Added is the Gliese Catalogue of Nearby stars for red and white dwarfs. Purple lines highlight important evolutionary bands. Credit: Richard Powell.

1.3 Stellar Variability

When looking at the stars at night, it is not unusual to notice that they seem to twinkle. This twinkle is merely a function of light being refracted as it goes through the Earth's atmosphere. However, this does not imply that light coming from stars is always stable. As it turns out, all stars fluctuate to varying degrees.

Stellar variability is caused by either internal processes or interaction with a nearby companion. Often these changes are regular or even periodic. The remainder of this section will focus on two types of variability which are frequently seen in stars of all types: companion interactions (binarity) and pulsations.

1.3.1 Binarity

1.3.1.1 Close Binaries

The term "close binary" is not well defined. It appears to date back to Pickering (1890) where a new class of binaries was discovered whose components were too close to be separated by ordinary means. Roberts (1895), citing Pickering (1890) was the first to refer to this class as close binary systems. This definition is not helpful since more than half of all stars are in systems where two (or more) objects orbit around a common center of mass (see Carroll & Ostlie 2007) and most of those meet the above criterion. "Close binary" later came to mean a system in which the stellar radii and the semimajor axis of the orbit are of similar size (see Kallrath & Milone 2009). A more physical description of this is put forth by Plavec (1968) which states that the system may be considered a "close binary" if (or when) the interaction between components causes the star to fill its Roche Lobe.

The subject of tidal interaction between stars and the concept of the "Roche Lobe" is crucial, especially from a computational standpoint, to the study of close binary systems. Around any massive object it is possible to define surfaces (lobes) where the gravitational potential
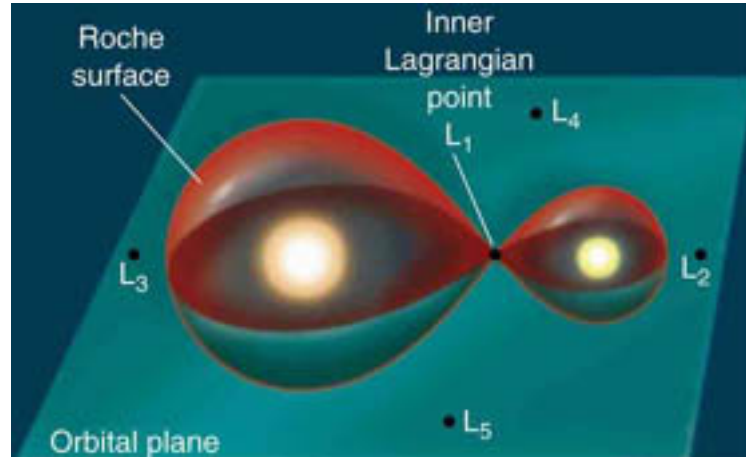
Figure 1.2   The Roche lobes of both stars in a binary system are shown. Where the two lobes meet is a Lagrangian point where gravitational force is zero. Picture obtained from http://www.daviddarling.info.

is constant. Close to the star these lobes are roughly spherical, but when there is a second body, the farther this equipotential surface is from the star's center of mass, the more affected it will be by its companion. Eventually, the two equipotential surfaces will meet at a single point. The surface created in this configuration is defined as the star's Roche lobe. If during its evolution the star fills this lobe, then some of the star's mass will be affected more by the companion than by the star itself. The definition of Plavec (1968) describes the problem well, but in practice it is a hard criterion to evaluate. In addition, while a system may be defined as a close binary, it may not exhibit those properties at the time it is being observed. Therefore, for the purposes of this dissertation, close binaries will be defined with an observational bias. If there is a noticeable change in the light curve of the system due to the presence of a companion, then the binary system can be considered "close".

There are many ways to identify close binary systems. Orbital motion can be detected through Doppler shifting of spectral lines: redder as the star moves away and bluer as the star moves towards our line of sight. In some cases small changes in the lateral position of the star on the sky can signify the presence of a companion. The most prevalent and accessible means of detection is through variations in the observed brightness of the object.

1.3.1.2 Eclipsing Systems

All binary systems orbit around a center of mass and have a well defined orbital plane. The orientation of this plane with respect to the line of sight determines the presence of eclipses. The inclination of the system is the angle of the rotation axis to our line of sight. Thus, an inclination of 90° would mean that the orbital plane is directly in the line of sight and eclipses are guaranteed[1]. Similarly an inclination of 0° means that, provided both components are resolved, their orbital motion would be visible on the plane of the sky (visual binary). Eclipsing systems are not necessarily "close binaries" as discussed above, but there is a higher likelihood as the larger the separation between the components, the smaller the range of inclinations which will allow for an eclipse. This is illustrated in the following inequality:

$$\sin(90 - i) \leq \frac{(r_1 + r_2)}{a\,(1 + q)},$$

(1.1)

where i is the inclination angle, a is the semimajor axis, q is the mass ratio, and r is the radius of the star (see Fig. 1.3).

Knowledge of the inclination angle constrains the binary system considerably and can be used to determine the mass. This is why eclipsing systems are so valuable. Even in the most extreme cases the inclination is at most 20° from perpendicular. The importance of accurately measuring the inclination can be derived from the general version of Kepler's third law:

$$P^2 = \frac{4\pi^2}{G(m_1 + m_2)a^3},$$

(1.2)

where P is the period, G the gravitational constant, a is the semi-major axis and m is the mass. P is well known from observations, but a cannot be directly calculated without knowledge of the absolute distance from the observer to the system.

Therefore, a can be expressed in terms of the velocity v of the star which is

$$a = \frac{vP}{2\pi}.$$

(1.3)

---

[1]This assumes that the rotation axis is in line with the orbital axis. This is a reasonable assumption based on our knowledge of binary formation.
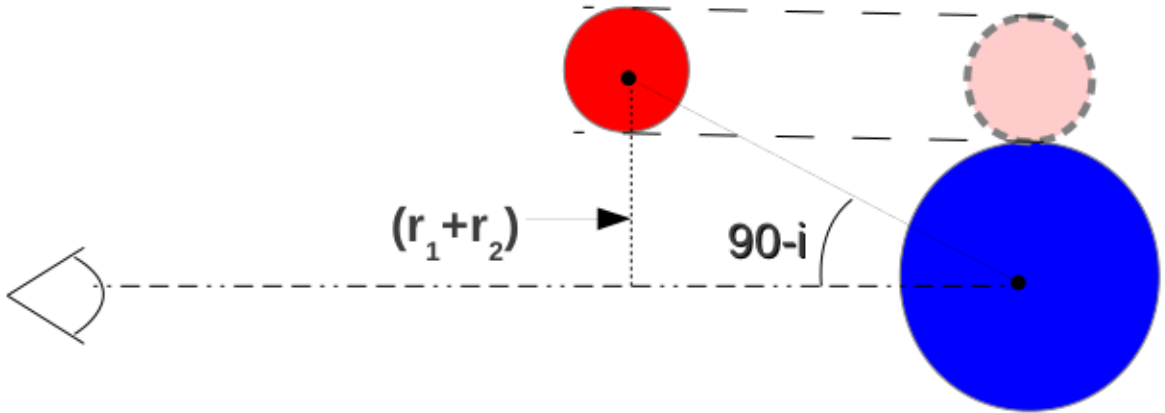
Figure 1.3 This shows the maximum inclination angle for eclipse. The eye shows the line of sight to the observer, and the semi-transparent circle shows the projection of the companion star on the sky.

This relationship is useful as spectroscopy provides a measure of the velocity. However, this is the velocity along the line of sight v_r, related to the absolute v by

$$v_r = v\sin(i). \tag{1.4}$$

Now Eq. 1.2 can be rewritten as

$$m_1 + m_2 = \frac{P}{2G\pi}\frac{(v_{1r} + v_{2r})^3}{\sin^3 i}, \tag{1.5}$$

from which we can determine a long list of parameters including M, a, and the radius of each component (see Table 4.1 for a complete list).

1.3.1.3 Ellipsoidal Binaries

When one star is markedly larger in mass than its companion, tidal effects can be significant. In these cases, the lower mass star will be distended in the direction of the primary (more

massive) star creating an oblong "gumdrop" shape with one "pointy" and one "blunt" end. Projections of this shape on the sky will result in different surface areas. This creates a sinusoidal pattern in the light curve with a periodicity half the of the orbital period (provided the massive companion is invisible). This is illustrated in Figure 1.4.
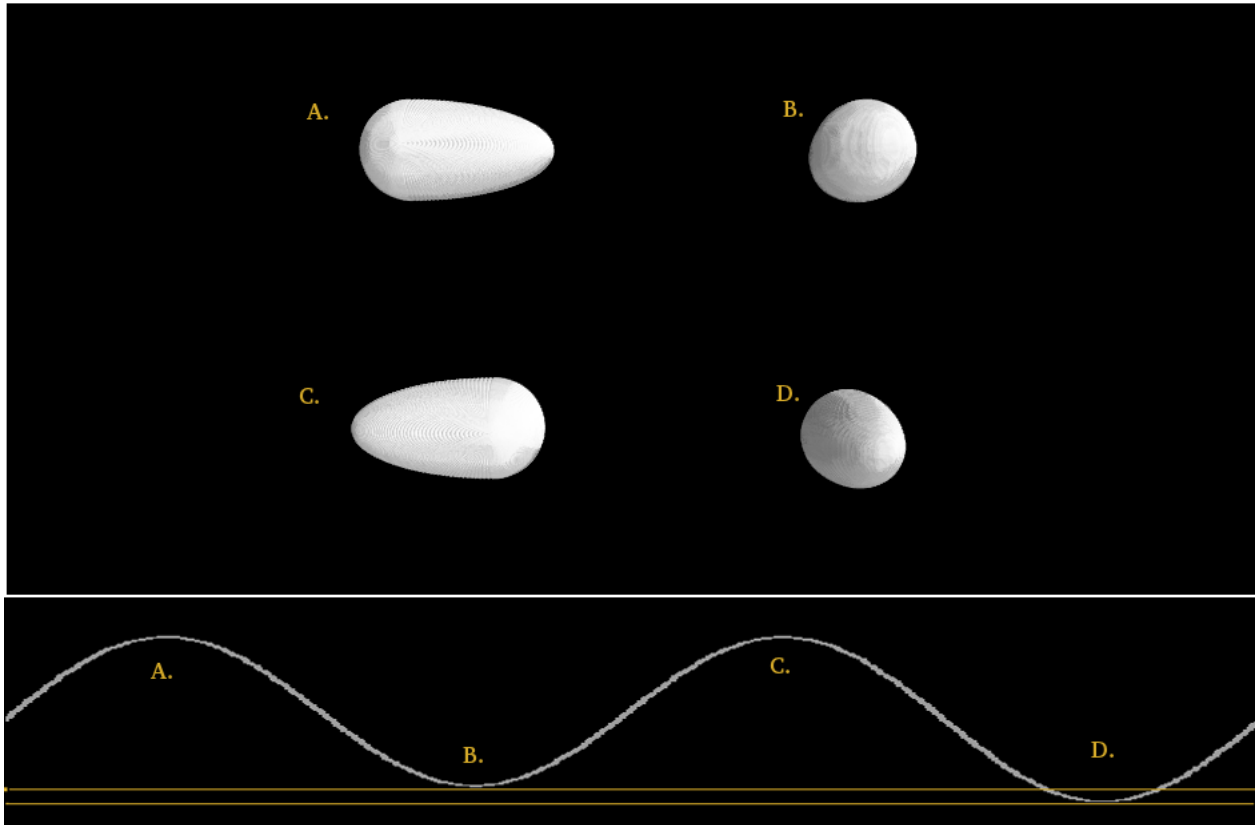
Figure 1.4   The top panel shows 4 different phases (labeled a-d) of a star distended by tidal forces. The light curve of the object is given in the bottom panel along where the location of each phase is marked. Gold lines at the bottom highlight the different depths of the minima.

Noticeable in Fig. 1.4 is an assymetry in the minima signifying that the "pointy" and "blunt" ends do not have the same surface brightness. This is explained by the concept of limb darkening. Since temperature decreases toward the star's exterior, and the line of sight terminates at higher layers as it approaches the limb, there is a negative brightness gradient in this direction. This means the limb darker than the projected center. The "pointy" end of an ellipsoidal star has a much larger fraction of the projected surface which terminates in the

star's outer layers than the blunt end. The minima with the pointy end in our direction (D in Fig. 1.4) are therefore less luminous than minima with the blunt end pointing toward us (B).

1.3.1.4   Tidal effects on rotation

The overriding force between astronomical bodies, particularly those in binary systems, is gravity. It is the reason stars coalesce and why binary systems stay bound. In close binary systems not only does gravity keep the systems bound, but it can affect the internal structure in complex ways through tides. A notable consequence is a change in the individual rotation rate of each star. The side of the star facing its companion feels a larger gravitational force than the far side. If the rotation period is not the same as the orbital period then this non-uniformity will cause friction as the star rotates. Over time this will spin up/down both components of the binary system to match their orbital period. Since the energy required for this comes from the orbit, the orbital period is also changing, but by a much smaller amount. This process is known as synchronization. Further study is required to discover how quickly synchronization occurs, and how angular momentum is transported during this process, but current theories will be discussed in Chapters 4 and 7.

1.3.1.5   Reflection Effect Binaries

Two gravitationally bound stars can vary greatly in the values of their individual parameters. In some cases this results in a large temperature difference between the objects. The hotter star will then irradiate one hemisphere of the cooler star causing the temperature on this side to increase (Eddington, 1926; Milne, 1926; Kopal, 1939). This effect can be quite large, in some cases dwarfing ellipsoidal variations and eclipses (e.g., Østensen et al. 2010a). The signature created in the light curve is a sinusoid with the same frequency as that of the orbit. Maxima occur when the irradiated face is towards our line of sight. Its impact on the light curve is similar to that of ellipsoidal variation. However, when eclipses are present, there will be two full sine curves between each eclipse in an ellipsoidal variable, but only one in a reflection effect variable. If there are no eclipses, then without an independent measure of the orbital period identification relies on the asymmetric minima present in the case of ellipsoidal

variation (see section 4.2.1).

1.3.1.6 Doppler Beaming

The shifting of spectral lines due to the motion of the binary allows us to measure radial velocities. With sufficient sensitivity the same effect is visible in the lightcurve as well. As the star travels towards the observer it receives a boost in light; as the star travels away it receives a reduction. By itself, the signal would be small with a relative amplitude of

$$A = (3 - \alpha)\frac{v_r}{c}, \tag{1.6}$$

(Loeb & Gaudi, 2003) where α (defined in section 4.3.3.) is less than 3. In a fast binary ($v_r \approx 350\frac{\text{km}}{\text{s}}$) this only amounts to an amplitude change of about 1 part in a thousand. Because proximity strongly affects v_r beaming is typically be found in close binary systems. To date it has only been observed as a perturbation on ellipsoidal variables (Bloemen et al., 2010; van Kerkwijk et al., 2010). In these cases it results in maxima of different heights which we can be used to determine the radial velocity of primary star from Eq. 1.6.

1.3.2 Pulsations

Pulsation, like binarity, is a fairly common cause of light variation among some classes of stars. The main difference is that the variations in light that occur are typically smaller and the periodicity is shorter. As a result, we need a faster sampling rate and nearly continuous data for detailed study. The field dedicated to understanding these pulsations, asteroseismology, has flourished with the advent of better instrumentation and perhaps most notably, the ability to do continuous observations from space (see section 1.4).

Stars spend the majority of their life as stable objects. The change in their luminosity is minimal as is that of their fundamental parameters. For this to be true, stars must be able to react quickly to changes in order to maintain mechanical equilibrium. This time scale is often referred to as the dynamical timescale:

$$\tau_{dyn} = \sqrt{\frac{R^3}{GM}}. \tag{1.7}$$

As the star attempts to "right" itself, it will overshoot and oscillate. Eventually it will come back to equilibrium. Therefore, pulsations must have periodicities comparable to τ_{dyn}.

Pulsation occurs when the star varies cyclically by some small amount. This causes a change in the surface area of the star which in turn causes a change in luminosity. Then as the star shrinks, the luminosity decreases in a predictable way provided T_{eff} is not changed (although it generally is). In the light curve this appears as small, nearly sinusoidal, oscillations. While damping of oscillations occurs through radiation and friction, some driving is also present. The driving mechanism is not universal, but there are two which cover the vast majority of pulsators: the κ mechanism and stochastic excitation.

In the κ mechanism, opacity (often from HeII, but sometimes from Fe or He) blocks the transfer of radiation. This causes the heat and pressure to increase, thus causing the star to swell. This partially ionizes the material increasing the opacity and heating further. Ultimately the opacity falls, radiation escapes, the layer cools and pressure drops. This mechanism is common in evolved pulsators (those that are no longer burning hydrogen in their core). Stochastic oscillations are more prevalent in solar–like stars and some red giants, where there is enough acoustic energy in the turbulent convective outer layers that it causes the star to resonate at natural frequencies, which are then transferred into global oscillations.

Observing pulsations is made difficult by the fact that there is rarely just one pulsation mode. These mechanisms drive several modes and these modes are independent. They can combine in a number of ways to produce a very complex light curve. However, their study can provide us with valuable information such as the star's mean density (τ_{dyn}) and its interior structure.

1.4 Subdwarf B stars

This dissertation focuses on using binarity and pulsation to probe a specific class of stars – subdwarf B stars. The sdB stars are blue in color, indicative of a rather high temperature.

Indeed the temperature of these objects is between 25000–30000 K (Heber et al., 1984). This puts them in the B spectral class. However, unlike main sequence B stars, sdB stars are compact with local gravities between $\log g = 5.0 - 5.5$. Another significant difference is that main sequence B stars are several times more massive than our Sun, whereas sdB stars have masses $\approx 0.47\ M_\odot$ (Saffer, 1994). Stranger still, hydrogen, which is a main component in all but the most evolved stars, makes up less than 1 per cent of the sdB's mass, all of which is in a thin hydrogen envelope (Saffer, 1994). Their position on the horizontal branch of the H-R diagram indicates a helium-burning core. The question then becomes, how does an evolved star lose virtually all of its outer layers? There is no simple answer to this question, but several possibilities will be discussed below.

1.4.1 Evolution

The transformation of a red giant into a sdB requires the star to relinquish most of its envelope, while nearly simultaneously igniting helium in its core. Although there are several viable methods for creating sdB stars, they are all connected by a common thread: mass loss on the red giant branch. This can occur in single stars, but the reason for this mass loss is not known (D'Cruz et al., 1996). Loss of mass in binary systems is much easier to explain and is associated with one of three basic scenarios (Han et al., 2002, 2003). The first and likely most common formation channel is through common envelope ejection. This occurs when the sdB progenitor evolves off the main sequence and grows large enough to engulf its companion. This companion, which can either be a low-mass main sequence star ($M < 0.5 M_\odot$) or a white dwarf, spirals in. It loses angular momentum through interaction with the envelope. This leads to envelope ejection. However, the progenitor must be close to helium ignition or else this mass loss can drastically alter conditions in the star preventing ignition. The end result of this channel is an sdB binary system with a period of hours to days.

Formation can also occur through Roche Lobe overflow. In this scenario, as the sdB progenitor becomes a giant, it transfers the majority of its mass to a main sequence companion just before helium ignition. This condition is not difficult to meet since the red giant radius is

just before helium ignition, and the star's hold on its outer layers is tenuous. The end product in this scenario will be a wide binary with an orbital period ranging up to 5000 days.

Finally, an sdB star can be produced through a merger of two white dwarfs (Han et al., 2002, 2003). In this formation channel two helium white dwarfs will spiral in due to gravitational wave radiation. During this merger helium is reignited and the end result is an sdB star with no companion. This is the only binary channel which produces individual sdB stars, and given that observational surveys have shown that a majority of sdB stars are in binaries, (e.g. Maxted et al. 2001) it does not appear to be common.

After creation sdB stars evolve much like any other horizontal branch star and continue to burn helium for around 10^8 years (Dorman et al., 1993; Kawaler, 2010). Once the sdB exhausts its supply of helium, it will become a white dwarf. Detailed information on sdB formation and evolution is given in Han et al. (2002), Han et al. (2003) and D'Cruz et al. (1996).

1.4.2 Variability

While not all sdB stars are currently known to have binary companions, this fraction could be as high as 89 per cent (Han et al., 2003; Green et al., 2004). When paired with a white dwarf, ellipsoidal variation is common, while a low mass companion often produces a reflection effect. Some of these stars are also in eclipsing systems. In addition, conditions are ripe for pulsations. Based on their temperature and gravity–which presumably is a function of their age–sdBs can pulsate in one of two different modes, or not at all. These two modes are observationally identified through their oscillation frequencies. Faster oscillations are p-modes and slower ones are g-mode (see Chapter 3 for more information). Not only are sdB stars variable, both intrinsically and extrinsically, but they allow us to probe a portion of binary evolution and stellar evolution about which little is known.

1.5   Entering the Space Age

Stellar variability is a great resource. It is the best way to provide insight into the dynamics of the interior and exterior conditions of a star. Despite these advantages, it is not always practical. Variability time scales for many interesting objects are on the order of hours. This is too long to gather useful information in the course of a single night. The Earth's rotation prevents us from observing these objects continuously from a single site on the ground as the sun drowns out all other astronomical signals. This leads to light curves where there is more information absent than gathered. A simple way of circumventing this problem is observing from space.

The *Kepler* spacecraft was designed for this exact purpose. While its primary mission is the search for extrasolar planets, it is valuable for all those who are interested in stellar variation (Prsa, 2012; Kjeldsen et al., 2010; Koch et al., 2010). This is because *Kepler* continously observes a single portion of the sky for years. Planets, especially Earth-like planets, will have Earth-like orbital periods. Most of the aforementioned sources of variabilty occur at fractions of that time scale. Therefore, even though planets are of higher priority for *Kepler*, the number of binary systems and pulsating stars found are an order of magnitude (or more) higher than the number of planets found. *Kepler* has already completely redefined what is possible in the field of asteroseismology. The wealth and quality of the data has made much of the analysis software inadequate. Its data also provides the foundation for this thesis.

CHAPTER 2.   FROM PHOTONS TO FOURIER TRANSFORMS

The study of stellar variability requires patience. Many stars are relatively stable throughout their life, varying on timescales far longer than humans have been in existence. These we can only hope to understand by examining populations of stars at different ages. However, as discussed in Chapter 1, there are more accessible variations on the order of days, hours, or even minutes. While these variations are a far more practical investigatory tool, they require excellent photometric precision and constant monitoring. Here I present some of the fundamental characteristics of times series photometry and analysis used in my research.

2.1   Time Series Photometry

Time series photometry consists of precise brightness measurement taken in rapid succesion and sustained over long periods of time. One of the most common uses for time series data is discovery and observation of periodic signals. The time interval between observations is highly dependent on the periodicities one expects or intends to observe. The smallest period we would like to observe sets our minimum sampling frequency. If our observations are spaced any farther apart than this value, the signal cannot be unambiguously retrieved. This is discussed in more detail in 2.3.3.

The integration time chosen for observation is subject to specific limitations. The first is target-based, as the integration time must be sufficiently long so that the instrument receives enough light from the star. If this does not occur, then background noise and Poisson (counting) statistics will mask small variations in the star's light. We are also limited by the instruments readout time (the time it takes to read and store the information).

2.1.1 CCD Photometry

Charge-coupled devices (CCDs) have become the standard imaging device for astronomical observations, including time series photometry. They have many advantages over photoelectric photometers mainly because the CCD's spatially sampled field of view provides simultaneous measurement of many comparison stars conjointly with the sky background. In addition, they have a maximum quantum efficiency[1] of 95 per cent compared to 20 per cent for photoelectric devices (Birney et al., 2006). Until recently though, photoelectric photomultiplier tubes were the chosen detectors for differential photometry for one very simple reason: speed. It can take a relatively long time to read out a CCD chip and time sampling is limited by readout time. This is especially problematic when looking for variations on short time scales (a few minutes), which is quite common in pulsations of sdBs, white dwarfs, and other stars (Gautschy & Saio, 1996). However, CCDs have now become the standard detector for asteroseismology because of sufficiently reduced readout times in their current generation.
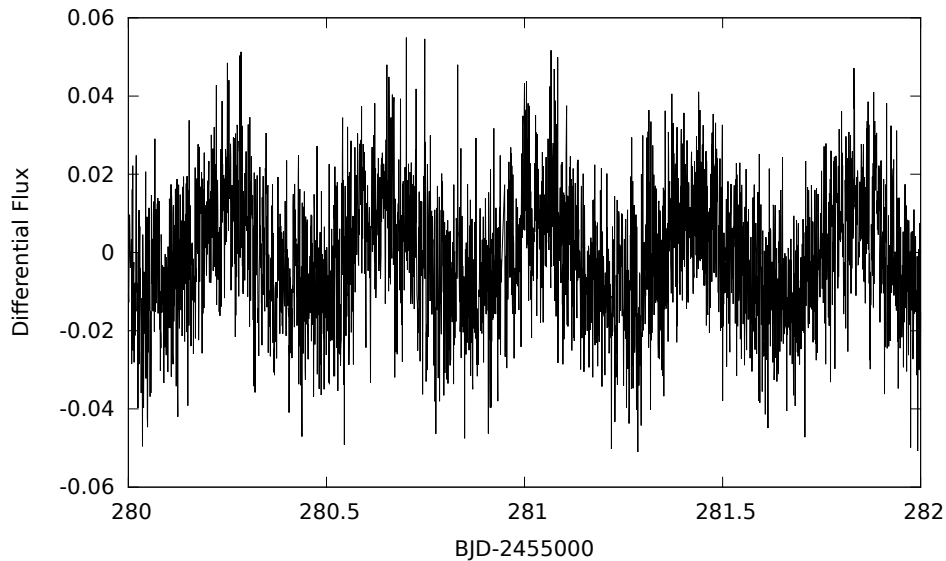
Figure 2.1   A small segment of the reduced *Kepler* Q5 data on KIC-11179657. This light curve is the final data product provided by time series photometry.

---

[1]This is the ratio of detected to incident photons. A quantum efficiency of 50 per cent means that half of the incident photons are detected.

It requires several procedures to transform a sequence of CCD images into the light curve used for asteroseismic analysis (e.g. Fig. 2.1). These techniques aim to remove systematic and instrumental effects. The first is called bias subtraction. CCDs have residual charge unassociated with astronomical sources. We can measure this charge by simply reading out the CCD chip while the camera's shutter is closed. The associated bias image gives a baseline of the initial charge in each pixel. It is common to take several bias images throughout the observing night and average them. This averaged image is then subtracted from each frame obtained on a given night.

A second step is the subtraction of "dark frames." Thermal electrons will create a dark current that also serves as a source of observational noise. The amount of current produced can be drastically reduced by cooling the CCD (often to 77 K with liquid nitrogen). An estimate of the residual current can be acquired by taking a long exposure (several minutes to hours) with the shutter closed. This is repeated several times to produce an average "dark frame" that is subtracted from all images.

Another issue associated with CCD detectors is that the response of each pixel is not uniform. We can correct for this by a process called flat fielding. This requires capturing images of a uniform light source; it can be a calibration lamp or the sky at twilight. The exposure time will vary when using the sky, which will brighten (or dim) substantially during twilight. Each observation should be long enough to allow sufficient counts while remaining in the CCD's linear regime[2]. Using flat fields, we can map pixel to pixel variation. For a night of observation all flat-field images are combined and an average flat-field image is made. The observations are then divided by this flat-field to establish uniformity. A more robust description of CCD photometry and reduction can be found in Birney et al. (2006).

---

[2]In this regime, there is a linear relationship between the length of observation and the number of counts received.

2.2   Observations

The difficulty involved with differential photometry comes from the precision required. Stellar variations can be a few parts per thousand and smaller. Attaining this level of precision requires the background to be very low. On the Earth, minute changes in the transparency of the atmosphere can mask the signal of stellar varation. While differential photometry can overcome some of this, it cannot eliminate it. Substantially smaller background variation can be easily obtained from space. In this dissertation, virtually all observations were taken with the *Kepler* spacecraft (see below). This high level of precision allows us to observe fainter objects and probe smaller variations than are attainable on the Earth. In addition, the data continuity provided by *Kepler* are crucial to this project. We will also discuss one ground based observation and some ground-based photometry using the Whole Earth Telescope (see Chapter 4).

2.2.1   *Kepler*

2.2.1.1   Spacecraft

The *Kepler* spacecraft was launched on March 7th, 2009. It is in an Earth–trailing, sun–centered orbit. This orbit allows *Kepler* to observe its chosen field continuously (24/7 365). The initial mission was designed to last for 3.5 years, with the possibility of an extension for another 3 years; it enters this extended mission phase in Nov. 2012. Currently it is the best resource that exists for differential photometry (Koch et al., 2010) and stellar asteroseismology (Gilliland et al., 2010a).

Kepler is designed to simultaneously obtain photometry on 150,000 stars with the primary goal of observing transits of extrasolar planets across their host stars. It continuously views 105 square degrees located just off the west wing of Cygnus (see Figure 2.2 and Koch et al. 2010). While the field of view remains constant, the telescope is rotated a quarter turn every 3 months. This rotation coincides with telescope down time during which the data are downloaded. Even though the *Kepler* field contains millions of stars, the data download limits our

analysis to a small fraction of them. There are 95 Megapixels on 42 CCDs, but only data from a small subset of pixels in each image will ever make it to the ground.
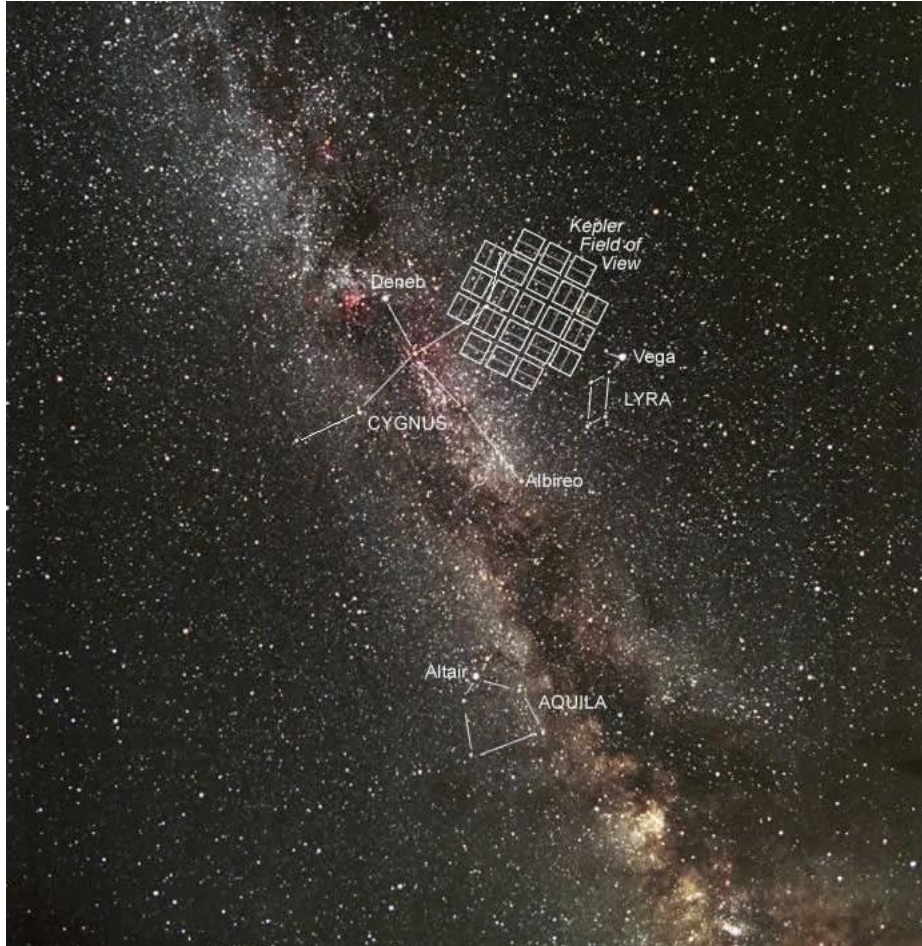
Figure 2.2   *Kepler* Field overlayed on the sky. Credit: Carter Roberts.

The instrument has two modes for data download: Long Cadence (LC) and Short Cadence (SC). The exposure time for the CCD is 6.02 seconds with a read out time of 518.95 ms. The integration times are relatively short to avoid saturation of the detector. There are 9 total integrations in a single SC observation of 58.8489 s. Each LC data point contains exactly 30 SC points. The data is then distributed to observers in 3 month increments or quarters[3] (e.g Q1, Q2). More information on the design specification for the *Kepler* CCDs is given in Koch et al. (2010). All the data for this project use the SC mode of which is necessary for looking

---

[3]Q0 and Q1 took place during the survey phase of the mission and are only 10 days and 1 month respectively.

at changes on the order of a few minutes.

2.2.1.2 *Kepler* Asteroseimology Science Consortium

A key element of *Kepler's* primary science goal is the determination of stellar properties (e.g. M, R) for stars that harbor planetary systems (Borucki et al., 2008). For this reason asteroseismology was a key secondary component to the mission and the *Kepler* Asteroseismology Science Consortium (KASC) was developed (Kjeldsen et al., 2010). The KASC is subdivided into 11 working groups. Each group oversees specific types of asteroseismic targets. In the following chapters, data obtained for the compact stars (Working Group 11) and pulsating stars in binaries (Working Group 9) is displayed.

2.3   Data Reduction

2.3.1   Reduction Pipeline

Data are downloaded from *Kepler* once every month (causing a small gap in the observations). These data must then go through a variety of procedures before they are provided to the observer for analysis. The data pass through three principle modules: Calibration, Photometric Analysis and Pre-Search Data Conditioning. During Calibration raw data are taken from the spacecraft along with "collateral" pixels. These pixels are designed to calibrate the data pixels. Much of the rest of the calibration is done using models of the instrument response derived from pre-launch tests performed on the CCD. These models include linearity, gain and flat-fielding (pixel to pixel variations).

The second step is Photometric Analysis. Here cosmic ray hits are cleaned, the background is estimated and removed, and each observation receives a barycentric timestamp correction[4]. Next, an aperture is drawn to select pixels containing data from the star and all the light within this aperture is summed. However, aperture selection is optimized for transit detection

---

[4]To correct for the motion of the spacecraft time is transformed to a non-moving reference frame at the solar system center.

and as such may not be optimal for asteroseismology[5].

The last step is Pre-Data Search Conditioning. This module specifically prepares the data for planet searches in several ways, most notably through the removal of flux outliers and the filling of data gaps. This is not necessary and sometimes harmful to asteroseismology efforts. As such these results have been ignored in our analysis. More information on the specifics of these modules can be found in Klaus et al. (2010a,b); Middour et al. (2010); McCauliff et al. (2010).

2.3.2 Post-pipeline Reduction

Although the data provided from the *Kepler* pipeline have undergone several reduction steps, this does not imply that the data are ready for asteroseismic analysis. The data may still show artificial long term variations due to instrumental effects. The reasons for these variations are not always known and are often different from quarter to quarter. To remove these trends we implement a simple boxcar smoothing. Here chunks of data over which there are no significant variations (≈ 5 days) are averaged together. A numerical function is created from these points through nearest neighbor interpolation. This function is then subtracted from the data removing long term trends. It should be noted that tools have been created which use the actual *Kepler* data from all nearby targets to remove systematic trends. However, this software was not designed for SC data and could not be used for our analysis. At this point we have a "flat" light curve with no variation on time scales longer than a day.

Another issue is that the base-level for the star may have changed over time because of changing CCD sensitivity, differential abberations or other effects. This is treated through normalization, where the mean value is subtracted from all points in a given quarter. The data are then divided by the mean so that we are left with the fractional deviation of the intensity

---

[5]Users can now process photometry from individual pixel data. However, this project was completed before this became available. The improvement is not significant in most instances relevant for this work.

from the mean. Finally, it is not uncommon to have single points which lie far above or below the data set. To eliminate these points, we apply a "sigma clip" on the data such that anything that is further than 4 sigma away from the local mean is removed from the light curve. Further details for specific targets are given in Ch. 5 and 6.

2.3.3 Fourier Analysis

Binary variations in a light curve are relatively easy to identify. They are, except in rare cases, hours (or longer) in period, show a significant change in brightness and produce an obvious signal in the light curve. In contrast, that same star can have thousands of multiperiodic pulsation modes that are typically much smaller variations in brightness on a time scale of minutes. Analysis of such a light curve in the time domain makes it virtually impossible to distinguish coherent pulsations from stochastic variations, much less determine the number of pulsation modes which exist. Untangling these signals requires transforming them into the frequency domain which allows the individual periodicities to manifest themselves. Although these pulsations persist across the entire time domain (assuming the signal is stable), they each have a distinct frequency. In the frequency domain the pulsations tranform into a series of unambiguous peaks each representing an oscillation mode (see Fig. 2.3a).

In the frequency domain we are still limited by the time sampling of our observations. Only frequencies that are less than half of the sampling frequency can be unambiguously determined. This is called the Nyquist frequency ($Ny = \frac{1}{\Delta t}$) and it is the maximum relevant signal in the Fourier transform.

2.3.3.1 Prewhitening

Once in the frequency domain, our goal is to identify the frequency of all pulsation modes, along with their phase and amplitude. Since there can be a multitude of peaks, some caused by noise, our first task is to determine which of these peaks is significant. We do this by first identifying the average noise level in a region of the Fourier transform that is devoid of peaks. We then assume that any peak which is larger than 4 times this noise level is real (Aerts et al.,
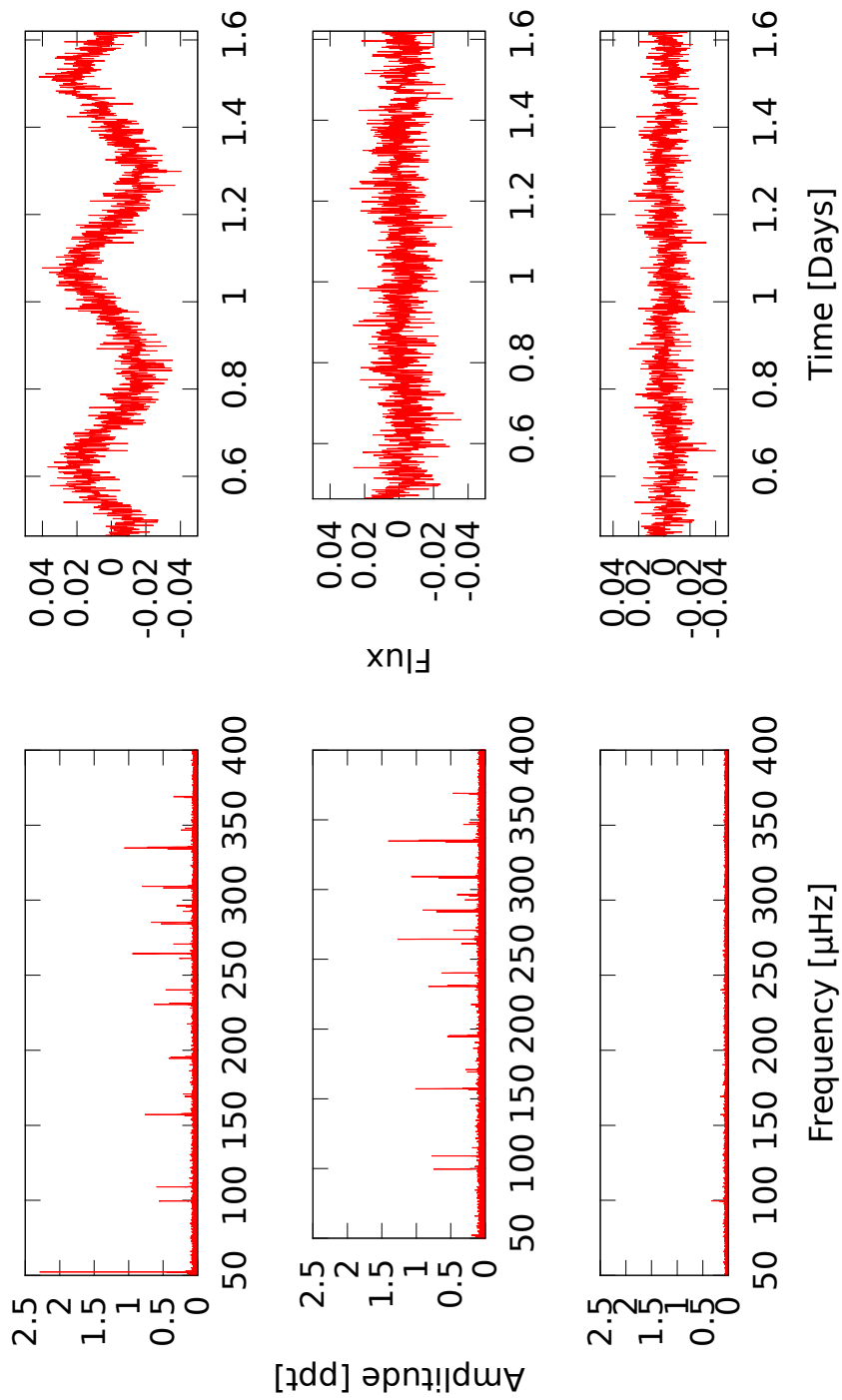
Figure 2.3 This Fourier transform (left) and corresponding light curve (right) of KIC-02991403. The top panel is unadulterated, the middle panel has prewhitened the binary signals and the bottom panel has prewhitened all signficant peaks.

2010). Once all candidate peaks have been identified we must model and remove them. This is accomplished by removing a sinusoid that has a period, phase and amplitude corresponding to each periodicity. Sine curve parameters are found using non-linear least squares fitting to determine the values of those parameters which minimize the spread in the new light curve (see Fig. 2.3). This procedure is then repeated, adding new peaks each time, until all significant peaks have been removed from the Fourier transform (see Fig. 2.3).

If two such peaks are closely spaced, we must check whether or not both peaks are resolved. The frequency resolution is equal to

$$\Delta\nu = \frac{1}{N\Delta t}, \tag{2.1}$$

where N is the total number of observations in the data set. If the frequency separation is smaller than this value, then only one peak can be considered real. Originally, this process was done using Period04 (Lenz & Breger, 2005). However, this particular program uses a discrete Fourier transform and as the size of the *Kepler* data sets increased to hundreds of thousands of points, it became much too slow to adequately process the data. Thus for data sets longer than 6 months we use a fast Fourier transform program, FASPER implemented for time series photometry (Press & Rybicki, 1989).

2.3.3.2 Ground-based Data Issues

The analysis described above is relatively simple when the sampling rate is uniform and the overall span of the data is long and continuous. However, this is often not the case. Gaps will exist if observations are taken from the ground even in the best observing conditions, because of the Sun. This limits the continuity of data and can also create false periodicities due to periodic gaps. While this is a problem for any pulsation signal, it is devastating for periods on the order of a few hours. This is because the oscillation times are similar to the observation time and, more importantly, to the time over which we are **not** able observe. Gaps of similar size to the intrinsic periodicities of the star will inevitably hamper the discrimination between true frequencies and their aliases (Nather et al., 1990). Multi-site campaigns are

useful for reducing aliasing effects, as their duty cycle can reach 60-70 %, but they generally only operate for a month or less at a time. Space-based observations can completely eliminate these problems. Not only is it possible to have virtually continuous data, but in the case of *Kepler* these observations have been on-going for multiple years, something that simply is not possible from the ground.
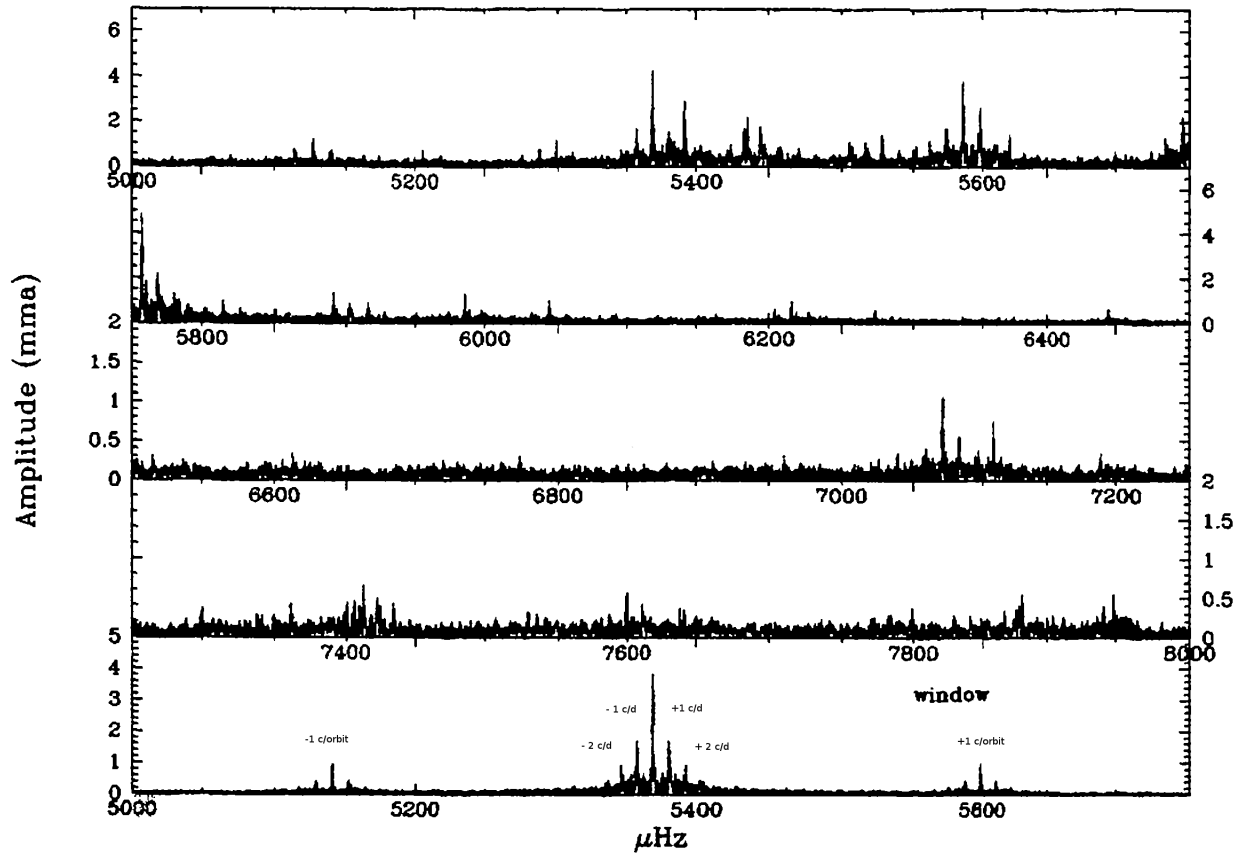
Figure 2.4   This is the Fourier transform and window function of pg1336 reduced from data taken on the Whole Earth Telecope run XCov 17. The window function (bottom) corresponds in frequency to the top frame in the Fourier transform where its effects are clearly visible. Adapted from Reed et al. (2000).

To illustrate this point, we can look at a single periodicity. If it is a perfect sinusoid it will appear as a sinc function in the Fourier domain, but if resampled periodically alias peaks will appear at offsets equal to the periodicity of the interruptions. The resulting form in the

Fourier transform is the "window function" equivalent to a point spread function in imaging. When examining time series data, one can try to compare with the window function to identify false periodicities and recover true pulsation frequencies (see Fig. 2.4). However, the *Kepler* observations are so close to this sinc function that using a window is not necessary.

2.4   Summary

In this chapter we have provided a framework for the analysis of time series photometry, specifically as it relates to asteroseismology. We have explained the identification and removal of peaks. We have also discussed the benefits of using space-based data: continuity and lack of atmosphere. This is a practical but incomplete picture of stellar asteroseismology as we have said little about what we can learn from this analysis. A proper understanding requires a brief introduction into the theory of stellar oscillations which will be discussed in the next chapter.

CHAPTER 3.   ASTEROSEISMIC TOOLS

Stars are often seen as unchanging objects in the night sky. While there are many exceptions, the majority of stars are stable, producing roughly the same amount of luminosity for the majority of their life. However, even the most constant main sequence star experiences oscillations. When an instability presents itself, the star acts as a self-regulating system to correct the anomaly. Such an instability is typically random and shows no periodic structure. However, in many stars these instabilities produce small changes in density and temperature (for example) that propagate out to the edges of the star and back again setting up standing waves at normal mode frequencies. This results in periodic oscillations in the light coming from the star.

Pulsations vary in strength and become most apparent at specific stages of stellar evolution during which their amplitude is sufficiently large. Additionally, they can exhibit a wide range in frequency and geometry. In this section we will examine the types of pulsations which can occur as well as the the information they can provide. The ideas will be general, but particular attention will be paid to sdB stars.

3.1   Pulsations

To understand what drives oscillations to observable levels we must first determine what is taking place. Somewhere in the star's interior there is a build up of heat which causes the star to expand. This expansion cools off the star, causing it to contract. Generally this process maintains a strict equilibrium. Under certain circumstances though, an instability can develop causing macroscopic oscillations around this equilibrium configuration. The relevant

quantities which determine the local perturbation of the radiant luminosity, δL_{rad}, are given in the expression

$$\frac{\delta L_{rad}}{L_{rad}} \approx -(\kappa_T - 4)(\Gamma_3 - 1) + \kappa_\rho \frac{\delta\rho}{\rho} \ , \tag{3.1}$$

where κ is the opacity, $\kappa_T = \left(\frac{\delta ln\kappa}{\delta lnT}\right)_\rho$, $\kappa_\rho = \left(\frac{\delta ln\kappa}{\delta ln\rho}\right)_T$, $\Gamma_3 = \left(\frac{dlnT}{dln\rho}\right)_{ad}$ and $\frac{\delta\rho}{\rho}$ is the relative change in density (Aerts et al., 2010). Typical values for these quantities lead to a situation where δL_{rad} increases outward which is a stable configuration (Aerts et al., 2010). If there are places where the flow of luminosity is blocked, the system will tend toward instability. This can occur in regions of high opacity, specifically in the ionization zones of abundant elements. In these zones there can be large increases in the opacity with temperature, κ_T. Because these regions have high values of κ_T it is shown clearly from Eq. 3.1 that they are a sink for δL_{rad} and as such a driving region for pulsations. This mechanism for excitation of pulsation modes is known quite aptly as the κ mechanism.

The κ mechanism is not the only method of excitation, but it is one of the most common driving pulsations in Cepheids, RR Lyrae, and white dwarfs (Gautschy & Saio, 1996). It also explains why different stars pulsate at different T_{eff}. Different T_{eff} leads to ionization of different elements and at different depths within the star. In sdB stars, this opacity is affected by iron-group elements that are concentrated by radiative levitation allowing large enhancements of iron in the hydrogen envelope. Charpinet et al. (1996) show how the κ effect in iron can drive pulsations in sdBs.

3.2   Distinguishing Oscillations

In a stellar model, it is possible to numerically obtain the frequencies of the oscillations being driven, albeit with certain simplifications. The first simplification is that of spherical symmetry. This implies that the for any wave propagating outwards in a star the angular direction of travel is inconsequential. An additional assumption is that the modes themselves are spherically symmetric. For some stars such as Cepheid variables this is true, so it is a

reasonable justification. These spherically symmetric modes are known as radial oscillations. In some scenarios we can relax the second assumption and consider non-radial oscillations in a spherical star. In sdB stars, which are of the greatest importance to this project, this is the appropriate assumption. Despite the mathematical headaches that arise from these so-called non-radial pulsations, their value makes such efforts worthwhile.

3.2.1 Non-radial Oscillations

Non-radial oscillations is a complex subject. Therefore, we present some highlights and features, but make no effort to be comprehensive. There are a number of rigorous treatments and reviews available (Unno et al., 1979; Cox, 1980; Aerts et al., 2010).

A star is a giant ball of gas under a large amount of pressure; motion inside of a star is described via fluid dynamics. We can describe this fluid with three basic equations. The first is known as the continuity equation showing that the mass flux through the star is a conserved quantity

$$\frac{\delta \rho}{\delta t} + \nabla \cdot (\rho v) = 0. \tag{3.2}$$

Here v represents the local fluid velocity. How the fluid flows is dependent on what forces are acting on it. In stars, the dominant force is that of gravity. The potential due to gravity, Φ, can be described by a Poisson equation:

$$\nabla^2 \Phi = 4\pi G \rho. \tag{3.3}$$

Finally the motion of the fluid under the influence of this potential and pressure gradients is given by the equation of motion

$$\rho(\frac{\delta}{\delta t} + v \cdot \nabla)v = -\nabla P - \rho \nabla \Phi. \tag{3.4}$$

We now have a description of our fluid (Cox, 1980). The pulsations are driven by changes in heat content which we discussed above. This acts upon a displacment of fluid from its

equilibrium position. This displacement causes departure from the equilibrium values of other properties. To see how they relate, we can express each of the quantities in Eq. 3.2–3.4 in terms of their equilibrium value plus the perturbation in each. All that remains is solving this new system of equations and we can in principle describe the different pulsations modes that occur in the star. Unfortunately, the solution to this system is difficult if we retain all the high order derivatives in both time and space. A recasting of these equations is needed, but we will not go into great detail here. The first thing we will do is make an assumption that the time dependence of all quantities can be expressed as $e^{i\sigma t}$ where σ is the oscillation frequency. Since we are expecting wave-like motion this is a logical jump. Then the radial perturbation, ξ, can be expressed as

$$\xi(\mathbf{r}, t) = \xi(\mathbf{r})e^{i\sigma t}. \tag{3.5}$$

Next we need to pick a coordinate system. It is natural to pick spherical coordinates since the star itself is spherical (to first order). This choice of coordinate system allows us to separate the perturbation into three separate equations in terms of r, θ, and ϕ. The radial component is still quite complicated, but the θ and ϕ components (which have no dependence on ρ) are just the solution to Laplace's equation (Aerts et al., 2010). This is a well known problem who solution is the set of spherical harmonics

$$Y_{l,m}(\theta, \phi) = \sqrt{\frac{(2+\ell)}{4\pi}\frac{(\ell - m)!}{(\ell + m)!}}P_\ell^m(cos\theta)e^{im\phi} \tag{3.6}$$

where P_ℓ^m is the set of Legendre polynomials (Laplace & Young, 1832). The consequence of this is that the oscillation frequencies are quantized, not just in l and m, but also with respect the radial component n. In the following sections we will describe the implications.

3.3   Oscillation Systematics

Understanding the pulsation modes inside stars requires the ability to model them numerically. This is extremely difficult to do in 3–D and several simplifications are made to arrive at a solution. The solution provides information about the inner workings of the star. As wave

solutions, the spatial parts take the form e^{ikr}, where k is just the wavenumber. An asymptotic analysis results in a dispersion relation for the radial wavenumber k_r:

$$k_r^2 = \frac{k_t^2}{\sigma^2 S_\ell^2}(\sigma^2 - N^2)(\sigma^2 - S_\ell^2) \tag{3.7}$$

where k_t is the transverse wave number, σ is the oscillation frequency and N and S_ℓ are the Brunt Väisälä and Lamb frequencies respectively (Hansen, Kawaler & Trimble, 2004). We have not defined these frequencies yet, but the equation adequately describes much of what we need to know about them. They are the critical frequencies for wave propagation. As long as σ^2 is greater than or less than both N^2 and S_ℓ^2 then k_r^2 will be positive which leads to sinusoidal solutions. If not then the the wave will be evanescent.
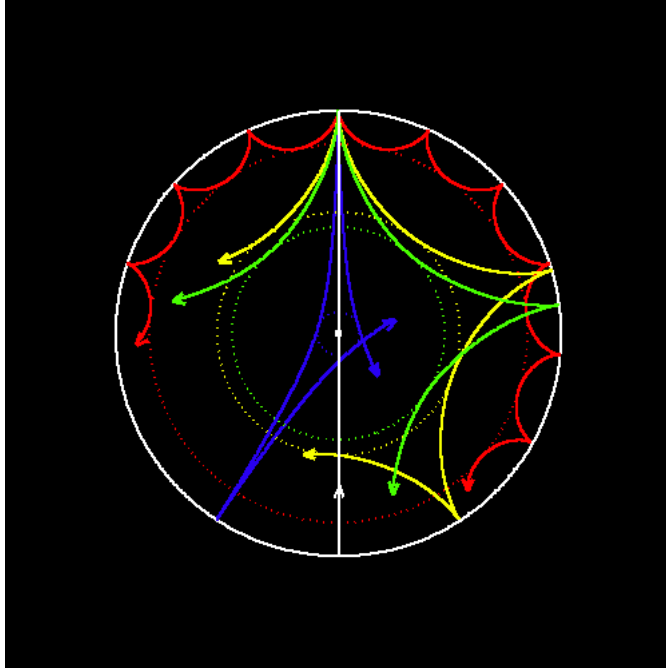
Figure 3.1   This figure shows is a simple stellar cross section that illustrates how p-modes of different ℓ propagate within a star. Credit: Theoretical Astrophysics Center, Institute of Physics and Astronomy, Aarhus University, http://www.astro.phys.au.dk.

Here it is important to notice that there are two possible conditions for wave propogation, and it is these two conditions which lead to the two types of oscillations which occur within a star. The first condition occurs when σ^2 is larger than both S_ℓ^2 and N^2. When S_ℓ is larger

32

than $|N|$ this means that the propagation of the wave depends mainly on S_ℓ. S_ℓ, called the acoustic frequency (or Lamb frequency), is proportional to the sound speed v_s. It is therefore logical that the propagating waves are sound waves. Since sound waves are pressure waves, these types of oscillations are known as p-modes. As they propagate radially towards the center of the star, the sound speed increases. This causes the wave to bend in much the same way that a light ray bends as it passes from water to air. Eventually the wave will be propagating back towards the surface, where it is reflected back down. This is illustrated nicely in Fig. 3.1.
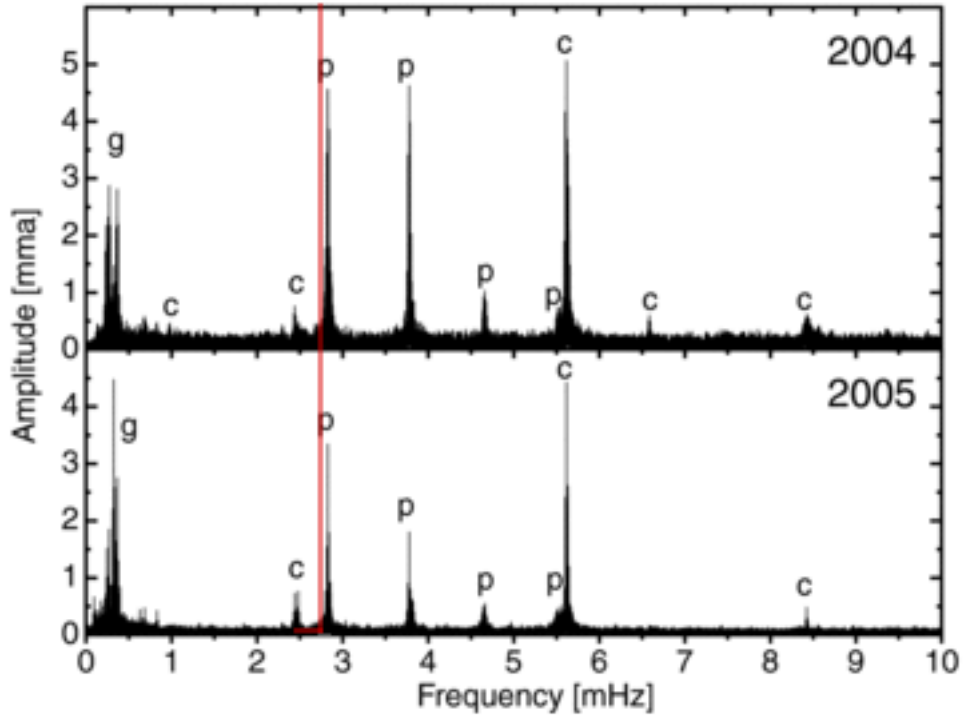
Figure 3.2   This figure is adapted from Baran et al. (2006) shows the hybrid pulsator Balloon09010001. The p-modes (p), g-modes (g) and combined frequencies (c) are labeled on the diagram. The top and bottom panels show the difference between two data runs: one in 2004 (top) and one in 2005 (bottom). The red line shows the frequency associated with τ_{dyn}.

On the other hand, when σ^2 is less than both quantities, the wave number is most sensitive to N. This frequency describes motion when buoyancy is the restoring force. Here, it is gravity acting on small changes in density which causes oscillatory motion. These modes are often

referred to as gravity-modes or g-modes. It is not as easy to draw analogies to light waves as with p-modes, but they are analogous to ocean waves. These waves tend to propagate deep into the star, probing a different region than p-modes.

These two types of waves need not be mutually exclusive. While many stars show only p or g-modes, there are hybrid stars in which the conditions are right for both types of waves to propagate (see Fig. 3.2). Even when both are present in a single star they are typically easy to distinguish. The p-modes will have freqencies on the order of the sound crossing time within the star or higher; g-mode frequencies are generally **much** lower (on order the free-fall time). For sdB stars this amounts to p-mode periods of 3–8 min and g-mode periods of 45 min to 2 hrs. In frequency space this will amount to two clusters of frequencies at different places in the Fourier transform.

3.3.1   g-mode period spacing

If we simplify k_r for the case of g-mode propagation ($\sigma^2 << N^2, S_\ell^2$) it becomes

$$k_r \simeq \frac{\ell(\ell+1)}{r^2}\left(\frac{N^2}{\sigma^2-1}\right). \tag{3.8}$$

We can use this to determine the frequencies of the g-modes by integrating between the boundaries of the g-mode propagation region (Tassoul, 1980). The quantization condition means that $\int_{r_1}^{r_2} k_r dr = \left(n - \frac{1}{2}\right)\pi$. For high order and low-degree g-modes ($n > l$) we note that $\sigma \ll N$. From this we can determine a period given by

$$\Pi_{\ell,n} = \frac{\Pi_0}{\sqrt{\ell(\ell+1)}}n + \epsilon, \tag{3.9}$$

where $\Pi_0 = \int_{r_1}^{r_2} \frac{N}{r} dr$ and ϵ are constants determined from stellar structure. This leads to a period spacing of

$$\Delta\Pi_\ell = \frac{\Pi_0}{\sqrt{\ell(\ell+1)}}. \tag{3.10}$$

Therefore modes with same ℓ value will be equally spaced in period (Tassoul, 1980). This relationship has been verified with several sdB stars in Reed et al. (2011b). While this spacing holds true for most modes, some g-modes can be trapped in specific regions of the star where the boundary conditions, and by extension $\Delta\Pi$, will be different.

3.4 Rotation

Although it was not mentioned above, implicit in the derivations is the idea that the star is not rotating. Since all things are in motion and stars coalesce from large clumps of gas, rotation is not something that can be properly ignored. However, it can be inferred from the angular dependence of oscillation modes. To understand this let us write down our full wavefunction

$$\xi(\mathbf{r}, t) = A\xi(r)P_\ell^m(\cos\theta)e^{im\phi}e^{i\sigma t}, \tag{3.11}$$

where A is an arbitrary constant. If we rewrite the exponentials in terms of trigonometric functions as outlined in Aerts et al. (2010), it becomes (ignoring the imaginary part)

$$\xi_t(t) \propto \cos(m\phi - \sigma t + \delta_0), \tag{3.12}$$

where δ_0 is just a phase shift. This immediately shows that the wave's azimuthal velocity is tied to m. If m is zero, there is a standing wave; if $m \neq 0$, then the wave's azimuthal velocity is $\frac{\sigma}{m}$. This is where the effects of rotation become apparent. When the star is not rotating, there is no way to distinguish the running waves from standing waves. However, the star's rotation breaks the m degeneracy and in so doing produces multiple peaks where originally there was only one.

The new frequencies that occur when breaking this degeneracy are well defined and can be expressed in the following way

$$\sigma_{n,\ell,m} = \sigma_{n,\ell,0} \pm m\Omega\left(1 - C_{n,\ell}\right), \tag{3.13}$$

where Ω is the rotation frequency of the star. The Coriolis force is also relevant and is included in $C_{n,\ell}$, known as the Ledoux constant, which can be found for a given oscillation mode (Ledoux,

1951). This relationship tells us that the star's rotation creates evenly spaced multiplets ($\ell(\ell + 1)$) in frequency (i.e. triplets for $\ell = 1$) which can be identified in the Fourier transform. These serve two main functions: allow for mode identification (l,m) and determine the global rotation rate of the star. For sdB stars this is extremely important as the other methods for determining rotation rates are either very difficult or simply not applicable. Additionally, since these waves probe deep into the star, this method measures the average **internal** rotation rate.

3.5   Mode Identification

We have mentioned that asteroseismology has the ability to tell us details about the star, some of which it is impossible to get in any other way. Non-radial modes are a powerful probe, especially if we can identify n, l, and m. While it is nearly impossible to observationally determine the value of n for most modes, multiplets allow us to find the ℓ and m number. We can use these to classify other similar modes through period spacing relationships inherent in g-modes (or frequency spacing in p-modes). Once these modes have been identified, stellar models and their calculated equations provide a link between observation and theory allowing us to measure values of stellar parameters (i.e. M, R, and g). The more modes that are identified, the more data that can be put into the models and the better the constraints on the input physics and derived parameters. This again points to us back to why continuous observation and short sampling rates are so crucial, especially to g-mode asteroseismology.

CHAPTER 4.   PULSATING sdB BINARIES

4.1   Importance of Pulsating Binaries

In Chapter 1, we discussed the importance of binaries, especially ones that show eclipses. Having **only** eclipse data is of limited use. Fortunately, high precision light curves are capable of providing several different types of constraints, including asteroseismic and even radial velocity (Loeb & Gaudi, 2003). A solitary sdB binary light curve which exhibits pulsations can not only provide a complete binary solution but also information on the evolution of the system.

4.1.1   Fundamental Parameters

Maximizing the information provided by an eclipsing binary typically requires a light curve and two radial velocity curves, one for each component[1]. A single radial velocity curve is difficult to obtain; obtaining both requires untangling spectral lines. More problematic for sdB binaries is that their size makes them on average much fainter than other stars with similar temperatures. In addition, as the sdB companion is likely a white dwarf or an M–dwarf, the companion is so faint that it is virtually impossible to identify the companion's spectral lines.

When the primary star is a pulsator though, it can eliminate the need for radial velocities. With a good stellar model it is possible to find the mass and radius of the primary star which, in combination with the system's inclination, is enough information to uniquely solve for the binary parameters. In the absence of a good stellar model fit, a solution to the system is still possible, provided the stellar pulsations are accurately measurable, through a "new" technique employing frequency modulation. This allows one to measure not only the radial velocity, but

---

[1]When both stars fill their Roche Lobes it is possible to find the mass ratio q from the light curve and a second radial velocity is not needed.

Table 4.1   Photometric Determination of Fundamental Parameters

	Eclipses	Ellipsoidal/ Reflection	Doppler Beaming	Pulsations	Eclipses+ Beaming	Eclipses+ Pulsations[a]	Eclipsing+ Pulsations[c]
P	$\checkmark$	$\checkmark$	$\checkmark$		$\checkmark$	$\checkmark$	$\checkmark$
i, $\frac{R_{1,2}}{a}$, $\frac{L_2}{L_1}$	$\checkmark$		$\checkmark$	$\checkmark$	$\checkmark$	$\checkmark$	$\checkmark$
$a_1 sini$					$\checkmark$	$\checkmark$	$\checkmark$
M_1, R_1				$\checkmark^a$		$\checkmark$	$\checkmark$
a, $R_{1,2}$, $M_{1,2}$						$\checkmark$	$\checkmark$
P_r				$\checkmark^b$			
q				$\checkmark^c$		$\checkmark$	$\checkmark$

[a] Stellar Model

[b] rotational multiplets

[c] phase modulation

the mass ratio of the binary system (Shibahashi & Kurtz, 2012). Table 4.1 shows a number of parameters that can be solved for with a single high precision photometric light curve.

4.1.2   Synchronization and Evolution

As discussed in Chapter 3, one unique aspect of asteroseismology is the ability to measure rotation rates. In binary systems, this is particularly useful as it gives us information about the tidal evolution of the system. Normally determining the rotation rate would also require spectroscopy to measure the rotational broadening[2]. For sdB stars, even high resolution spectroscopy may not yield a rotation rate because of the large natural width of sdB absorption lines. However, asteroseismology allows us to accomplish this feat with a single light curve. Comparing the rotation and orbital period allows us to determine if tidal interactions have equalized them. In addition, since the sdB mass and radius are well known, we are able to calculate expected tidal synchronization times for these objects. Comparing both pieces of

---

[2]As the star turns one side is red shifted while the other is blue shifted broadening the line. The main difficulty in using this to determine the rotation velocity is that there are several other sources of line broadening which can swamp the rotational effect.

information enables us to pinpoint much more precisely where the system is in its evolution. A non-synchronous system will have an upper limit on its age, while a synchronous system will have a lower limit.

We are also able to place limits on the system's formation state. The common envelope phase that all close sdB binaries have gone through is extremely short (≈ 100 yrs) (Shankar et al., 1991) and, for that reason, still much of an enigma. Knowing the state of the system currently and its synchronization rate allows us to back track and constrain the sytem's initial conditions. These conditions can tell us the state of the system as it exits the common envelope.

4.2   Disentangling Pulsating Binaries

We showed in the previous section the usefulness of studying pulsating sdB stars in binaries. This is true as long as both signals can be identified. Unfortunately, both binarity and pulsationsaffect the light curve in similar ways. The end result often more resembles noise than two (or more) coherent signals (see Figure 4.1). Therefore, these signals must be separated before they can be analyzed.
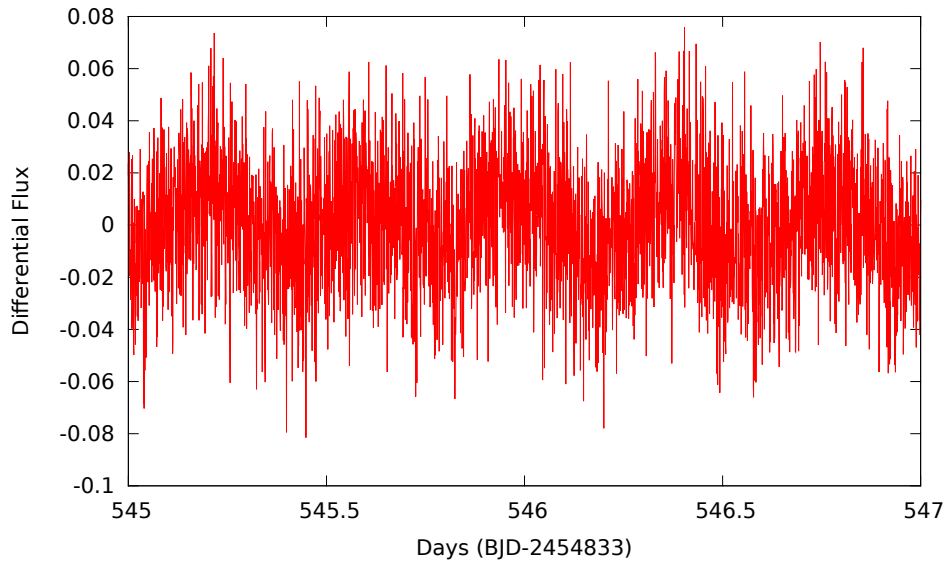
Figure 4.1   This is a two day sample of the *Kepler* observation of B4. Since the pulsations are of the same order as the reflection effect it is very difficult to disentangle them.

4.2.1 Distinguishing Binary Characteristics

In Chapter 1 we briefly discussed the three major types of variability that occur due to the presence of a companion:

1. Eclipses

2. Ellipsoidal variation

3. Reflection effect.

A single binary light curve can show the presence of one or all of these effects. When an eclipse is present, it is easy to distinguish the difference between an ellipsoidal variable and one showing the reflection effect. The eclipse in an ellipsoidal variable will occur at a minimum in the light curve when the "pointy" or the "blunt" end is facing us (see Figure 1.4). In a reflection effect variable, the heating is at its greatest when the companion is being eclipsed, so an eclipse will appear at a maximum in the light curve as well as the minimum (see Fig. 4.2).
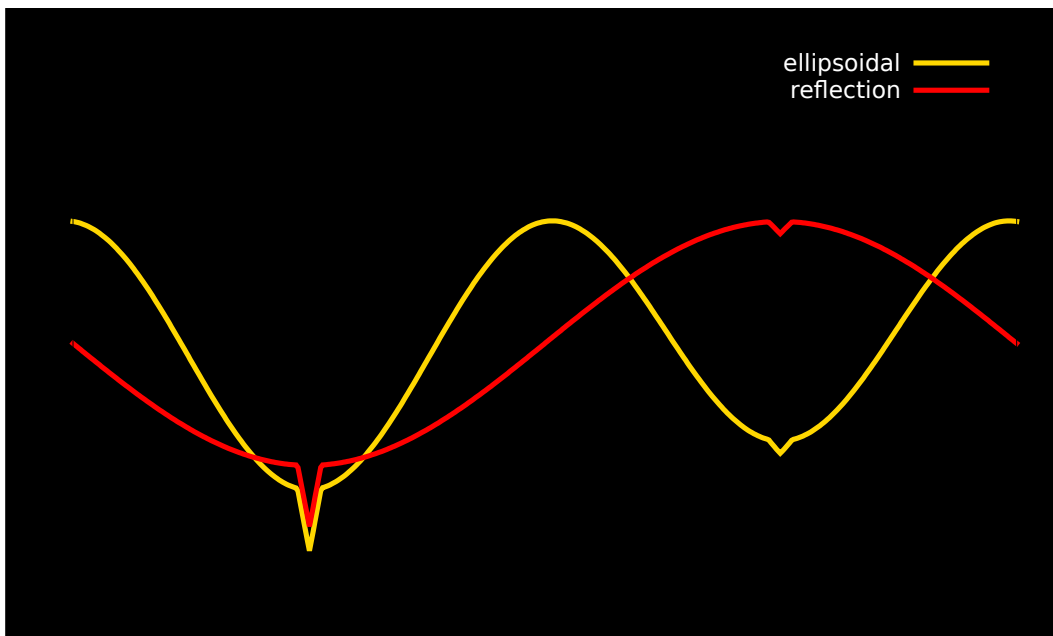
Figure 4.2   This simple illustration shows the differences between a reflection effect (red) and ellipsoidal variable (gold).

None of the binaries we will discuss in future chapters show eclipses. The only noticeable difference between the light curves in this case is that an ellipsoidal variable will have minima of different depths. If this variance is not large, or the star is pulsating, the two light curves can be virtually indistinguishable. In such cases we must look at the Fourier transform. An ellipsoidal variable should have a peak at the orbital frequency and also one at half the orbital frequency. This is still not sufficient as orbital harmonics are common in the Fourier transforms of binaries and expected in close pulsating binary systems (Willems & Aerts, 2002). The only option left to us is to fit the two peaks. If the maxima of the signals represented by the two peaks are in phase then we know it is a reflection effect.

4.2.2 Frequency Space

While it is difficult to pinpoint closely spaced signals in the time domain, they are much more distinct when transformed to the frequency domain (see Chapter 3). This, while standard for pulsation analysis, does not help untangle them from the binary signal. However, close sdB binaries, including those discussed here, have orbital periods ranging from hours to several days (Han et al., 2003; Maxted et al., 2001). The pulsations, though, are all shorter than 3 hours (Hu et al., 2010). This means there is a distinct gap in the Fourier transform between the orbital frequency and the forest of peaks associated with p and g-mode oscillations (see Fig. 3.2).

While this is true of the actual binary period, orbital harmonics can be located in the p-mode and/or g-mode range of the sdB, interfering with asteroseismic analysis. Luckily, these peaks are easy to separate as they lie at precise multiples of the orbital frequency. What is both more problematic and interesting is that such peaks may not simply be orbital harmonics. Instead they could be indicative of tidally induced oscillations common in close binaries (see section 7.2). It is difficult to confirm as it requires precise seismic modeling (large numbers of well identified peaks) or spectroscopy (Willems & Aerts, 2002). To date this has not been identified in an sdB binary.

4.3   An Example: The Curious Case of KPD 1930+2752

KPD 1930+2752 (hereafter KPD1930) is the only sdB binary that is discussed in detail in this dissertation which will be analyzed using ground based observations. While there are many interesting things to learn from these binaries, the following section will serve as an illustration of both the potential these systems hold, and also the necessity for space-based observations.

4.3.1   Observations

KPD1930 was first discovered in the Kitt Peak Downes survey (Downes, 1986). Further observations revealed it to be a pulsating p-mode binary (Billéres et al., 2000). This binary is very interesting as its white dwarf companion puts the total system mass very close to the Chandresekhar mass (1.44 $M_\odot$). Since a white dwarf exceeding this mass would result in a supernova (type Ia[3]) KPD1930 is seen as a possible progenitor system of this event.

For these reasons it became the target of the Whole Earth Telescope (WET) run XCov 23 (Reed et al., 2011a). This multi-site campaign lasted from August 15 to September 9 2003, during which time series photometry was obtained at 17 observatories. The observational duty cycle of this run was 36 per cent. The pulsation analysis for this data set is discussed at length in Reed et al. (2011a); here we will discuss its binarity.

Combining data from several different observatories increased the noise level and masked some of the more minute light variation. Therefore we chose to use the data from a single source: the Nordic Optical Telescope. These observations were taken from Aug 20-22[4] 2003. The observations were taken with a CCD photometer using a cadence of 10 seconds and a filter with similar properties to $CuSO_4$.

---

[3] This type of supernova occurs when the white dwarf mass is sufficient to break electron degeneracy causing the star to collapse further in a massive explosion.

[4] Data was also taken on the 23 of August, but not used due to large continuity gaps.

4.3.2 Reduction and Spectral Filtering

WET CCD data are reduced on site by each observer (Reed et al., 2011a). This means that the CCD reductions discussed in detail in Chapter 2 have already been applied. Before beginning analysis a 3.5 σ clip was performed removing less than 0.3 per cent of the data points. These data are shown in Fig. 4.3. Since the amplitude of the pulsations are of the same order as the binary variation, it was necessary to filter them in order to explore the systems binarity. The simple smoothing created by phasing over the orbital period and then binning the data was insufficient, as shown in Fig. 4.4a.
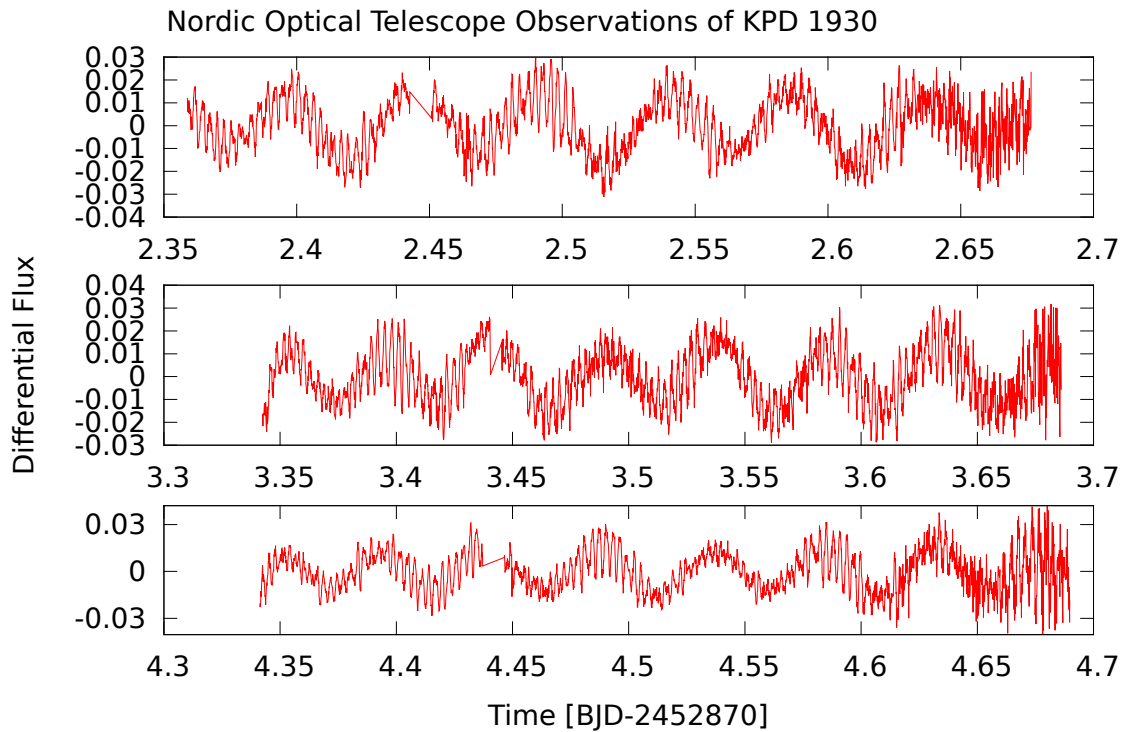
Figure 4.3   These are observation of KPD1930 taken at the Nordic Optical telescope Aug. 20-22, 2003. Pulsations are clearly evident as is a longer period whose uneven minima denotes ellipsoidal variation.

For this reason it was necessary to filter out the pulsations. This is done in the Fourier domain where the distinction between the two sources of variation is clear. Typically each peak is fitted and removed one by one in a process called pre-whitening (see Chapter 2). However,

KPD1930 shows at least 68 significant peaks and another 13 suspected peaks (Reed et al., 2011a). Also, the pulsations show amplitude and frequency variations on daily time scales. Therefore it was determined that even careful prewhitening would not sufficiently remove the pulsations.
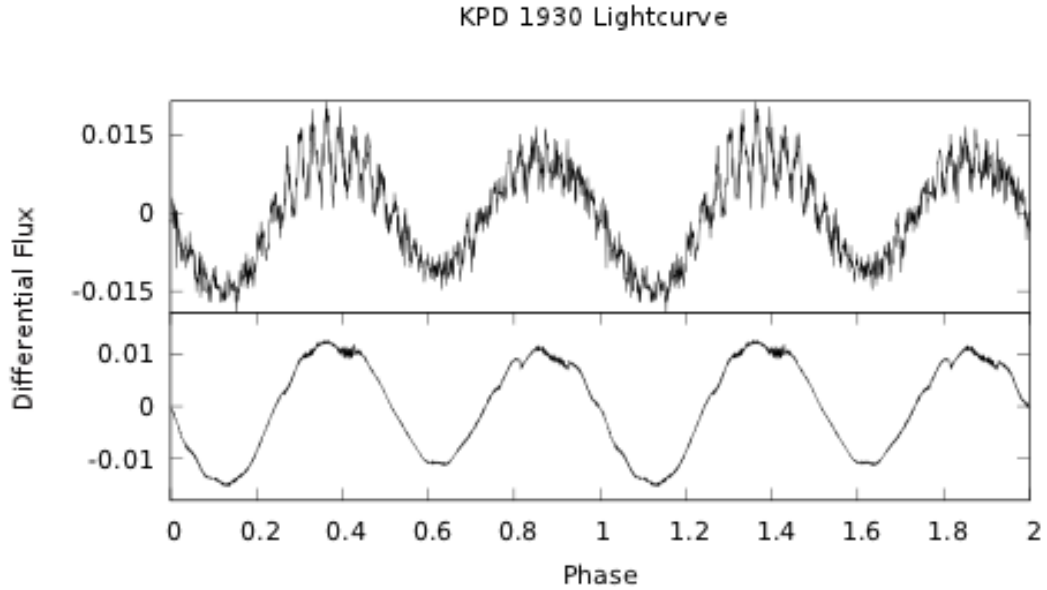
Figure 4.4   a.)The phased and binned light curve on the unfiltered data. The presence of pulsation is indicative of pulsation modes that are in resonance with the orbital period. b.) The phased and binned light curve of the filtered data. When compared with a.) the lack of pulsations is evident. Both are binned at 0.001 in phase and show two orbital cycles.

After experimenting with various low and high pass filters we decided on simply zeroing out the Fourier transform in the range of the pulsation frequencies. The inverse transform would then result in a light curve relatively free of pulsations. For the resulting light curve to retain all relevant information, the number of data points during both the transform and the inverse must be the same. Also, the transform must be taken to twice the Nyquist frequency.

We used an FFT to create the frequency spectrum. Since this method requires a constant

sampling rate, the data was interpolated using a nearest neighbor interpolation creating evenly spaced data over the entire run. Even though the actual sampling rate is around 10 seconds, we interpolated with a 5 second interval to create an oversampled transform. It is much easier to identify peaks when this is done. The filtered light curve is shown in Fig. 4.4b.

4.3.3 Hidden Information

Closer inspection of the filtered light curve reveals not only the asymmetric minima denoting ellipsoidal variation, but also a similar feature in the maxima. These differences are not noticeable in the unfiltered light curve as some of the pulsations seem to be resonant and in phase with the maxima. This type of variation is generally attributed to Doppler beaming (Loeb & Gaudi, 2003; Zucker et al., 2007). In addition, the highest maxima follows the deepest minima, consistent with this idea. To test the Doppler beaming hypothesis, we fit the light curve using 4 parameters and 3 sinusoids (Fig. 4.5).   The ellipsoidal variation was fit using

Table 4.2   Doppler Beaming Fit

Amplitude	Value
Binary	0.01217 ± 0.00005
Ellipsoidal	0.001901 ± 0.00005
Beaming	0.00065 ± 0.00005

two sinusoids: one at twice the orbital period, and a second at the orbital period to account for differences in the minima. A third sinusoid at the orbital period was fit to account for differences in the maxima (Doppler). The amplitude of each sinusoid was allowed to vary along with the overall phase of the light curve, but the offset between each of the sinusoids was fixed. This fit used a linear least square minimization and the results can be found in Table 4.2.

This change in flux at the maxima is wavelength specific, but can be related to the radial velocity v_r. Following Zucker et al. (2007) this relationship is given as

$$F_\nu = F_{\nu\text{o}} \left[1 + (3 - \alpha) \frac{v_r}{c} \right], \tag{4.1}$$

where F_ν is the observed flux, $F_{\nu o}$ is the emmited flux and α is a factor that gives the relationship between the spectrum of the star and the wavelength of the observations. For a blackbody

$$\alpha = \frac{e^\beta}{e^\beta - 1}\beta, \tag{4.2}$$

where $\beta = \frac{h\nu}{kT_{\text{eff}}}$. We use the temperature quoted in Maxted et al. (2000) of 33000 K. This leads to $v_r = 197 \pm 29$ km/s. The maximum v_r determined through spectroscopy is $\approx 341 \pm 1$ km/s. Our result is off by a factor of 2 and clearly not within error. We tried to correct for this discrepancy by varying the frequency range filtered out, but it makes little difference and the fit in each case is almost identical. The poor measure of the Doppler amplitude is probably due to the to the resonance seen in Fig. 4.4a which filtering is unable to adequately remove. Still, this is a promising result, and one of the first ground-based measurements of Doppler boosting confirming the suspicions of Maxted et al. (2000).
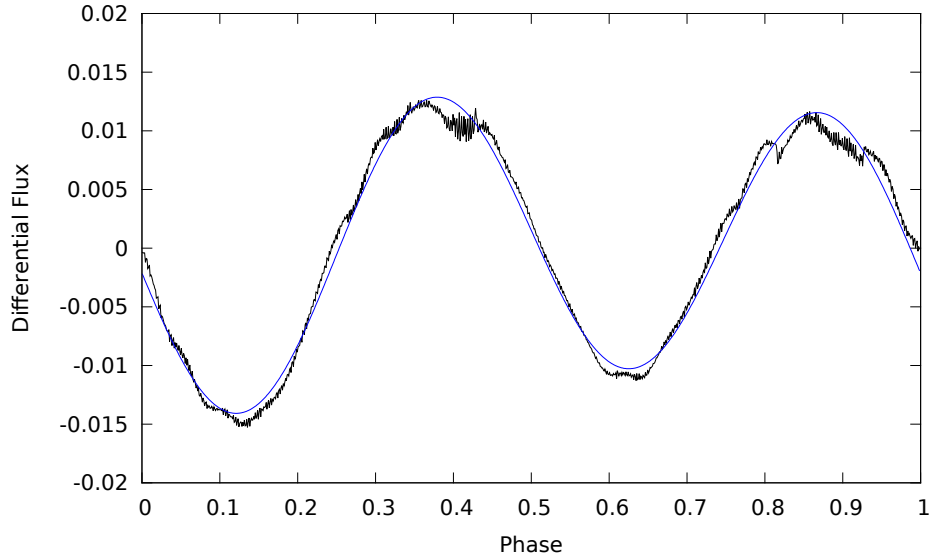
Figure 4.5   This figure shows the phased binned light curve (black) with a fit to the data (blue). The parameters and results of this fit can be seen in Table 4.2.

4.4   Space Observation

KPD1930 should not discourage one from looking at these complex systems. In fact, it is a great example of the untapped potential which lurks inside sdB binaries. However, it is also an unfortunate example of the limitations faced when studying these systems from the ground. The lack of continuity in observations, and the number of different instruments involved in maintaining gapless data from the ground are constant problems. In addition, it is simply not feasible to run campaigns for much longer than a month. These problems and others like it led to the development of the *Kepler* mission (although primarily for exoplanets). In the subsequent chapters it will become apparent just how much the area of binary pulsators has grown as a result of this mission.

CHAPTER 5. EXPLORING B4: A PULSATING sdB STAR, IN A BINARY, IN THE OPEN CLUSTER NGC 6791

Herbert Pablo, Steven D. Kawaler, & Elizabeth M. Green

This chapter is taken from a paper published in Volume 740 article id. L47 of the Astrophysical Journal 2011 of which I did the majority of the work. Fig. 5.1 has been replaced with the erratum version printed in Volume 750.

Abstract

We report on *Kepler* photometry of the hot subdwarf B (sdB) star B4 in the open cluster NGC 6791. We confirm that B4 is a reflection effect binary with an sdB component and a low-mass main-sequence companion with a circular 0.3985 day orbit. The sdB star is a *g*-mode pulsator (a V1093 Her star) with periods ranging from 2384 s to 7643 s. Several of the pulsation modes show symmetric splitting by 0.62 μHz. Attributing this to rotational splitting, we conclude that the sdB component has a rotation period of approximately 9.63 days, indicating that tidal synchronization has not been achieved in this system. Comparison with theoretical synchronization time provides a discriminant between various theoretical models.

5.1 Introduction

Subdwarf B (sdB) stars are evolved low-mass stars that have helium cores surrounded by a thin hydrogen envelope (Saffer, 1994). Their effective temperatures range from 22000 to 40000 K; typical masses are approximately $M \approx 0.47\ M_\odot$ (Heber et al., 1984, 2009). Since these stars have survived the core helium flash, they provide an opportunity to study a rapid phase

of stellar evolution (Kawaler, 2010) and perhaps a direct probe of the post-flash helium core.

Many sdB stars are non-radial multiperiodic pulsators, which can be used in asteroseismic analysis (Charpinet et al., 2008a; Østensen, 2010b, and references therein). This analysis can allow us to determine the mass, internal rotation, compositional stratification, and other interior properties. There are two main classes of sdB pulsators. The first class to be discovered were the shorter period V361 Hya stars (O'Donoghue et al., 1997), which are primarily p-mode pulsators with periods typically between 2 and 4 minutes. The V1093 Her stars are g-mode pulsators with periods ranging from 0.75 to 2 hr with typical amplitudes of less than 0.1% (Green et al., 2003; Østensen, 2010b). Generally, the pulsation amplitude is higher in the V361 Hya stars (about 1%) than in the V1093 Her stars (Kilkenny, 2007; Reed et al., 2007).

The formation of stars with such thin surface hydrogen layers (less than 0.1% of the stellar mass) is still not completely understood. There are several proposed formation channels. One channel that has significant observational support involves mass transfer to a companion and ejection of a common envelope (Han et al., 2002, 2003). Observationally, many of the known sdB stars are indeed in close binary systems, with orbital periods on the order of hours (Maxted et al., 2001; Morales-Rueda et al., 2003; Karl et. al, 2004; Heber et al., 2009).

Given the short orbital periods, these stars are generally thought to rotate synchronously as the result of tidal effects. However, two theoretical treatments of tidal synchronization provide a range of estimates for the timescale for synchronization (Tassoul, 1987; Zahn, 1975); for sdB binaries, they can differ by orders of magnitude. B4 provides a potential test of these scenarios. At these rotation velocities, it is not possible to measure rotational broadening in the H or He lines. The narrow metal lines can show broadening, but the lines are very weak, necessitating high resolution and high signal–to–noise (S/N) spectroscopy requiring large telescopes. Therefore, spectroscopic verification of tidal synchronization is difficult, though Geier et al. have addressed this issue with the sdB star PG 0101+039 (Geier et al., 2008). However, asteroseismology provides a possible way to test for synchronization by measuring rotational

splitting of oscillation modes. In the few cases where this has succeeded, tidal synchronization seems to be verified: (van Grootel, 2008) report that the sdB star Feige 48 appears to be in synchronous rotation. It is in a binary with a white dwarf companion, with an orbital and rotation period of 9 hr. Another sdB that shows evidence for rotational splitting at the orbital frequency is PG 1336-018 (Charpinet et al., 2008b), with an orbital period of 2.42 hr and a low-mass main-sequence companion.

These successes have been limited by the difficulty faced by ground-based photometry in resolving the pulsation spectra. *Kepler* provides long-term nearly continuous high-precision photometry, eliminating aliasing problems associated with ground-based data. Early results from *Kepler* observations of sdB stars (Østensen et al., 2010a; Kawaler et al., 2010; Østensen et al., 2011, for example) show that *Kepler* provides exquisite time-series photometry of these stars. For single *g*-mode pulsators, the *Kepler* data have already allowed detailed seismic modeling of two sdB stars (van Grootel et al., 2010; Charpinet et al., 2011). These investigations have determined that the mass of the sdB g-mode pulsators is close to what is expected based on standard stellar evolution models. They also place tight constraints on the hydrogen layer thickness for these stars and indicate that the convective core may be significantly larger than current evolutionary models suggest.

A particularly interesting star that could shed light on the origins of sdB stars is the hot subdwarf B4 in the old open cluster NGC 6791 (Kaluzny & Udalski, 1992). The broadband colors suggested that it was indeed hot enough to be an sdB star. Spectroscopy by Saffer (1994) confirmed it was an sdB star, and that it was likely a member of NGC 6791 based on its spectroscopic distance. B4 was identified as a binary through a significant brightness modulation (Mochejska, 2003; De Marchi et al., 2007). However, since no eclipses were seen and the data points were sparse it was not possible to tell whether this was an ellipsoidal or a reflection effect variable.

The temperature determination by Saffer (1994) placed B4 within the range of the V1093

Her stars, but it had not been observed with a high enough time resolution to detect pulsations. Photometric variations from binary effects and constraints given its membership in NGC 6791 would make it a uniquely valuable asteroseismic target: a non-radially pulsating sdB star, in a close binary, in a cluster. Its presence within a cluster provides stringent constraints on its age (and metallicity) for comparison with models of sdB formation. For example, since the lifetime of an sdB star is short ($\approx 10^8$ yr) compared to the cluster age ($\approx 8 \times 10^9$ yr), the mass of the sdB progenitor must be close to the turnoff mass of 1.1–1.2 $M_\odot$. With this potential in mind, B4 was observed as part of the *Kepler* Guest Observer (GO) program during Cycle 2.

In this Letter, we report the discovery of multiperiodic g-mode pulsation in B4. We confirm that it shows a longer period variation associated with a reflection of light from a companion with a much lower temperature. This variation signals an orbital period for the binary system of 0.3985 days. Our analysis of the pulsations reveals that the sdB star is not in synchronous rotation. We also estimate the synchronization timescale using two prescriptions for tidal spin-up and show that the results favor that of Zahn (1975) but are dependent on the details of the structure of the sdB star.

5.2   Observations

While the primary mission of the *Kepler* spacecraft is the search for extrasolar planetary transits (Koch et al., 2010; Borucki et al., 2010), it is also very well suited for asteroseismic observations (Gilliland et al., 2010a). Observations of B4 were obtained in late 2010 and early 2011 by the *Kepler* spacecraft during Cycle 2 of the GO program. In this Letter, we analyze the first 6 months of data (Q6 and Q7) on this star. The data were taken at the short cadence mode, with individual integrations of 58.85 s. The data acquisition and pipeline reductions are as described in Gilliland et al. (2010) and Jenkins et al. (2010). The data coverage is continuous except for short, monthly gaps for data retrieval and occasional brief safe mode events. The data pipeline produces both a raw and "corrected" flux value for each integration. Since the corrected value accounts for estimated background contamination (which may change with follow-up photometry in the future), we use the raw flux. For analysis of the photometric

variations, we quote fractional variation from the mean flux.

We removed outliers beyond four times the rms deviation from the local mean (determined via a boxcar filter with a width larger than any expected pulsation but smaller than the timescale for binary variation). This filtering removed 225 points from the original data. B4 has a V magnitude of 17.87 (De Marchi et al., 2007) and a *Kepler* magnitude (Kp) of 18.27. The noise level is approximately 3.4×10^2 per integration; in six months of data, this reduces to a noise level of 6.7×10^5.

5.3   Analysis

5.3.1   Binary Variation

This star is quite faint even for *Kepler*, so to establish a binary ephemeris we use phased data to get a better sense of the overall light curve shape. We found each point of maximum, rather than keying on another phase, because the light curve shows more sharply peaked maxima and the time of each maximum could be defined more precisely than the flatter minimum. We assumed that the period did not change on timescales smaller than days. This allowed us to add several days of data together with a block–phasing procedure. We achieved the best results by averaging over 10 orbital cycles. Using this procedure, we found the period to be 0.3984944(35) days and T0 to be 55372.6002(9) (in BJD − 2,400,000).

If this modulation is caused by ellipsoidal variation, then the period of 0.3985 days would represent one-half of the orbital period, since in an ellipsoidal variable, there are two minima and two maxima per orbit. Furthermore, ellipsoidal variables often display minima of unequal depth (Hutchings, 1974; Wilson & Sofia, 1976; Bochkarev et al., 1979), producing a peak in the Fourier transform at the subharmonic of the highest-amplitude periodicity.

Figure 5.1 shows the light curve phased at twice the period determined above. This light curve shows minima of equal depth and maxima of equal height. There are no eclipses apparent.
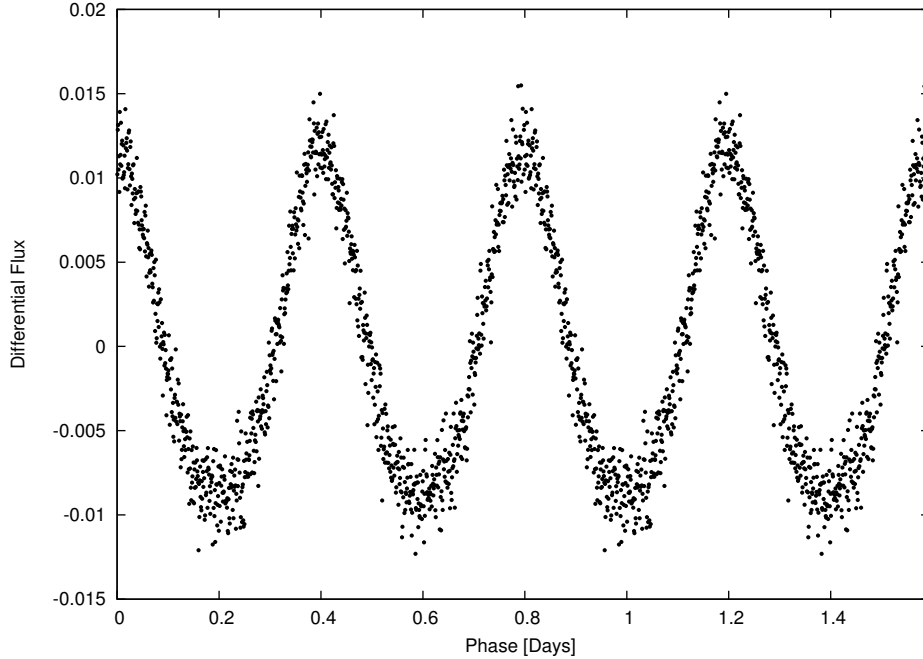
Figure 5.1 Photometric data on B4, phased on twice the suspected orbital period (2×0.3885 d). The equal–depth mimina rule an interpretation of the light curve as being caused by ellipsoidal variation.

In the Fourier transform of the light curve, the largest amplitude peak corresponds to the 0.3985 day period and the next-highest frequency peak corresponds to the first harmonic of this orbital period. We note that the frequency of the first harmonic of the orbital period (in Table 5.1) is slightly more than 1 σ away from exactly $2 \times f_{orb}$. We do not think that this difference is significant. We see no significant peak at the subharmonic.

5.3.2 Pulsation

The Fourier transform of the g-mode region, with the peaks identified, is shown in Figure 5.2. B4 shows many periodicities in the frequency range from 120 to 420 μHz, which are characteristic of g-mode pulsation in V1093 Her stars. We followed the "standard" procedure of successive removal of periodicities by nonlinear least-squares fitting of sinusoidal signals at the frequency peaks (see Kawaler et al. (2010) and references therein). Each successive pre-whitening was performed in the time domain. We continued this process until no peaks remained at or above four times the rms noise level in the residuals. This 4σ limit was 0.29

Table 5.1   Periodicites of B4. Quoted errors are formal least-squares errors.

ID	Frequency [μHz]	Period [s]	Amplitude [ppt]	Orbital splitting	fine structure
	Binary period and first harmonic				
f_{orb}	29.04430 ± 0.00022	34430.17 ± 0.26	10.310 ± 0.064		
$2f_{orb}$	58.0901 ± 0.0014	17214.63 ± 0.42	1.579 ± 0.064		
	Pulsation frequencies				
f1	130.8784 ± 0.0032	7640.68 ± 0.19	0.700 ± 0.064		
f2	216.2851 ± 0.0016	4623.527 ± 0.034	1.427 ± 0.064		
f3	216.8996 ± 0.0038	4610.428 ± 0.068	0.081 ± 0.064		= f2+0.615
f4	217.4811 ± 0.0036	4598.101 ± 0.076	0.631 ± 0.064		= f3+0.582
f5[1]	229.0105	4366.61	0.314		
f6	229.6014 ± 0.0031	4355.374 ± 0.058	0.740 ± 0.064		= f5+0.591
f7	241.5107 ± 0.0028	4140.604 ± 0.048	0.800 ± 0.064	= f3+24.60	
f8	273.4754 ± 0.0048	3656.637 ± 0.065	0.467 ± 0.064	=f7 +2×15.98	
f9	291.7086 ± 0.0024	3428.079 ± 0.028	0.948 ± 0.064		
f10	316.8387 ± 0.0034	3156.180 ± 0.034	0.664 ± 0.064		
f11	318.1220 ± 0.0062	3143.448 ± 0.062	0.363 ± 0.064		= f10+1.283
f12	342.4285 ± 0.0030	2920.318 ± 0.026	0.744 ± 0.064	= f11 + 24.27	
f13	343.7004 ± 0.0052	2909.511 ± 0.044	0.432 ± 0.064		= f12+1.272
f14	372.6323 ± 0.0037	2683.611 ± 0.027	0.613 ± 0.064		
f15	373.8966 ± 0.0027	2674.536 ± 0.020	0.828 ± 0.064	=f12+2×15.73	= f14+1.264
f16	404.7753 ± 0.0042	2470.506 ± 0.026	0.538 ± 0.064	=f15+2×15.44	
f17[1]	405.45	2466.4	0.27		=f16+0.68
f18[1]	406.04	2462.81	0.307		=f17+0.61
f19	419.3662 ± 0.0069	2384.551 ± 0.039	0.325 ± 0.064		

[1]Frequencies near the detection threshold; not included in the fit.

parts per thousand (ppt). Above this we found 16 unique frequencies which are given in Table 1. There are three more frequencies near the detection threshold which await confirmation with further data, but we include them in Table 5.1 for reasons noted below.
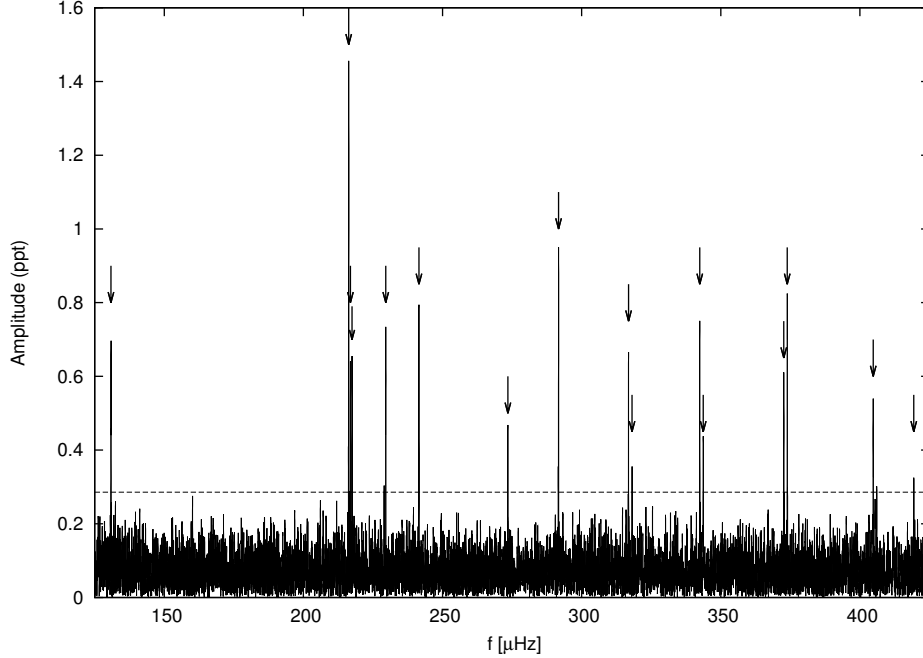
Figure 5.2   The g-mode region of B4. The arrows show all pre-whitened frequencies The 4 σ level above the noise is represented by the dotted line.

The g-mode period distribution in B4 resembles, quite closely, that seen in non-binary sdB pulsators. In high-overtone g-mode pulsators (where n l), the periods of consecutive overtones should be equally spaced, with a period spacing that scales with . Here, we use the standard labeling of non-radial modes, where n, l, and m are the radial, angular, and azimuthal quantum numbers. This behavior is seen in pulsating white dwarf stars (Winget et al., 1991, 1994) and in g-mode sdB pulsators (Reed et al., 2011a). For the sdB stars observed by *Kepler* the period spacings range from 231 s to 272 s, with that spacing identified with $l = 1$ modes (Reed et al., 2011a).

Figure 5.3 shows that B4 also follows this trend. This echelle diagram plots points associated with each periodicity; the vertical axis is the period and the horizontal axis is the period
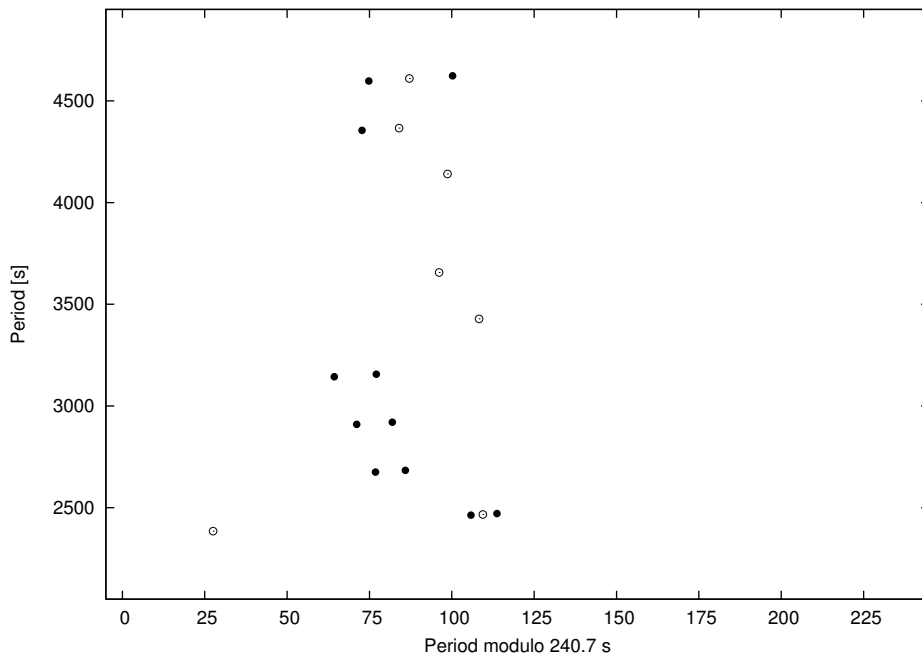
Figure 5.3   Echelle diagram of the periodicities f2-f18 of B4 with a folding period is 240.7s. Filled circles are suspected $m = \pm 1$ modes, and open circles are $m = 0$ modes (or modes for which m cannot be determined).There is a clear ridge around 85 s.

modulo the average period spacing of 240.7 s. For equally spaced modes, the periodicities should line up vertically, with (small) departures to be expected as a result of mode trapping by composition gradients within the star. The "best" period spacing of 240.7 s is in very close accord with $l = 1$ pulsations in sdB stars (Reed et al., 2011a). One periodicity, f1 ($P = 7640$ s), does not lie near the ridge (it would be at 226 s on the abscissa of Figure 5.3). Another lower amplitude mode, f19, also does not fall along the ridge.

As indicated in Figure 5.3, there are multiple periodicities for a given order in the diagram (i.e., three successive, nearly horizontal points). This multiplet structure results from rotational splitting: non-radial modes with the same values of n and l can be split into equally spaced multiplets by rotation, with the frequency splitting proportional to the rotation frequency. The well-known relationship between frequency splittings and rotation (see, for example, Ledoux 1951) is

$$f_{n,l,m} = f_{n,l,0} + m\Omega(1 - C_{n,l}) \tag{5.1}$$

where Ω is the (assumed solid-body) rotation frequency and $C_{n,l}$ is the Ledoux constant. For B4, we adopt values for $C_{n,l}$ from Kawaler et al. (2010) of 0.48 for $l = 1$ and 0.16 for $l = 2$ modes.

As can be seen in Figure 5.2 and in the table, there is one well-defined triplet in the data with an average spacing of 0.60 μHz consisting of f2, f3, and f4. Triplets are expected for rotational splitting of $l = 1$ modes. We also see many doublets with spacing of nearly twice that value (f10, f11), (f12, f13), and (f14, f15), along with two peaks separated by 0.59 μHz (f5, f6). Taken together, these multiplets, if $l = 1$, indicate a rotation frequency of 1.20 μHz, (a rotation period of 9.63 days). The structure of the amplitude spectrum surrounding each of these frequencies is shown in Figure 5.4.
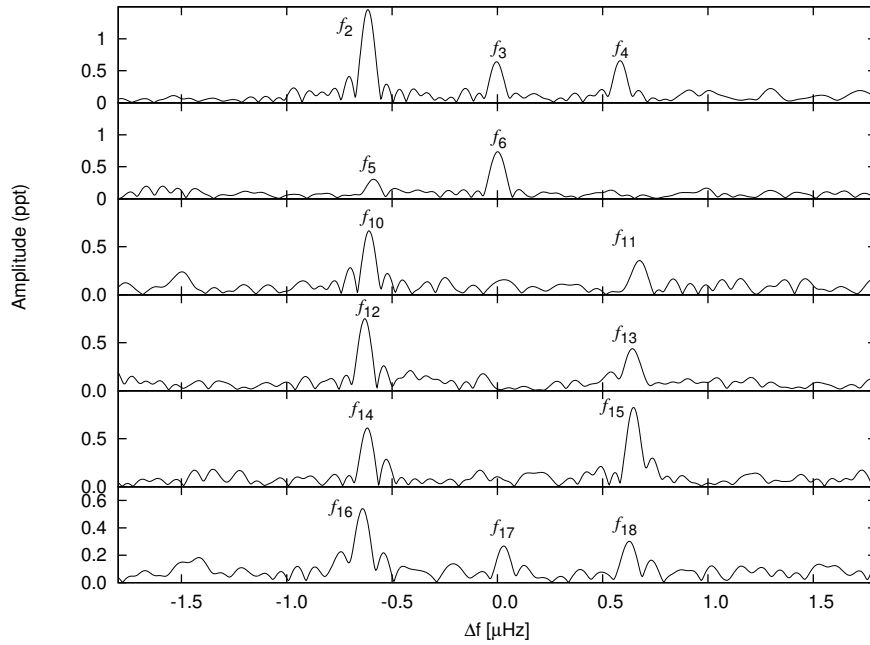
Figure 5.4   Amplitude spectrum of several g-modes in B4, centered on the suspected rotational multiplets. The frequencies of each peak can be found with corresponding labels in Table 5.1. There is one triplet (top) with an average spacing of 0.6 μHz. Several doublets show twice this splitting. Some of these doublets show signs of a peak halfway in between enhancing the likelihood that 0.6 μHz is the rotational splitting.

B4 is a close binary; if in synchronous rotation, we would expect to see splittings that are approximately 15.4 μHz for $l = 1$ modes and 24.4 μHz for $l = 2$ modes. The measured splittings are much smaller than this orbital frequency, leading to the surprising conclusion that the sdB component is most likely not in synchronous rotation. Though one might expect the system to be in complete spin-orbit resonance, with the sdB rotating at the orbital frequency, this does not seem to be the case.

The fifth column of Table 5.1 shows that some of the frequency spacings between periodicities approach the orbital frequency. This is, we believe, the result of an unfortunate coincidence: the average period spacing between g-modes of 240 s corresponds to a frequency spacing ranging from 11.3 μHz at the long-period end to 34 μHz at the short-period side. Thus, some of the apparent frequency spacings that might match those expected for synchronous rotation arise instead as a consequence of equal period spacings for high-overtone g-modes.

5.3.3 Synchronization Timescales

Recent seismic studies of sdB binary systems with short periods suggest that they are in synchronous rotation; e.g., Charpinet et al. (2008a) and van Grootel (2008) looked at systems with orbital periods of 2.42 hr and 9.02 hr, respectively. Geier et al. (2008, 2010) claim synchronous rotation in systems with orbital periods up to 14 hr. But B4, with an orbital period of 9.56 hr does not rotate synchronously.

There are two prescriptions to calculate the timescale for synchronization: Tassoul (1987, 1988) and Zahn (1975). Tassoul (1987, 1988) argue that large meridional currents driven by tidal effects can drive changes in the rotation rate in nonsynchronous systems. For stars with radiative envelopes, Claret, Gimenez & Cunha (1995) provides an estimate for the Tassoul (1988) synchronization time:

$$\tau_{syn} = 2.13 \times 10^4 \left(\frac{1+q}{q}\right) \left(\frac{L}{L_\odot}\right) \left(\frac{M}{M_\odot}\right)^{\frac{5}{4}} \left(\frac{R}{R_\odot}\right)^{-3} \times \left(\frac{P}{days}\right)^{\frac{11}{4}} \qquad (5.2)$$

where q is the mass ratio of the system (assumed to be close to 1) and P is the binary period. For parameters typical of sdB stars ($M = 0.48\ M_\odot$, $R \approx 0.2\ R_{odot}$, and $L \approx 30\ L_\odot$), $\tau_{syn} \approx 2 \times 10^5$ yr for $P = 0.4$ days, assuming a mass ratio of 1. We would thus expect B4 to be synchronous since it has an evolutionary timescale that is a factor of 500 times longer. While the Tassoul (1988) prescription is not easily extended to low-mass ratios, a mass ratio of 0.2 used in Equation 5.2 yields a synchronization time that is still short compared to the evolutionary timescale.

Zahn (1975) explores how tides couple to non-radial oscillations in the star. The oscillations propagate through the convective core and the radiative zone, and provide a torque. For stars with radiative envelopes, the resulting synchronization timescale, from Claret & Cunha (1997) can be written as

$$\tau_{syn} = 3.43 \times 10^6 \text{yr} \left(\frac{\beta}{0.13}\right)^2 \left(\frac{1+q}{q}\right)^2 \left(\frac{M}{M_\odot}\right) \left(\frac{R}{R_\odot}\right)^{-7} \times \left(\frac{P}{\text{days}}\right)^{\frac{17}{3}} \left(\frac{E_2}{10^{-8}}\right)^{-1} \quad (5.3)$$

where β is the "radius of gyration" (the moment of inertia, I scaled by MR^2) and E_2 is a tidal constant for a given stellar structure. E_2 depends sensitively on stellar structure, and in particular on the fractional size of the convective core. For large cores, E_2 can reach values of 10^5; for small convective cores, its value approaches zero (Claret, A. , 2004).

Though we do not have values for E_2 calculated directly for sdB models, Claret, A. (2004) provides E_2 for convective core burning main-sequence models with similar convective core mass fractions to the sdB stars (approximately 0.14). Though the sdB stars burn helium in the core, the presence or absence of convection is the most important factor for tidal coupling. Claret, A. (2004) main-sequence models with that size core generally have values of E_2 between 5×10^9 and 1.3×10^8, somewhat independent of mass. We choose 10^8 as a representative value. Using the same representative values for mass, radius, and orbital period, Equation 5.3 provides $t_{syn} \approx 10^9$ yr for $q = 1$. For a lower-mass companion (lower q), the timescale is even longer. We note that for Equation 5.3 to reduce to 10^8 yr for B4, E_2 would need to be 10^7. For sdB stars with a comparable orbital period but more massive companion (i.e., Feige 48), synchronization should be swifter than for B4.

This leads us to the conclusion that the Zahn (1975) mechanism may be slow enough to allow the B4 binary to be out of spin-orbit synchronization. However, conclusive analysis requires direct calculation of E_2 for evolutionary stellar models at the correct T_{eff} and $\log g$.

5.4   Discussion

The hot blue sdB star, B4, in the old open cluster NGC 6791 is a pulsating member of a short-period reflection-effect binary with an orbital period of 0.3984944(35) days. Frequency splittings in the g-mode pulsation spectrum reveal that the sdB component rotates with a period of 9.63 days, and therefore is not in synchronous rotation. The nearly equal period spacings resemble the pattern seen in many other g-mode sdB pulsators being observed with *Kepler*. Thus, the *Kepler* sdB pulsators form a homogenous class, independent of their binarity.

B4's membership in NGC 6791 provides its (overall) age and metallicity; its initial main-sequence mass is close to the turnoff mass of 1.15 $M_\odot$. Further asteroseismic probing subject to these initial constraints should provide a new opportunity to address the riddle of the formation of sdB stars in general. Given that B4 is not in synchronous rotation, it will be important to compute the synchronization timescale for sdB stars in close binaries to evaluate the accuracy of current theoretical models of tidal synchronization. A spectroscopic determination of T_{eff} and $\log g$ (as well as the mass ratio of the system) is essential for this.

We plan continued photometric monitoring of B4 with *Kepler* for as long as possible. In addition to refining the observed frequencies, increasing S/N could reveal lower-amplitude modes, allowing us to fill out the $l = 1$ pulsation spectrum and expose modes with higher values of l. In addition, extended photometry may allow us to measure the evolution of the sdB component through secular period changes as the star continues its nuclear evolution. If it is a newly formed sdB star that is experiencing tidal spin-up, we may also be able to measure the increasing rotational frequency through the pulsations.

CHAPTER 6.   TWO CLOSE sdb+dM BINARIES: SEISMIC EVIDENCE for NON-SYNCHRONIZATION IN TWO CLOSE sdB+dM BINARIES FROM *KEPLER* PHOTOMETRY

Herbert Pablo, Steven D. Kawaler, M. D. Reed, S. Bloemen,S. Charpinet, H. Hu, J. Telting,R. H. Østensen, A. S. Baran, E. M. Green, J. J. Hermes, T. Barclay, S. J. O'Toole, Fergal Mullally, D. W. Kurtz, J. Christensen-Dalsgaard, Douglas A. Caldwell, Jessie L. Christiansen, K. Kinemuchi

Abstract

We report on extended photometry of two pulsating sdB stars in close binaries. For both cases, we use rotational splitting of the pulsation frequencies to show that the sdB component rotates much too slowly to be in synchronous rotation. We use a theory of tidal interaction in binary stars to place limits on the mass ratios that are independent of estimates based on the radial velocity curves. The companions have masses below 0.26 $M_\odot$. The pulsation spectra show the signature of high–overtone g-mode pulsation. One star, KIC 11179657, has a clear sequence of g-modes with equal period spacings as well as several periodicities that depart from that trend. KIC 02991403 shows a similar sequence, but has many more modes that do not fit the simple pattern.

6.1 Introduction

Close binary systems are typically those in which the semi-major axis of the orbit is of comparable size to the radii of the stars themselves. In such systems, circularization of the orbit and synchronization of the components through tidal interactions is often assumed. The precise mechanisms of tidal coupling, and the resulting time-scales, have been under debate for a number of years. Observational tests have been difficult to implement. While orbital period determination is usually straightforward (through radial velocity curves and/or photometry), measuring the rotation of the component stars is challenging. Determinations of rotation periods using starspots becomes difficult in binary systems and impossible when those systems are evolved. It is possible to measure rotational broadening of spectral lines, but that requires metal lines which are inherently weak and need high S/N; in binaries with compact components other broadening mechanisms swamp the rotational broadening signal for rotation rates of interest. When there are pulsations in one of the stars, asteroseismology can provide an alternative method for measuring rotation. The spinning of the star breaks degeneracy in the pulsation modes of non-radial pulsators causing single peaks to split into multiplets. This splitting can, through a simple relation, yield the rotation rate of the star (Ledoux, 1951).

One class of nonradially pulsating stars that can be ideal for this type of analysis is the pulsating subdwarf B (sdB) stars. These stars, remnants of low mass stars that have undergone helium core ignition, lie along the extreme horizontal branch with temperatures 22000-40000 K and masses of $\approx 0.47 M_\odot$ (Saffer, 1994; Heber et al., 1984). Their surface gravities ($\log g$ ranging from approximately 5.0 to 6.0) are typically higher than main sequence stars with corresponding temperatures. The formation process for a star with these characteristics is difficult to identify; one proposed formation channel is through common envelope ejection (Han et al., 2002, 2003). This implies that a significant number of these objects are members of binary systems.

In addition, a selection of these stars pulsate nonradially. These pulsations fall into two distinct classes. The p-mode pulsators, also called V361 Hya stars, have periods that are generally in the 2-4 min range, with pulsation amplitudes ≈ 1 per cent of their mean brightness (Kilkenny, 2007; Reed et al., 2007). The g-mode pulsators, also known as V1093 Her stars,

have pulsation periods between 45 min and 4 h and typical amplitudes less than 0.1 per cent of their mean brightness (Green et al., 2003; Østensen, 2010b; Reed et al., 2011a).

Given their small pulsation amplitudes and multiperiodic nature, resolving the oscillation spectra of these g-mode pulsators is extremely challenging using ground–based facilities. In particular, the periods of the g-mode pulsators result in only a few cycles for a single night's observing. To use the pulsations to measure rotational effects requires identification of the azimuthal order of the modes, meaning that small frequency spacings between individual periodicities in the Fourier transform need to be measured unambiguously. Even with multi-site campaigns it is challenging to obtain a sufficient baseline for detailed study.

Recently, data on sdB pulsators provided by the *Kepler* mission have spurred rapid progress in our understanding of these stars. The broader science goals, mission design, and overall performance of *Kepler* are reviewed by Borucki et al. (2010) and Koch et al. (2010); Gilliland et al. (2010a) review the asteroseismology component. The *Kepler* Asteroseismic Science Consortium (KASC) working group on compact pulsators has made significant strides toward our understanding of the non-radial g-mode pulsators as a group (Reed et al., 2010, 2011a; Gilliland et al., 2010a; Kawaler et al., 2010), and have provided detailed seismic fits to two $g-$mode pulsators (Charpinet et al., 2011; van Grootel et al., 2010). Many of these multiperiodic pulsators show distinct sequences of modes that are equally spaced in period, as is expected for high–overtone $g-$modes (Reed et al., 2011a).

Two of the KASC targets are g-mode pulsators in close reflection–effect binary systems with periods of approximately 0.4 d: KIC 02991403 and KIC 11179657. 30 d of *Kepler* data from the survey phase hinted that neither system was in synchronous rotation, though the data durations were too short to fully resolve the pulsations (Kawaler et al., 2010). In a separate examination of an sdB star in the old open cluster NGC 6791, (KIC 02438324, identified as "B4" by Kaluzny & Udalski 1992), Pablo et al. (2011) used 6 months of *Kepler* data to show that it too is in a close reflection–effect binary. B4 rotates with a period that is significantly longer than the orbital period of the system. The similarity between these three systems suggests that the binary properties are closely related to their origin.

In this paper we report on results from longer duration observations of KIC 02991403 and

KIC 11179657 with *Kepler*. We identify several rotational triplets, demonstrating that the stars are not in synchronous rotation. These results are consistent with the results of B4 shown in (Pablo et al., 2011), and suggests that sdB stars in $\approx$ 0.5-d binary systems with low-mass M dwarf companions do not appear to be in synchronous rotation. KIC 11179657 shows a clear sequence of equally spaced periods as seen in many other g-mode sdB pulsators, including B4 (Pablo et al., 2011). KIC 02991403 also shows a sequence of modes that share a constant spacing in period, but shows many more modes that do not follow this pattern.

6.2   Observations

All observations were obtained by the *Kepler* spacecraft between 2010 March and 2011 March. *Kepler* data are made available in 3–month spans and identified by quarter number. The observations we are analysing are from quarters Q5-Q8. The data were obtained in short cadence (SC) mode (Gilliland et al., 2010) which has a cadence of 58.85 s. Data were processed through the standard pipeline (Jenkins et al., 2010). All data products received through KASC have undergone Pre-search Data Conditioning. However, since this conditioning is optimized for exoplanet science, we used the simple aperture photometry flux. These fluxes are converted to fractional variations from the mean (i.e. differential intensity $\delta I/I$). The data show (mostly) subtle baseline changes from month to month, and so we treated each month of data individually, resulting in a light curve that is continuous across each quarter. We further edited the data by removing outliers; we clipped individual data points that departed from the (local) mean by 4σ. This resulted in a reduction of 1847 points (out of 486336) in KIC 02991403 and 947 points (out of 392532) in KIC 11179657.

Under normal operating circumstances, data received from *Kepler* is continuous with the exception of small gaps, the largest of which is due to the quarterly roll of the spacecraft. For this reason *Kepler* has a duty cycle of over 90 per cent. There are a small number of instrumental artefacts in the data commensurate with the long cadence (LC) readout rate $(1/30 \times \text{SC})$ producing peaks at multiples of 566.44 μHz, with the highest amplitude peaks generally lying in the 4000-7000 μHz region (Gilliland et al., 2010). These artefacts are at a significantly higher frequency than the physical periodicities in these stars, and so do not

impact our analysis.

We obtained 12 months of data (Q5-Q8) on KIC 02991403, resulting in a (formal) frequency resolution ($1/T$) of 0.032 μHz. The actual frequency precision achieved through least-squares fitting of sinusoids to the data (Montgomery & O'Donoghue, 1999) is significantly higher, but the higher precision is only realized if the individual periodicities are isolated from any other signal. Kawaler et al. (2010) identified 16 independent oscillation frequencies using 1 month of data from Q1. This star is a reflection effect binary with an orbital period of 10.633762 ± 0.000015 h. No significant signal is seen at the subharmonic of this periodicity, and the first harmonic is present at the 13% level. The phase of this harmonic peak is such that the maxima of the harmonic are at the extrema of the main peak, as is expected for a reflection-effect binary. Preliminary radial velocity measurements on the sdB star have an of amplitude 36 ± 2 km s^{-1} (Telting et al., 2011). This velocity implies that the (unseen, except for the reflection effect) companion is lower in mass than the primary ($M < 0.47 M_\odot$) if the inclination angle of the system is greater than 15°. The absence of an eclipse places an upper limit on the inclination of approximately 80°, and places a lower limit on the companion mass of ≈ 0.089 $M_\odot$. The sdB star has $T_{\rm eff} = 27300 \pm 200$ K and $\log g = 5.43 \pm 0.03$ (Østensen et al., 2010b).

For the second target, KIC 11179657, we obtained 9 months of data (Q5-Q7); in Q8, KIC 11179657 fell on the beleaguered Module 3 in the *Kepler* focal plane which is no longer functional. The resulting formal frequency resolution is 0.042 μHz, though as noted above, isolated frequencies can be determined to much higher precision. This star is also a reflection effect binary with an orbital period of 9.466936 ± 0.000024 h. It shows 8 oscillation frequencies in the 30-d survey data from Q2. The binarity in this reflection–effect system has also been confirmed via a measured velocity amplitude for the sdB star of 21 ± 2 km s^{-1} (Telting et al., 2011). Assuming a non-zero inclination angle the companion in this system is again of low mass, with a minimum mass ≈ 0.047 $M_\odot$ if seen nearly edge–on; the companion exceeds the mass of the sdB if the inclination is less than approximately 8.5°. The sdB star is slightly cooler and lower–gravity than its counterpart, with $T_{\rm eff} = 26000 \pm 800$ K, and $\log g = 5.14 \pm 0.13$ (Østensen et al., 2010b).

6.3   Analysis

We determined the frequencies of pulsation (and the orbital modulation period from the reflection effect) through Fourier analysis combined with non-linear least-squares fitting and prewhitening, as described in Kawaler et al. (2010); Reed et al. (2010); and Kawaler et al. (2010). This process identifies peaks in the Fourier transform and fits the amplitude, frequency and phase using a non-linear least-squares procedure. A sine curve with the fit parameters is then subtracted from the light curve to remove the periodicity. This process is then iterated until all significant peaks have been identified, fitted, and removed. A peak is defined as significant if it is more than 4σ above the mean noise level. This was calculated by finding the mean value of the Fourier transform, outside of obvious peaks, in the g-mode region of each star.

Normal modes of oscillation in stars are characterized by the set of indices n, l and m. The radial order n provides a measure of the number of nodes in the radial direction for the given oscillation mode. The angular indices l and m correspond to the spherical harmonic $Y_l^m(\theta, \phi)$. For nonradial oscillations, in the absence of processes that break azimuthal symmetry, the oscillation frequencies depend only on n and l; modes with different m values are degenerate in frequency. If the star is rotating (or has a sufficiently strong magnetic field), this can lift the m degeneracy, revealing an equally spaced multiplet of $2l + 1$ peaks if all m components are present and if the rotation is sufficiently slow (or the magnetic field sufficiently weak). For solid-body rotation with a period of P_{rot}, the frequency spacing is proportional to the rotation rate:

$$f_{n,l,m} = f_{n,l,0} + \frac{m}{P_{\mathrm{rot}}}(1 - C_{n,l}) \tag{6.1}$$

(Ledoux, 1951) where $C_{n,l}$ is the Ledoux constant. $C_{n,l}$ is determined by the oscillation eigenfunctions. For models appropriate to KIC 02991403 and KIC 11179657 the range of $C_{n,l}$ is discussed in Kawaler et al. (2010), with $C_{n,1}$ between 0.465 and 0.496 while $C_{n,2}$ is between 0.158 and 0.165. For these two targets, if the sdB components are in synchronous rotation, the rotational splitting should be approximately 13-15 μHz for $l = 1$ modes.

6.3.1 KIC 02991403

With a full year of data, the number of detected oscillation modes has increased significantly compared to what was found by Østensen et al. (2010b). All 16 modes previously identified are still present, and 18 additional periodicities lie above our significance threshold of 0.141 ppt (parts per thousand). The amplitude spectrum of the data is shown in Fig. 6.1, and the significant periodicities are listed in Table 6.1. In this table, frequencies identified in Kawaler et al. (2010) are f1 through f16; the new periodicities, ordered by increasing frequency, are f18 through f34. The phase is given as an offset from T_0 of the first time of maximum (for that periodicity).
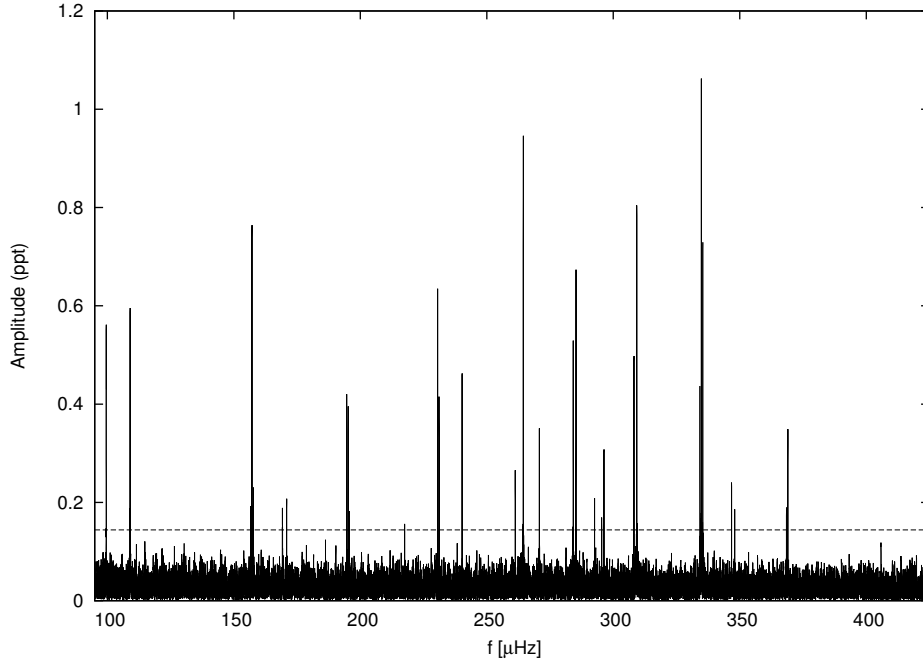
Figure 6.1   The g-mode region of KIC 02991403. The 4-σ significance threshold is represented by the dotted line.

As noted in Kawaler et al. (2010), there is little evidence for frequency spacings between modes that match the expectations from synchronous rotation. The few splittings that are near the orbital frequency can be explained by the common period spacing in $l = 1$ g-modes (see below). In the range of frequencies typical for g-modes, the period spacing coincides with the system's orbital frequency.

Table 6.1   Periodicities of KIC 02991403. Quoted errors are formal least-squares errors. Periodicities marked with an asterisk are slightly below the 4-σ cutoff but included in the fit.

ID	Frequency [μHz]	Period [s]	Amplitude [ppt]	$T^1_{\max}$[s]	Orbital splitting	fine structure
	Binary period and first harmonic					
1f$_{\text{orb}}$	26.122249(36)	38281.542(51)	17.657(35)	15971.0(24)		
2f$_{\text{orb}}$	52.24451(28)	19140.8(10)	2.279(35)	16062.0(93)		
f17	99.5625(11)	10043.94(0.11)	0.562(35)	7122.0(200)		
f18	108.994(11)	9174.816(88)	0.601(35)	3352.0(170)		
f19*	114.8141(48)	8709.73(0.37)	0.131(35)	5486.0(740)		
f20	156.6102(41)	6385.28(0.17)	0.153(35)	1678.0(460)		
f1	157.17197(82)	6362.458(34)	0.763(35)	2306.0(92)		=f20+0.562
f21	157.6653(35)	6342.55(0.14)	0.195(36)	1549.0(380)		
f22	157.7319(25)	6339.87(0.11)	0.255(36)	5551.0(290)		=f1+0.560
f23	169.2203(32)	5909.46(0.11)	0.200(35)	5618.0(330)		
f24	170.8781(29)	5852.124(99)	0.219(35)	3699.0(300)	=f22+13.146	
f25*	186.2481(48)	5369.18(0.14)	0.128(35)	4935.0(460)		
f2	194.6251(15)	5138.083(39)	0.434(35)	2350.0(130)		
f3	195.1789(15)	5123.50(4)	0.417(35)	5055.0(140)		=f2+0.554
f26	195.7147(37)	5109.477(97)	0.171(35)	1161.0(330)	=f24+24.837	=f3+0.536
f27	217.5162(41)	4597.358(87)	0.154(35)	3131.0(330)		
f4	230.554(10)	4337.386(19)	0.626(35)	1671.0(77)	=f27+13.038	
f5	231.1063(15)	4327.014(29)	0.409(35)	2463.0(120)		=f4+0.552
f28	240.2369(14)	4162.558(23)	0.466(35)	2530.0(99)		
f29	261.2529(23)	3827.709(34)	0.273(35)	479.0(150)		
f6	264.43948(66)	3781.5836(95)	0.956(35)	376.0(44)		
f7	270.7766(18)	3693.081(25)	0.345(35)	868.0(120)	=	
f8	284.1718(12)	3518.998(14)	0.541(35)	481.0(72)		
f9	285.2697(93)	3505.455(1)	0.684(35)	1768.0(57)		=f8+1.098
f30	292.5943(29)	3417.702(34)	0.218(35)	3399.0(170)		
f31	295.409(36)	3385.137(42)	0.174(35)	2719.0(210)		
f10	296.316(2)	3374.78(23)	0.311(35)	3061.0(120)		
f11	308.1784(12)	3244.874(14)	0.484(35)	1164.0(74)		
f12	309.27964(79)	3233.3199(83)	0.800(35)	1470.0(45)		=f11+1.101
f13	334.2474(16)	2991.796(14)	0.402(35)	2987.0(82)		
f14	334.81955(59)	2986.6835(51)	1.078(35)	728.0(31)		=f13+0.572
f15	335.37212(87)	2981.7625(77)	0.729(35)	1943.0(45)		=f14+0.553
f32	346.7506(25)	2883.917(21)	0.241(35)	71.0(130)		
f33	347.995(33)	2873.605(26)	0.194(35)	227.0(160)	=f14+13.145	=f32+1.244
f34	368.4757(36)	2713.883(25)	0.178(35)	1188.0(170)		
f16	369.0067(18)	2709.978(12)	0.350(35)	1881.0(86)		

[1] T_0 is BJD 2455276.4793502

With the improved frequency resolution and sensitivity available with 1 year of data, several equally-spaced triplets are now seen in the data, with spacing that is substantially smaller than the orbital frequency. One true triplet ($f13$, $f14$, $f15$) was identified by Kawaler et al. (2010), but its spacing was near the run resolution. We now see several doublets and triplets with very similar spacings of $\approx 0.56\ \mu$Hz; these are shown in Fig. 6.2. Of the 34 periodicities in Table 6.1, 16 are components of multiplets that show this spacing. The rotational period calculated using this frequency splitting assuming $l = 1$ is ≈ 11 d. This is an order of magnitude longer than the orbital period, confirming that this system is not in synchronous rotation. This ratio is very similar to that seen in B4 (Pablo et al., 2011). The possibility exists that the modes that are part of these multiplets with a 0.56 μHz spacing are $l = 2$ rather than $l = 1$, even though no quintuplets are present. If that were the case, the rotation period would be longer. A rotation period of 11 d corresponds to a rotation velocity of approximately 1 km s^{-1}. This rotation is slower than what is generally seen in more ordinary (cooler) Horizontal Branch stars both in clusters and in the field (Behr, 2003a,b). It is also consistent with spectroscopic measurements of many individual sdB pulsators (Heber et al., 2009). Since this is significantly longer than the orbital period, it is clear that not much spin up has occurred in these systems.

In many $g-$mode sdB pulsators, the periods of the modes display period spacings that are integer multiples of a common period spacing (Reed et al., 2011a), as expected from asymptotic theory for models without internal compositional discontinuities. To examine the possibility that KIC 02991403 shows this signature, we attempted to find a common period spacing. For $l = 1$ modes in sdB stars, this spacing has been observationally determined to be remarkably uniform; most stars show a spacing near 250 s, which is consistent with the asymptotic $l = 1$ spacing from theoretical models (Reed et al., 2011a). Kawaler et al. (2010) explored this question with one month of data and concluded that there might be a mix of $l = 1$ and $l = 2$ modes in KIC 02991403. With these new data, most of the periods corresponding to the centres of the triplets in Fig. 6.2 seem consistent with a spacing of 269.6 s. Folding all identified periodicities at that spacing leads to the échelle diagram shown in Fig. 6.3. A likely $l = 1$ sequence seems to be present near 60 s in this figure; however, many peaks are not associated with this group. Theoretical models of high–overtone $g-$modes (**?**, see, for example)]char11,
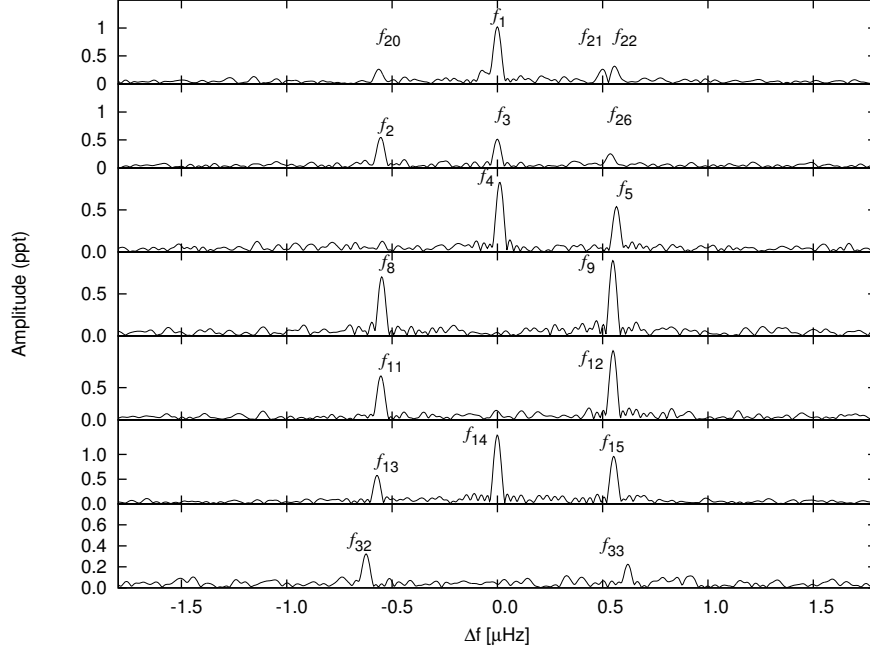
Figure 6.2   Amplitude spectra of several multiplets in the *g*-mode region of KIC 02991403.
The frequencies of each peak can be found with corresponding labels in Table 6.1.
There are three triplets with an average spacing of 0.56 μHz. Several doublets
show twice this splitting. There is some ambiguity in placement of f4 and f5 in the
third panel from the top; they could be shifted to lower frequencies by 0.56 μHz
since we cannot uniquely assign m values.

vg11 show periods that approximate this behavior, though large departures (up to 100 s)
are common. These departures from uniform period spacing are the consequence of internal
composition transition zones, which lead to mode trapping and departure from the asymptotic
relationship. In KIC 02991403, the spread of points in the échelle diagram (Fig. 6.3) may
be because some of the periodicities are $l = 2$ modes, or that the internal structure of this
star contains features that cause mode trapping. Thus the problem remains as far as clearly
identifying l for many of the modes of KIC 02991403.

6.3.2   KIC 11179657

Nine months of data *Kepler* photometry on KIC 11179657 brings the 4-σ noise threshold
down to an amplitude of 0.146 ppt. At this level, combined with the frequency resolution
gain, we can identify 18 periodicities in the light curve in addition to the 8 periodicities found
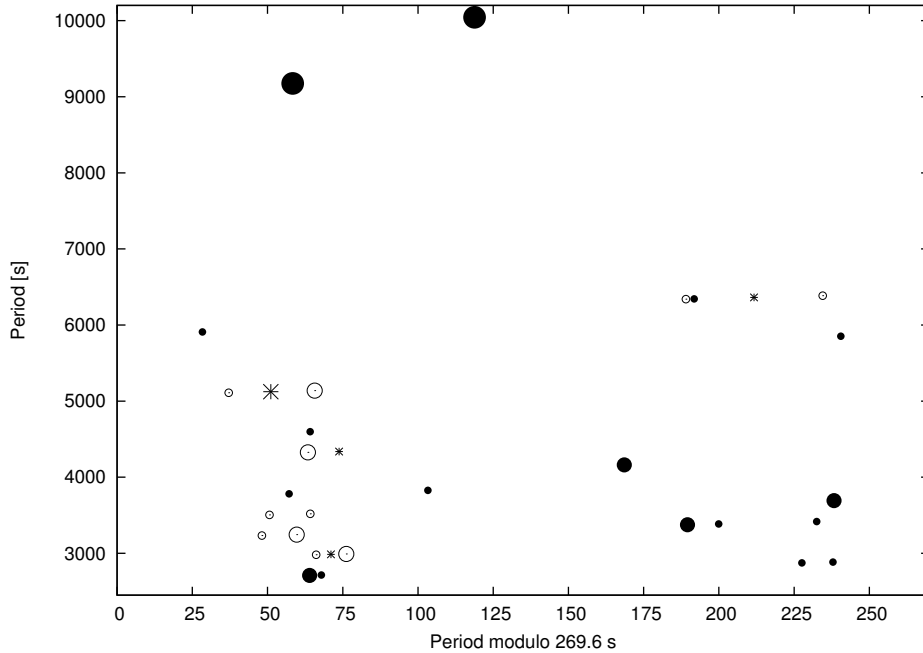
Figure 6.3   This échelle diagram contains symbols for all periodicities identified in KIC 02991403. The points are plotted modulo a fixed period spacing; those that have periods that are integer multiples of this period spacing will be aligned vertically. Stars denote $m = 0$ modes (those at the centre of triplets), and open circles are suspected $m = \pm 1$ modes. Filled circles are isolated periods. Larger symbols indicate higher amplitude peaks. A vertical column centered near 50-75 s contains most of the identified triplets. There are also several points that lie far away from this grouping, and may be indicative of higher l modes, or modes that are strongly affected by internal composition gradients. There is an artificial offset of 50 seconds imposed in the figure so the points do not fold across 0 s.

by Østensen et al. (2010b); two that were close to the detection threshold in Kawaler et al. (2010) are confirmed. Fig. 6.4 shows the amplitude spectrum of the new data over the range of frequencies where significant periodicities are found. Table 6.2 presents the frequency list; we use the same naming convention as used for KIC 02991403.

Kawaler et al. (2010) failed to identify any equally-spaced triplets using the one-month survey data. With the extended data from Q5-Q7, we find that all but one of the previously detected frequencies ($f5$) is a member of a triplet or pairs with another frequency at twice the triplet splitting. These common frequency spacings are much smaller than the orbital frequency. The most common spacing is approximately 0.78 μHz; 12 periodicities are parts of multiplets

Table 6.2 Periodicites of KIC 11179657. Quoted errors are formal least-squares errors. Periodicities marked with an asterisk are slightly below the 4-σ cutoff but included in the fit.

ID	Frequency [μHz]	Period [s]	Amplitude [ppt]	$T^1_{\max}$[s]	Orbital splitting	fine structure
	Binary period and first harmonic					
1f$_{\mathrm{orb}}$	29.341887(74)	34080.971(87)	9.36(3)	19462.0(35.0)		
2f$_{\mathrm{orb}}$	58.6836(11)	17040.53(0.31)	0.66(3)	2582.0(250.0)		
f9	119.6149(19)	8360.16(0.13)	0.36(0.03)	1152.0(220)		
f10	122.5558(24)	8159.55(0.16)	0.29(0.03)	838.0(270)		
f11	146.2958(24)	6835.47(0.11)	0.29(0.03)	560.0(220)		
f12	185.7243(35)	5384.3(0.10)	0.20(0.03)	5382.0(260)		
f1	186.4778(39)	5362.569(1)	1.77(0.03)	5157.0(29)		=f12+0.753
f13	194.925(2)	5130.169(51)	0.35(0.03)	5002.0(140)		
f2	195.72284(43)	5109.266(1)	1.63(0.03)	3465.0(30)		=f13+0.798
f14	206.5921(33)	4840.455(78)	0.21(0.03)	139.0(220)		
f15	218.2891(41)	4581.081(87)	0.17(0.03)	2368.0(260)		
f16	231.8228(23)	4313.64(0.43)	0.30(0.03)	1005.0(140)		
f17	260.39(3)	3840.391(45)	0.23(0.03)	2825.0(160)		
f18	261.6353(32)	3822.114(47)	0.22(0.03)	185.0(170)	=f16+29.8125	=f17+1.245
f19	262.873(4)	3804.117(58)	0.17(0.03)	2051.0(210)		=f18+1.238
f20	265.5517(33)	3765.746(46)	0.21(0.03)	861.0(170)		f19+2.679
f21	269.278(3)	3713.634(42)	0.23(0.03)	2098.0(160)		
f22	283.83(17)	3523.235(21)	0.42(0.03)	2681.0(81)		
f3	284.62843(78)	3513.3525(96)	0.90(0.03)	3283.0(37)		=f22+0.798
f4	285.4093(16)	3503.74(0.02)	0.44(0.03)	591.0(77)		=f3+0.781
f5	295.5828(25)	3383.15(0.03)	0.27(0.03)	890.0(120)		
f23	307.8559(25)	3248.273(28)	0.27(0.03)	1018.0(120)		
f6	308.6558(14)	3239.855(14)	0.52(0.03)	1356.0(60)		=f23+0.800
f24*	309.4427(48)	3231.62(0.05)	0.14(0.03)	71.0(210)		=f6+0.787
f7	337.17368(46)	2965.8306(41)	1.48(0.03)	1963.0(19)	=f23+29.3178	
f25	337.9506(38)	2959.013(33)	0.19(0.03)	470.0(150)	=f6+29.2948	=f7+0.777
f8	338.2984(12)	2955.97(0.10)	0.60(0.03)	698.0(47)	=f6+29.6426	=f7+1.125
f26	369.0297(19)	2709.809(14)	0.36(0.03)	2115.0(73)		

[1] T_0 is BJD 2455276.4801154
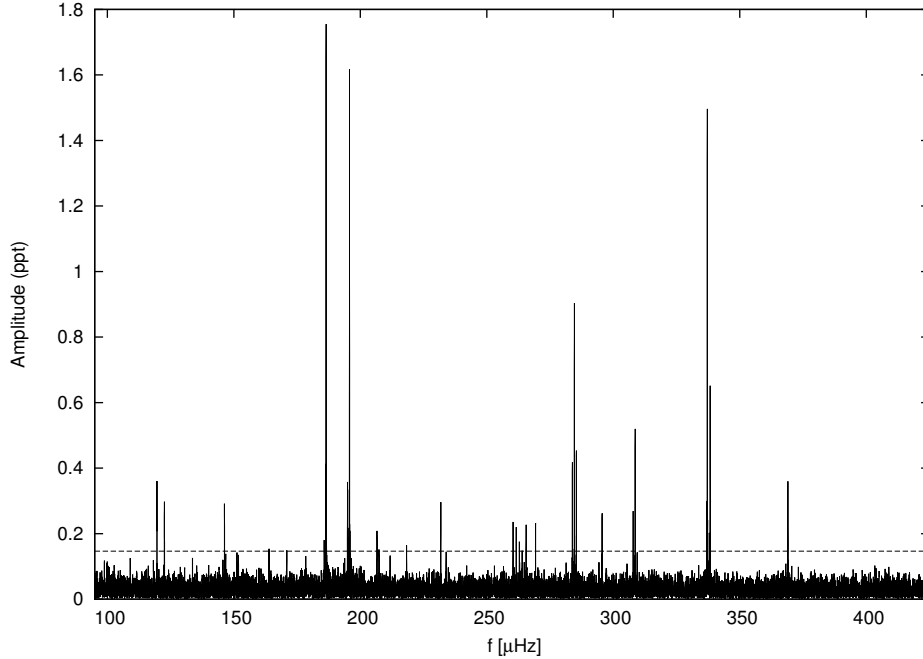
Figure 6.4   The $g-$mode region of KIC 11179657. The 4-σ level above the noise is represented by the dotted line.

with this splitting. The uniformity of this splitting is shown in Fig. 6.5 where we expand the Fourier transform around each multiplet. In two instances, the central peak has the largest amplitude, and we align the incomplete multiplets assuming the large amplitude component is the central one. The labelled peaks are all above or near our significance threshold as indicated by the number corresponding to the entry in Table 6.2. These modes are split by the same spacing of 0.78 μHz.

Four other periodicities (f17, f18, f19, and f20) show a spacing of ≈ 1.29 μHz. The ratio between the 0.78 μHz and 1.29μHz splitting is 1.65, consistent with that expected for $l = 1$ modes (0.78 μHz) and $l = 2$ modes (1.29 μHz). Thus the four frequencies appear to be part of an $l = 2$ quintuplet which is missing one peak. The calculation of the rotational period from these spacings is consistent with ≈ 7.4 d which, as in KIC 02991403 and B4, is much longer than the orbital period. We note that the frequency spacing between f7 and f8 is close to, but significantly smaller than, the $l = 2$ spacing.

Unlike KIC 02991403, most of the periodicities of KIC 11179657 have a consistent period
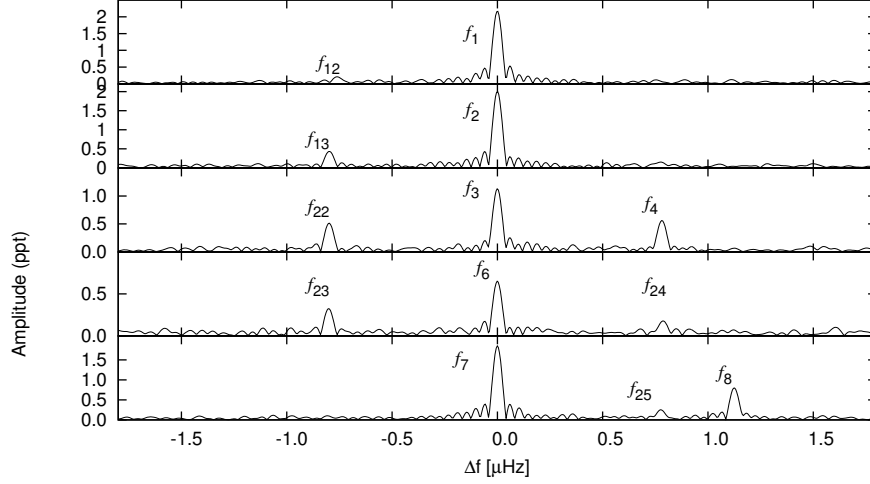
Figure 6.5   Rotationally split multiplets in KIC 11179657 associated with the suspected $l = 1$ spacing ≈ 0.784 μHz. The frequencies of each peak can be found with corresponding labels in Table 6.2. There are two triplets (middle and second to bottom) with an average spacing of 0.793 μHz, though we note that f24 is slightly below our formal detection threshold. There are several doublets which show this splitting. In the bottom panel centered on f7, f25 is spaced at the $l = 1$ rotational splitting distance. The f8 peak is separated by 1.12μHz from f7, which is smaller than the expected $l = 2$ splitting.

spacing. The period spacing found in this star is 265.3 s and appears to be fairly uniform. In Fig. 6.6 we see a well defined column of periodicities that are all consistent with being $l = 1$ modes. A few of the periodicities are offset from the ridge by about 140 seconds, which may indicate modes that are affected by mode trapping by internal composition transition zones (see above). Note that in Fig. 6.6 the suspected $l = 2$ multiplet is also offset from the $l = 1$ ridge.

6.4   Synchronization

Synchronization has not been reached in either KIC 02991403 or KIC 11179657, meaning that the synchronization time-scale must be significantly longer than the time that these sys-
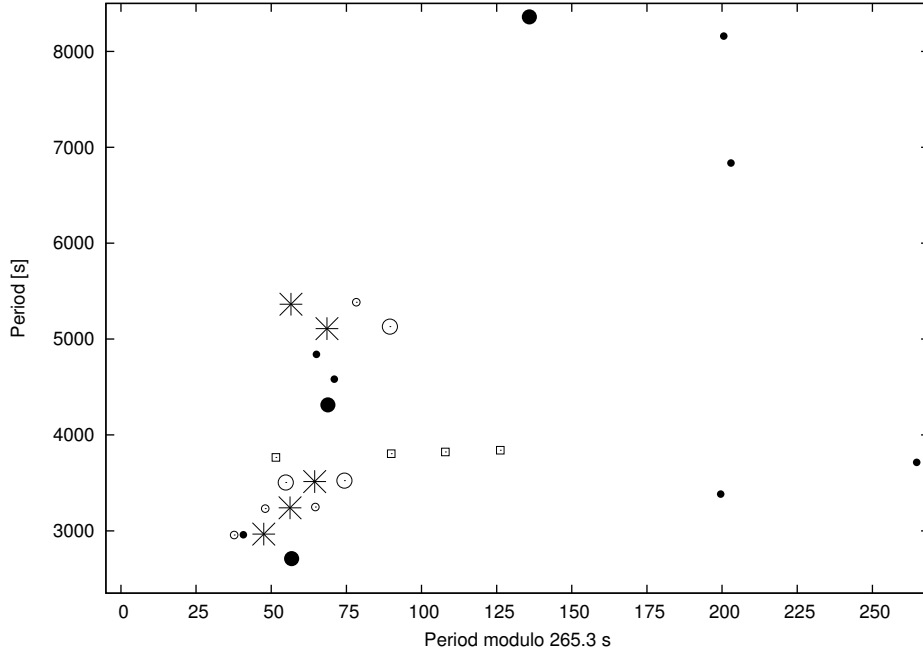
Figure 6.6 Échelle diagram of the periodicities $f1$-$f26$ of KIC 11179657 with a folding period is 265.3 s. Filled circles are undetermined peaks, stars are $l = 1$, $m = 0$ modes, open circles $l = 1$ $m = \pm 1$ modes, and open squares are suspected members of an $l = 2$ multiplet. The symbol size is proportional to peak amplitude. There is a clear grouping around 70 s which is most likely associated with $l = 1$. The members of the $l = 2$ multiplet are offset from the $l= 1$ ridge, though the highest frequency member (and the missing adjacent mode) do overlap with the $l = 1$ ridge. This overlap is not unexpected as they can have different values of n.

tems have been in their current configuration. The time-scale for life as a helium core burning sdB star is 10^8 years. Without more precise models of these stars (constrained by seismology) it is difficult to know their ages, but we can estimate the synchronization times using two prescriptions. KIC 02991403 and KIC 11179657 have very similar system parameters in terms of masses, rotation rates, and orbital periods. Therefore, the analysis below applies to both systems.

The model of Tassoul & Tassoul (1997) produces a synchronization time that is extremely short for sdB+dM binaries with these periods (as discussed in Pablo et al. 2011). On the other hand, synchronization through coupling via dynamical tides, as proposed by (Zahn, 1975), produces an approximate parametrized synchronization time-scale (Claret & Cunha , 1997;

Pablo et al., 2011).

$$\tau_{\mathrm{syn}} = 3.43 \times 10^6 \mathrm{yr} \left(\frac{\beta}{0.13}\right)^2 \left(\frac{1+q}{q}\right)^2 \left(\frac{M}{M_\odot}\right)^{\frac{7}{3}} \left(\frac{R}{R_\odot}\right)^{-7} \left(\frac{P}{\mathrm{day}}\right)^{\frac{17}{3}} \left(\frac{E_2}{10^{-8}}\right)^{-1} \qquad (6.2)$$

where β is "the radius of gyration" (the moment of inertia divided by MR^2), q is the mass ratio, and E_2 is the tidal constant, which is highly dependent on stellar structure. E_2 is difficult to calculate directly, but is proportional to $(r_c/R)^8$ where (r_c/R) is the fractional radius of the convective core (Zahn, 1977). Scaling from main sequence models by Claret (Claret & Cunha , 1997) we find that, to within a factor of three, $E_2 = (r_c/R)^8$ for sdB stars. The error introduced is small compared with our other uncertainties. As the sdB star evolves, (r_c/R), R, and (to a lesser extent) β can change causing τ_{syn} to vary.

This approach to synchronization can be integrated using the computed τ_{syn} as a function of time via

$$\frac{1}{\tau_{\mathrm{syn}}} = \frac{1}{\Omega - \omega} \frac{d\omega}{dt} \qquad (6.3)$$

where Ω is the orbital angular velocity and ω is the star's angular rotation velocity. Using the value of τ_{syn} as a function of age allows us to calculate $\omega(t)$. When $\omega \approx \Omega$ this system is synchronized. Conservation of total angular momentum implies that spinning up the sdB star will come at the expense of orbital angular momentum. However, since the rotational inertia of the star is less than 1 percent of the orbital angular momentum, spin-up of the star will occur on a time scale that is approximately 100 times shorter than the rate of change of the orbital angular momentum, regardless of the companions mass. We therefore assume that Ω is constant. We also assume that the secondary star is in synchronous rotation so its angular momentum evolution can be ignored. We can also compute the synchronization time as a function of the mass ratio q for comparison with the data – smaller mass ratios imply longer synchronization times. With a typical mass for the sdB star of $\approx 0.47\ M_\odot$, and values for R and (r_c/R) from representative sequences of evolutionary models (Kawaler, 2010; Kawaler & Hostler, 2005), the fact that these stars are not yet synchronized (at an upper limit to the age of 10^8 years) we should be able to place limits on the mass of the companion. For values of E_2 greater than $(r_c/R)^8$, if the age of the system is half the mean lifetime (5×10^7 y) then $M_c < 0.26 M_\odot$. On the other hand, if E_2 is much less than $(r_c/R)^8$ then it is likely that the

system will never spin-up. In that case for the system to have spun-*up* to the value observed starting from a rotation period of 100 d, M_c must be greater than 0.16 $M_\odot$. The value of M_c is valid for rotation periods longer than about 50 d.

6.5 Discussion

KIC 02991403 and KIC 11179657 are two very similar sdB *g*-mode pulsators in binary systems. Both systems have several triplet spacings, which imply rotation periods of 10.3 d and 7.4 d, respectively. This assumes solid body rotation, but as the *g*-modes are sensitive to virtually all depths in the star, our conclusions should change little. Since the orbital period in both systems is ≈ 0.4 d both systems are in non-synchronous rotation. These properties are shared with the sdB binary in NGC 6791 investigated by Pablo et al. (2011). These results can place tight constraints on theoretical models for tidal synchronization. For example, the Tassoul & Tassoul (1997) mechanism would synchronize these stars in a very short time.

On the other hand, if the analysis following Zahn (1977) and Pablo et al. (2011) in the previous section is accurate, then we can use the *lack* of synchronization to place limits on the mass ratio and therefore on the mass of the secondary star. This mass limit, along with the radial velocity amplitude, can in turn provide a lower limit on the orbital inclination. If $E_2 > (r_c/R)^8$ this turns out to be $\approx 23°$ for KIC 02991403 and $\approx 13°$ for KIC 11179657. However, if $E_2 < (r_c/R)^8$ then we can set a maximum inclination of $\approx 35°$ for KIC 02991403 and $\approx 19°$ for KIC 11179657. Using the fact that there are no eclipses we can set a independent maximum inclination that is $\approx 80°$ for both stars. While the estimates are rough the synchronization and spectroscopy yield consistent results.

Intriguingly, despite their similar parameters, the period distributions in these stars are quite different. The periods are well-behaved, with a clear period spacing, $l = 1$ multiplets and, in the case of KIC 11179657, an $l = 2$ multiplet. While KIC 2991403 does show an $l = 1$ sequence, there is no clear evidence of $l = 2$ multiplets despite having a longer baseline and more pulsation modes than KIC 11179657. Compared to KIC 11179657, KIC 02991403 shows a large number of periodicities that are clearly separated from the $l = 1$ ridge, suggesting that it has several $l = 2$ modes that are not parts of multiplets and/or it has a significant number

of modes that are influenced by internal composition transition zones.

We expect to obtain at least two years of data on these targets, and perhaps much more, over the course of the *Kepler* mission. With more data, lower-amplitude modes may be revealed that could complete additional multiplets. Given the current observed modes, however, seismic modelling may be able to reveal subsurface composition transitions that would explain the g-mode period distribution.

Acknowledgments

CHAPTER 7.   TIDAL EVOLUTION IN CLOSE sdB BINARIES

7.1   Close Binary Dynamics

Tidal interactions between stars in a close binary system act to bring both components towards angular momentum equilibrium (tidal locking). This equilibrium configuration is realized when the following conditions, outlined in Kopal (1978), are met:

1. The relative orbit of the two stars is circular.

2. The axial rotation has been synchronized with that of revolution.

3. The equatorial plane of each component is coplanar with that of their orbit.

In a binary, this is achieved through the influence of a variable external gravitational field. The star acts to balance the gas pressure and all internal and external gravitational forces to mantain a mechanical equilibrium. The condition of stability results in an instantaneous shape for the star, known as the equilibrium tide. Perturbations away from equilibrium in the interior of the star caused by non-synchronicity are referred to as the dynamical tide. This generates forced oscillations of g-modes within a star (Cowling, 1941). It is dissipative effects acting on these oscillations and tides which work to bring the star into a tidally locked state.

For late-type main sequence stars ($M < 1.5\ M_\odot$) viscous dissipation in the convective envelope causes the tidal bulge (resulting from the equilibrium tide) to lag with respect to the gravitational force (Zahn, 1966). In such systems the tidal bulge does not lie along the line connecting the two stars. This leads to a torque which acts to spin the star up or down so that it matches the orbital period (see Figure 7.1).
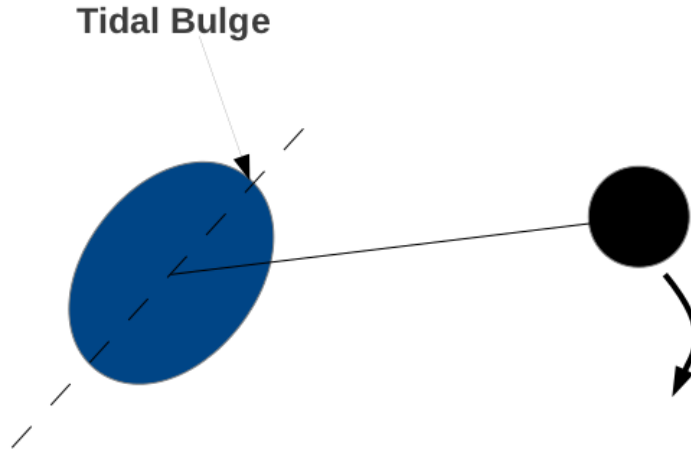
Figure 7.1   The lag between the tidal bulge and the line connecting the centers of mass of two stars. Since the gravitational force is along this line, the lag causes a torque which changes the rotation rate of the star.

In early-type stars ($M \geq 2M_\odot$) with radiative envelopes and convective cores, the torque produced from the equilibrium tide is not sufficient to change the rotational angular momentum of these stars. Two approaches to this problem (Tassoul, 1987; Zahn, 1975) give alternative methods for synchronization. In the following section we describe each method in detail. We then apply both theories to sdB binaries to consider their viability and evolutionary consequences which are hinted at in Chapters 5 and 6.

7.2   Zahn's Tidal Approach

The ineffectiveness of the equilibrium tide in massive stars in producing significant tidal torque caused Zahn (1975) to look more closely at the dynamical tide. The time scale of variability of the external gravitational field falls within the periods belonging to g-modes. Forced oscillations in this regime studied by Cowling (1941) and Zahn (1970) were not found to differ significantly from equilibrium distortions in driving angular momentum evolution. However, in both cases the adiabatic approximation was assumed and the oscillations were treated as purely mechanical.

Zahn (1975) re-explored the dynamical tide with a more realistic model. In this model the star is broken into two parts, where oscillations in the interior are still adiabatic, but oscillations in the outer envelope can be affected by radiative damping. The oscillation equations are then solved in these regions and matched at the boundary. Rather than solving this 4th-order differential system directly he introduces the variables X and Y.

$$X \equiv \rho x^2 \chi',$$

(7.1)

where x is the fractional radius, and χ is the sum of the perturbation in the gravitational potential and that of the relative density. Y is slightly more difficult to define but

$$Y \equiv \frac{x^2 \Phi}{g},$$

(7.2)

where Φ is the total gravitational potential. The perturbations on the stellar structure can now be described by the following differential equations:

$$X'' - \frac{\rho'}{\rho} X' - n(n+1) \frac{X}{x^2} = 0,$$

(7.3)

$$Y'' - 6 \left(1 - \frac{\rho}{\bar{\rho}}\right) \frac{Y'}{x} - \left[n(n+1) - 12(1 - \frac{\rho}{\bar{\rho}}\right] \frac{Y}{x^2} = 0,$$

(7.4)

where n is the spherical harmonic eigenvalue of the oscillation ($n = 2$ is the dominant term of the tidal potential). These two equations must be solved numerically, X in the convective core and Y throughout the star. This leads us to the determination of a stellar structure constant

$$H_n = \frac{2n+1}{(n-3)Y(1) + Y'(1)} X(x_f) \int_0^{x_f} \left[Y'' - n(n+1) \frac{Y}{x^2}\right] X \mathrm{d}x,$$

(7.5)

where the subscript f represents the value of a given quantity at the convective core boundary. These oscillations, unlike the g-modes described in Chapter 3, dissipate in energy near the boundary of the star. It is this damping which allows for the transfer of angular momentum and also creates the phase lag of the tidal bulge. The effect of the gravitational potential on the dynamical tide is dependent on the tidal coefficient

$$E_n = \frac{3^{\frac{8}{3}} \left[\Gamma\left(\frac{4}{3}\right) \right]^2}{(2n+1) \left[n(n+1) \right]^{\frac{4}{3}}} \left(\frac{\rho_f R^3}{M} \right) \left[\frac{R}{g_s} \left(\frac{N^2}{x^2} \right)'_f \right]^{-\frac{1}{3}}, \tag{7.6}$$

where

$$\Gamma(a+1) = \int_0^\infty t^a e^{-t} \, dt, \tag{7.7}$$

and $'$ is the spatial derivative with respect to x. The effort required to calculate E_2 led Zahn (1977) to derive an order of magnitude estimate:

$$E_2 \sim \left(\frac{R_f}{R} \right)^8, \tag{7.8}$$

which has been used in Chapters 5 and 6.

E_2 is then is used to find the tidal torque and from that the synchronization time t_{syn} given as

$$1/t_{syn} = 5(2)^{\frac{5}{3}} \left(\frac{g_s}{R} \right)^{\frac{1}{2}} \left(\frac{MR^2}{I} \right) q^2 (1+q)^{\frac{5}{6}} E_2 \left(\frac{R}{D} \right)^{\frac{17}{2}}, \tag{7.9}$$

where I is the moment of inertia, D is the orbital separation and g_s represents the surface value of the gravitational acceleration. Implicit in this calculation is that the change in the orbital frequency ω is negligible so that t_{syn} may also be written as

$$\frac{d}{dt} \left| \frac{(\Omega - \omega)}{\omega} \right|^{-\frac{5}{3}} = \frac{1}{t_{syn}}, \tag{7.10}$$

where Ω is the rotation frequency. Estimates of E_2 for sdB stars give values of τ_{syn} which are comparable to the horizontal branch lifetime. Therefore, this approximation is unsatisfactory for answering questions about synchronization in these stars.

The same processes that act to synchronize the rotation also work to make the orbit circular. We can derive a timescale for this change t_{circ}:

$$\frac{1}{t_{\text{circ}}} = \frac{1}{e} \frac{de}{dt}, \tag{7.11}$$

where e represents the eccentricity, the amount the orbit deviates from a perfect circle. Since there is considerably more angular momentum tied to the orbit than either of the stars, the timescale for synchronization tends to be much shorter than that of circularization. Therefore we make the assumption $\Omega = \omega$ and find that the circularization time is

$$\frac{1}{t_{\text{circ}}} = \frac{21}{2} \left(\frac{GM}{R^3} \right)^{\frac{1}{2}} q \left(1 + q \right)^{\frac{11}{6}} E_2 \left(\frac{R}{D} \right)^{\frac{21}{2}}. \tag{7.12}$$

Since it is difficult to measure rotation, especially for evolved stars like sdBs (see 4.1.2), eccentricity is a more commonly known parameter for a binary system. For this reason it is much easier to test Zahn's theory via circularization rates. However, certain inconsistencies arise from these examinations which will be addressed later in this chapter.

7.3 Tassoul's Theory of Meridional Flow

In the early 1980s, observational data had shown the curious result that while the method expressed in Zahn (1975, 1977) was accurate for circularization time scales, there were many more synchronized systems than expected (Giuricin et al., 1984a,b). This lead Tassoul (1987) to explore more efficient methods for synchronization using hydrodynamics. Tidal forces from the companion cause the star to lose axial symmetry. With this comes the development of large scale meridional flows. This analysis must satisfy 3 boundary conditions as enumerated in Tassoul & Tassoul (1982):

1. The gravitational potential must connect smoothly at the stellar boundary where the density vanishes.

2. The net stress vector acting on the free surface must equal zero.

3. Velocity normal to the outer surface must vanish.

These boundary conditions necessitate an "Ekman" boundary layer where there is a force balance between the pressure gradient, coriolis force, and turbulent drag. In this layer the flow is viscous, whereas throughout the rest of the envelope it is essentially inviscid. The mass

exchange between these two layers also constitutes an exchange of angular momentum which works to spin down/up the star. This leads to a spin down time of

$$t_{sd} = \frac{1}{4\pi} P_0 \left(\frac{\delta}{R} \right)^{-1} \epsilon_T, \tag{7.13}$$

where P_0 is the intial rotation period, δ is the height of the Ekman boundary layer and ϵ_T is the ratio of the tidal force to the star's own gravitational force given as

$$\epsilon_T = \frac{M'}{M} \left(\frac{R}{a} \right)^3, \tag{7.14}$$

where M' is the companion mass. The height of the Ekman boundary layer, δ as derived in Tassoul (1987) is:

$$\frac{\delta}{R} = 3 * 10^{-5 + \frac{N}{4}} \left[\frac{P}{\text{day}} \right]^{\frac{1}{4}} \left(\frac{L/L_\odot}{M/M_{odot}} \right)^{\frac{1}{4}}, \tag{7.15}$$

where L is the luminosity and N is a constant related to the radiative viscocity. $N = 0$ is often used for radiative stars as that is the value which best fits the observations (Claret, Gimenez & Cunha, 1995).

Calculation of t_{sd} is predicated on the assumption that the system is close to synchronicity. Tassoul (1987) suggests that this time can be use to make a conservative estimate of the synchronization time $t_{syn} = 10 t_{sd}$. Claret, Gimenez & Cunha (1995) found that $t_{syn} = 10^{1.6} t_{sd}$ was a better relationship based on observational constraints. It is immediately obvious that this timescale will be much shorter than Eq. 7.9 as its period dependence is P^4 whereas Zahn (1975) is $P^{8.5}$ (see Fig. 7.2). Since we have already shown in previous chapters that this P^4 dependence is not able to explain known rotation periods for sdB binaries, the rest of this chapter focuses on Zahn's theory.

7.4 Synchronization Computations

Calculating t_{syn} requires knowledge of the internal structure of the star and thus requires stellar models. These were made with the ISUEVO code and are described in Kawaler &
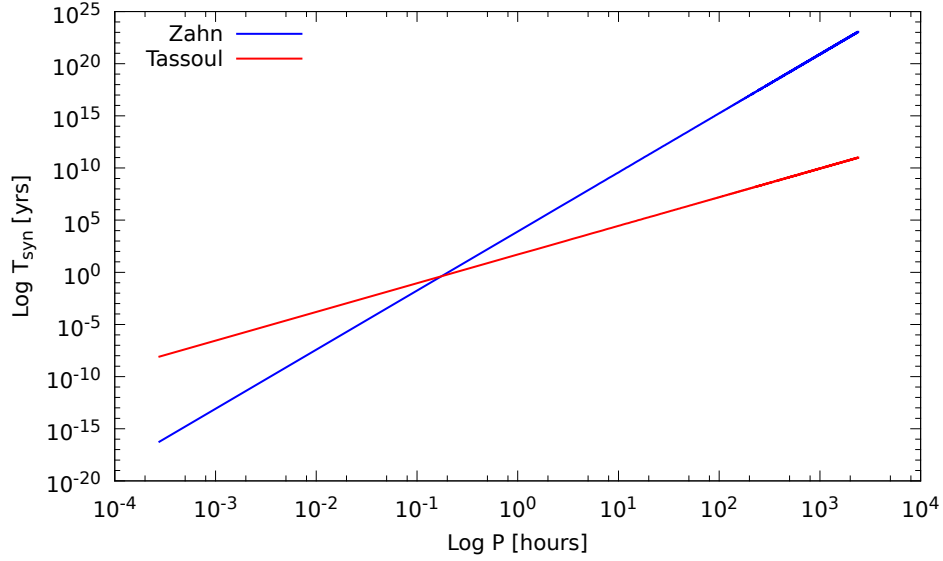
Figure 7.2   This shows the relationship between period and τ_{syn} for the Zahn (red) and Tassoul (green) prescriptions. This assumes and sdB model with $M = 0.478 M_\odot$ and a hydrogen layer of $0.008 M_\odot$. The mass ratio q is assumed to be 1.0.

Hostler (2005). All differential equations were integrated numerically using Mathematica 8 (see Appendix A).

7.4.1   Dynamical Tide

To solve Equations 7.3 and 7.4 we must first establish suitable boundary conditions. We know that the solution must be regular at the center. This means that

$$dr = 0 \text{ in } r = 0. \tag{7.16}$$

Applying this to the equations of nonradial oscillations, we find that this requires $\chi[0] = 0$ and $\chi'[0] = 0$. Since X depends on χ and x

$$X'[0] = 0 \text{ and } X[0] = 0. \tag{7.17}$$

We then solved Equation 7.3 using an implicit Runge-Kutta method. However, since singularities appear at $x = 0$ the equation was solved from $\epsilon \approx 10^{-16}$ to the convective core boundary.

In Eq. 7.4 we require Y be regular at the center which gives us our first boundary condition

$$Y[0] = 0. \tag{7.18}$$

For our second boundary condition it is beneficial to note that Eq. 7.4 is an alternate form of the Clairaut equation. As outlined in Kopal (1989) we can use the following substitution

$$\eta_n[x] = \frac{x}{Y}Y' \tag{7.19}$$

and Equation 7.4 becomes

$$x\eta'_n + \eta_n\left(\eta_n - 1\right) - 6\left(1 - \frac{\rho}{\bar{\rho}}\right)\left(\eta_n + 2\right) = n\left(n + 1\right). \tag{7.20}$$

For finite values of $\rho[0]$ it follows that $\frac{\rho}{\bar{\rho}} = 1$ as $x \to 0$. Applying this to Equation 7.20 we obtain our second boundary condition.

$$\eta_n[0] = n + 1. \tag{7.21}$$

We then solve Equations 7.19 and 7.20 for Y again using an implicit Runge Kutta method and avoid singularities by evaluating from $\epsilon \approx 10^{-16}$ to the edge of the star. Plugging solutions for X and Y into Equation 7.5 we find H_2 from which we can calculate E_2.

7.4.2 Results for a Representative sdB Model

We performed all the aforementioned calculations using an evolutionary sdB model calculated from ISUEVO. This model has a mass of 0.478 $M_\odot$ with a hydrogen layer 0.008 $M_\odot$. It was evolved from the zero age horizontal branch through core helium exhaustion with E_2 being computed at various stages. Since there is no precise indication of age in the systems outlined in Chapters 5 and 6, we must pick a representative model. We made our choice based on two criteria: proximity to the average sdB age $(5 \times 10^7$ yrs) and relative agreement of E_2 for nearby models. As shown in Figure 7.4 E_2 stays roughly constant until about 4×10^7 yrs at which point it balloons considerably. Therefore we chose the model whose age $\approx 4 \times 10^7$ yrs which has $E_2 = 10^{-9.41}$. The complete specifications for this model are given is Tab. 7.1.

Table 7.1   sdB Model

Parameter	Value
Age	4.011×10^7 yrs
Mass	0.478 $M_\odot$
Radius	0.298 $R_\odot$
Luminosity	17.31 $L_\odot$
T_{eff}	22074 K
log g	5.206
Y_c	0.57748

The rapid increase in E_2 during the last stages of the sdBs life is of little concern as very little time is spent in this stage (see 7.5.1). This value of E_2 agrees reasonably well with the estimates $E_2 \approx (R_f/R)^8$ Zahn (1977) of $log(E_2) = -8.53$. However, since time scales calculated in Chapters 5 and 6 from this estimate approach sdB lifetimes for systems, the need for the full derivation is clear.
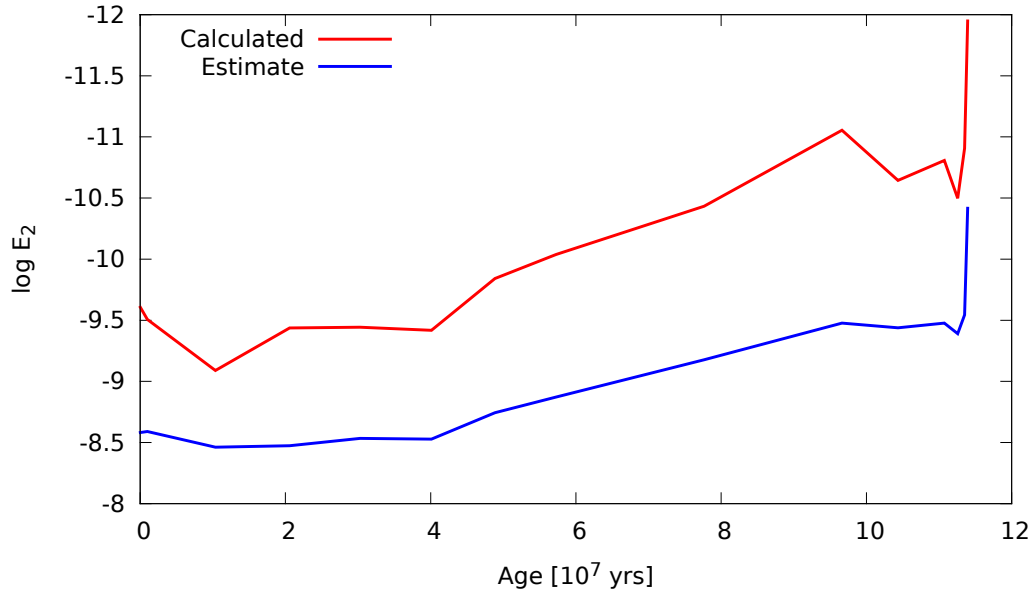
Figure 7.3 E_2 as a function of time for an sdB evolutionary sequence of mass 0.478 $M_\odot$ and hydrogen layer 0.008 $M_\odot$ directly calculated (red) and also estimates from $E_2 \approx (R_f/R)^8$ (green). It has been evolved from the sdB creation until helium burning has finished. At this point the core is no longer convective which makes further calculation invalid.
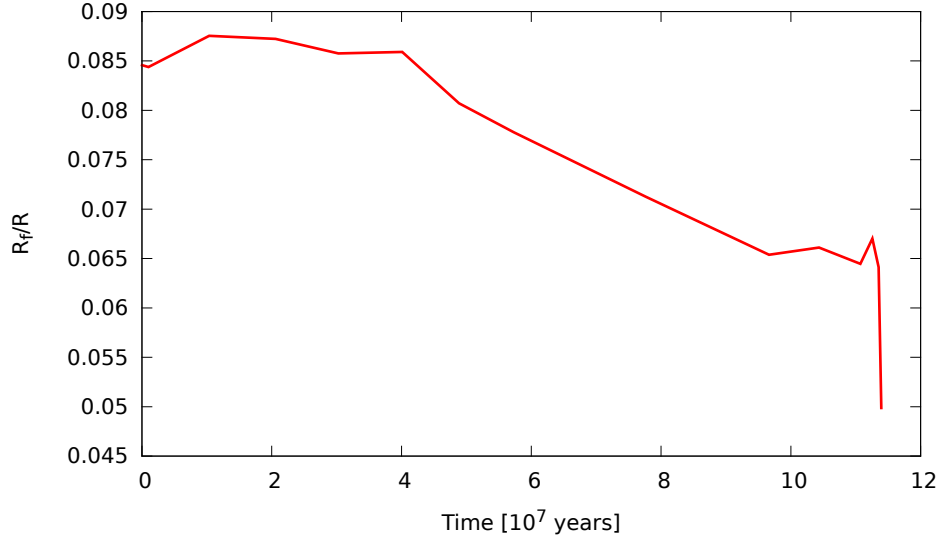
Figure 7.4 $\frac{R_f}{R}$ for a sequence of sdB evolutionary models of mass 0.478 $M_\odot$ and hydrogen layer 0.008 $M_\odot$.

It should be restated that all t_{syn} calculations made using Zahn's theory imply that changes in the orbital period are negligible. Since the lower limit on the angular momentum difference is $\frac{J_{orb}}{J_r} \approx 3 \times 10^3$ the assumption of constant ω is sound.

7.5   sdB Evolution

7.5.1   sdB Synchronization

Now that we have succesfully calculated E_2, we can use Eq. 7.9 to determine the synchronization time for known sdB binaries. Results for a selection of well known sdB binaries are shown in Table 7.2 where we assume the model sequence is representative of all sdB pulsators. For the sdB+dM binaries discussed in Chapters 5 and 6, we find that the observed non-synchronous rotation is consistent with the Zahn (1975) mechanism. This method predicts synchronization time scales which are over an order of magnitude longer than the evolutionary time scale.

Table 7.2   sdB Binaries

System	Orbital Period [d]	P_r [d]	$\log\tau_{syn}$ [yr] [1]	$\log\tau_{circ}$ [yr]
PG 1336	0.1010160	0.101016	6.9	13.8
KPD 1930	0.09511567	0.09511567	5.6	15.0
Feige 48	0.3760	–	9.0	23.4
B4	0.3980	9.63	9.4	22.6
KIC 02991403	0.443	10.3	9.7	23.3
KIC 11179657	0.3945	7.4	9.4	22.6

[1] This is a lower limit based on the maximum size for the unknown companion

Each binary's synchronization state matches the calculated τ_{syn} with one notable exception: Feige 48. Reed et al. (2004) observed a possible rotational multiplet in the fourier spectrum of Feige 48. van Grootel (2008) agreed with asteroseismic model fits that rule out differential rotation in the core. However, since τ_{syn} is an order of magnitude longer than the evolutionary timescale, it is unclear whether the interpretation of the pulsation spectrum is correct.

A reason for this difference may be found in recent spectroscopic observation of Feige 48 by M. Reed and collaborators (private comm.) which suggests that the peaks in the apparent triplet actually consists of two different orders of l. This misidentification could strongly affect the asteroseismic interpretation as being synchronous.

Table 7.3   Initial Rotation

System	Rotation Period [d]	$\frac{d\omega}{dt} s^{-2} \times 10^{-21}$	$P_{\rm o}$ [d]
B4	9.63	2.08	72
KIC 02991403	10.3	1.00	18
KIC 11179657	7.4	2.18	25

The rotation periods found in Chapters 5 and 6 can now be used to further constrain their respective systems. Assuming that the rotational frequency changes at a constant rate with time, we can determine an upper limit on the initial rotation period assuming the typical sdB evolutionary lifetime is 1×10^8 yrs. All pertinent information is given in Table 7.3. According to Zahn's theory we can see that $P_{\rm o} < 75$ days for all systems and $P_{\rm o} < 30$ d for two of the

three. If we instead assumed the average age for these systems (5×10^7 yrs) $P_0 < 17$ d. Since the currend sdB rotation rates are all greater than 7 days, this suggests a vary narrow window for P_0.

7.5.2 Evolution

We find that Zahn's theory adequately describes all three of the sdB binaries observed with *Kepler* and appears to be true for all sdB binaries. If this is indeed the case then we can make certain claims about their tidal evolution. For any sdB binary with a compact white dwarf companion, synchronization will not occur for orbital periods > 6 hrs within the 10^8 year sdB lifetime. Similarly, M dwarf companion binaries with periods longer than 5.3 hrs will not synchronize. Every sdB binary with a period < 3.6 hrs will tend toward synchronous rotation independent of mass(as long as the secondary is not substellar). These limits demonstrate that it is **incorrect** to assume that all close binaries with sdB stars are in synchronous rotation.

The only other attempt to constrain synchronization in sdB binaries was performed by Geier et al. (2010). They assumed synchronous rotation and calculated $v_{rot} = \frac{2\pi R_{sdB}}{P}$ using a mass-radius relationship to determine R_{sdB}. They then compared this value to the projected observational velocity $v_{obs} = v_{rot}(\sin i)$ to constrain the inclination angle and solve the binary systems. This method reproduced a consistent companion mass when compared with an independent analysis for systems with orbital periods up to 1.2 days[1]. They also noted the results of Zahn (1977) and Tassoul & Tassoul (1992), claiming that neither was sufficient for all cases. With a more rigorous calculation using Zahn's method we find synchronization times that are longer than those calculated in Geier et al. (2010).

Unlike the results discussed in Geier et al. (2010), we showed in the previous section that all but one of the pulsating sdB binaries are consistent with Zahn (1977). One possibility for this discrepancy is that the surface is rotating synchronously but the sdB's inner layers are not. Goldreich and Nicholson (1989) claims that Zahn's method works to synchronize the star from

---

[1]They also found consistent results for one outlier system with an orbital period of 1.6 days.

the outside in which may explain the Geier result. However, this theory is mainly heuristic and lacks quantitative computations so the rate at which the outer layer spins down is not clear. It is also worth restating that the rotation rates quoted in Geier et al. (2010) have not been observed, merely assumed and then confirmed (or not) based on binary fits. It is therefore at best inconclusive evidence contrary to Zahn (1977).

A second important consequence of consistent synchronization times is the ability to back track through the binary's evolution. P_{o} calculated above tells us the state of the system after it goes through it's common envelope phase. For periods of order 9 hours the $P_{\mathrm{o}} < 75$ days. Using the formation channels described in (Han et al., 2002, 2003) we have developed rather strong limits to test models for common envelope formation. These limits on P_{o}, though broader than we would like, are the only ones that, to our knowledge, currently exist in the literature.

Preliminary analysis of *Kepler* data on sdB pulsators not in binaries indicate rotation periods which are roughly consistent with those in binaries having values of P_{o} mostly between 20 to 50 days. One possible explanation for this consistency, is that rotation rate is independent of formation channel. If we assume initial solid body rotation, the value we measure is that of the core. Its rotation would be least affected by envelope ejection, especially if core and envelope were decoupled during the common envelope phase. Further study could indicate how the sdB progenitor transitions from a CE to life on the horizontal branch.

CHAPTER 8. SUMMARY AND FUTURE WORK

8.1 Summary and Implications

The preceeding chapters have outlined the study of three sdB binaries: B4, KIC02991403 and KIC 11179657 . We have shown that the equal g-mode period spacing, both observationally shown and theoretically predicted, exists in all three systems (Reed et al., 2011b). In addition, all three have rotational multiplets which show that sdB star is **Not** in synchronous rotation, contrary to conventional wisdom on close sdB binaries.

We find that for all of these systems, evidence supports the synchronization methods of Zahn (1975), those of Tassoul & Tassoul (1992) being much too short. While there is some evidence which contradicts this assessment (Geier et al., 2010; van Grootel, 2008), rotation periods of sdB stars in binaries have only been **measured** conclusively in the three binaries discussed in this work. We assume therefore, that Zahn (1975) is relevant for all sdB binaries.

Using this assumption we can assemble several constraints on sdB binary evolution. For the typical M dwarf or white dwarf companions, synchronization should not occur if P is longer than 6 hrs. Additionally, systems with an orbital period shorter than 3.7 hrs should synchronize before the sdB exhausts helium. We can even backtrack evolution and put an upper limit of 72 d on the intial rotation periods of these systems. Assuming an average age for the sdB stars of 5×10^7 yr, roughly half the total lifetime, suggests that the initial rotation period is well under 30 days.

Ultimately, what we learn from these pulsating sdB binaries have consequences for many

close binaries. This is because, as stated previously, close sdB binaries are a result of common envelope evolution. Limits on the rotation period coupled with knowledge of the orbital period for systems exiting the CE phase illuminate what occurs during the CE. This knowledge provides some of the only constraints with which to test the complex models associated with CE evolution.

8.2   Future Work

While we have made significant strides towards understanding sdB binaries, there are many questions left to answer. All three pulsating sdB binaries discussed in Chapters 5 and 6 are still under *Kepler* observation. Hopefully, continued observation will significantly aid identification of pulsation modes and allow for precise stellar modeling. This will give us exact values for the fundamental parameters of both the sdB and the system as a whole. However, to better explore sdB evolution, we will have need extend this work in different directions which are outlined in the sections below.

8.2.1   Backtracking Evolution

8.2.1.1   sdB Progenitors

Our current work has focused on sdB systems that have emerged after CE ejection. Our next step is to identify sdB progenitor systems. Many possible sdB formation channels exist, for which we know the binary specifications under which they will be created (Han et al., 2002, 2003). Since all of the systems above have M dwarf companions, we are most interested in finding progenitors to these systems. *Kepler* provides us with an excellent opportunity to accomplish this as a catalog of eclipsing binaries with over 2100 binaries already exists (Prsa, 2012). This archive of data will be public by November, 2012.

We can identify potential systems by the limits which can be placed on the mass $1.15 M_\odot < M_{sdBp} < 2.5 M_\odot$ (Pablo et al., 2011; Han et al., 2002). This constraint allows us to place limits on quantities such as the luminosity and radii ratios which are much easier to measure. For

promising systems which have either star spots or pulsations we have a strong possibility of measuring the rotation rate. Stars that show both could provide us a chance to test the claims of layer–by–layer spin down explained in Goldreich and Nicholson (1989) (see the following section). Once progenitor systems have been identified and rotation rates have been measured constraints can be placed on the system as it enters the CE phase. These constraints coupled with those outlined in Chapter 7 should give us unprecedented information with which to test our knowledge of the CE.

8.2.1.2 Common Envelope Systems

Since the CE has a timescale of tens to hundreds of years (Shankar et al., 1991), in contrast to red giant branch life times of $\approx 10^9$ yr, no objects have currently been observed in this evolutionary stage. Even though the *Kepler* data set includes extended observations on over 14000 red giants, there should not be a realistic expectation of observing and identifying a CE system. Despite this fact several candidate systems have been identified (Jordan Smith private communication).

The configuration of these candidate systems vary from strange to virtually impossible using the CE interpretation, but there is currently no better hypothesis. One of the more unusual binaries is show in Fig. 8.1. While the ellipsoidal variation, which is seen in several of these systems, could be a good indication of CE, eclipses should not be seen as the companion (P=1.4 d) would be inside the red giant. Current investigations suggest that, while contamination can be a large issue with *Kepler* data, it is not one for many of these candidates (including the one in Fig. 8.1). Regardless of the outcome, it is clear that these systems are worthy of further study.

8.2.2 Angular Momentum Transport

Goldreich and Nicholson (1989) provides an excellent semi-quantitative explanation for why stars appear synchronous well before Zahn (1975) suggests. This theory implies that while the surface layers of the star are in synchronous rotation, the interior of the star is not. It is pos-
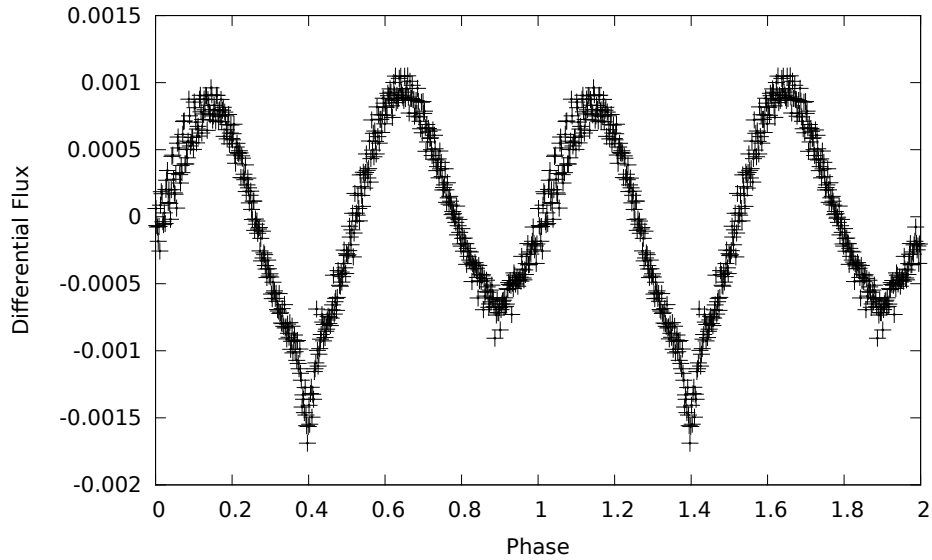
Figure 8.1   This shows the phased and binned light curve of KIC 6526377 (from Q1-Q11) on the suspected orbital period of 1.4 d. Since this system contains a red giant, the orbital period of an unseen companion would put it well within the red giant's envelope.

sible to test this hypothesis with sdB stars. The rotation rate achieved from asteroseismology is an average throughout the star. Spectroscopic observations can provide (with some effort) surface rotation rates in these systems. If surface rotation values are significantly different than asteroseismic ones, then we have concrete proof that star spins up/down from the outside in.

From a theoretical standpoint though, this re-interpretation of Zahn (1977) by Goldreich and Nicholson (1989) is still lacking a crucial element: a timescale for surface synchronization. While it is clear from angular momentum arguments that the surface will be spun up/down signficantly faster than the rest of the star, there is no indication of just how quickly this will occur. It requires knowledge of the amount of absorption experienced by the incident gravity wave as well the efficiency with which the angular momentum is transported outwards (Goldreich and Nicholson, 1989). It is also necessary to know the scale height of the star's surface layer. These questions are not easy to answer, but there are advanced stellar evolution and modelling codes such as MESA (Paxton et al., 2011) which may be useful in this endeavor.

APPENDIX A. MATHEMATICA E_2 COMPUTATION

A.1   Model Input

The necessary model inputs are r, rho, N^2, M and g.

fradius = Import["/home/hpablo/synstuff/fortides/sdB61-rf.txt", "list"]

rho = Import["/home/hpablo/synstuff/fortides/sdB61-rho.txt", "list"]

BV = Import["/home/hpablo/synstuff/fortides/sdB61-N2.txt", "list"]

g = Import["/home/hpablo/synstuff/fortides/sdB61-g.txt", "list"]

Mr = Import["/home/hpablo/synstuff/fortides/sdB61-M.txt", "list"]

rhom = Import["/home/hpablo/synstuff/fortides/sdB61-rhom.txt", "list"]

A.2   Preparation

Here constants are defined and model parameters are made into interpolated functions for use in differential equations.

len = 563

rcl = 77

mmax = 472

BV[[rcl]]

$6.38292500000000038618.80501974145667 \times 10^{-6}$

M1 = Mr[[len]]

$9.50741999999999982 \times 10^{32}$

R1 = 1.988754 $* 10^{10}$

1.98875×10^{10}

$l = \mathbf{2.0}$

2.

$G = \mathbf{6.67 * 10^{-8}}$

6.67*^-8

$\mathbf{rc = fradius[[rcl]]}$

0.0859123350600426161

$E_{2e} = \mathbf{rc^8}$

$2.96786529287574233321600829413627446709789063860871 8.030965536139846 \times 10^{-9}$

$\mathbf{Table[\{fradius[[x]], rho[[x]]\}, \{x, 1, len\}]}$

$\rho = \mathbf{Interpolation[\%]}$

$\text{InterpolatingFunction}[\{\{0.0110753466743498691, 1.00000000000000000\}\}, <>]$

$\mathbf{Table[\{fradius[[x]], rhom[[x]]\}, \{x, 1, len\}]}$

$\rho m2 = \mathbf{Interpolation[\%]}$

$\text{InterpolatingFunction}[\{\{0.0110753466743498691, 1.00000000000000000\}\}, <>]$

$\mathbf{Table[\{fradius[[x]], g[[x]]\}, \{x, 1, len\}]}$

$\mathbf{gs = Interpolation[\%]}$

$\text{InterpolatingFunction}[\{\{0.0110753466743498691, 1.00000000000000000\}\}, <>]$

$\mathbf{Table[\{fradius[[x]], BV[[x]]\}, \{x, 1, len\}]}$

$\mathbf{BV2 = Interpolation[\%]}$

$\text{InterpolatingFunction}[\{\{0.0110753, 1.\}\}, <>]$

$\mathbf{Table[\{Mr[[x]], R1 * fradius[[x]]\}, \{x, 1, mmax\}]}$

$\mathbf{rm = Interpolation[\%]}$

$\text{InterpolatingFunction}[\{\{9.50742 \times 10^{29}, 9.5074 \times 10^{32}\}\}, <>]$

A.3 Solve For X

bs = Block[{ϵ = \$MachineEpsilon},

NDSolve $\left[\left\{X"[x] - \left(\frac{\rho'[x]}{\rho[x]}\right) * X'[x] - l * (l+1) * \frac{X[x]}{x^2} == 0,\right.\right.$

$X'[\epsilon] == l * (l+1) * \rho[\epsilon] * \epsilon, X[\epsilon] == \rho[\epsilon] * \epsilon^2 * \epsilon\}, X, \{x, \epsilon, rc\},$

Method $\rightarrow$ "ImplicitRungeKutta", AccuracyGoal $\rightarrow$ 10, PrecisionGoal $\rightarrow$ 10,

MaxSteps $\rightarrow \infty$, MaxStepFraction $\rightarrow$ 0.00001]]

$\{\{X \rightarrow \text{InterpolatingFunction}[\{\{2.220446049250313\text{*^-16}, 0.0859123\}\}, <>]\}\}$

X2[x_] = First[X[x]/.bs]

InterpolatingFunction[$\{\{2.220446049250313\text{*^-16}, 0.0859123\}\}, <>][x]$

Plot $\left[\text{Evaluate}[X[x]/.bs], \{x, 1 * 10^{-6}, rc\}, \text{PlotRange} \rightarrow \text{All}\right]$
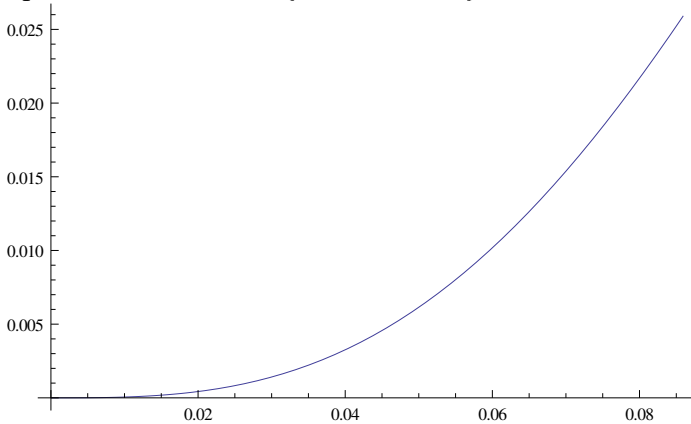
I1 = NIntegrate $\left[\text{rm}[z]^2, \{z, 0, M1\}\right]$

6.12736×10^{51}

$\rho2 = \text{Table}\left[\frac{3}{i^3} * \text{NIntegrate}\left[\rho[x] * x^2, \{x, 0, i\}\right], \{i, \text{fradius}\}\right]$

Table[{fradius[[x]], $\rho2$[[x]]}, {x, 1, len}]

$\rho\text{m2} = \text{Interpolation}[\%]$

InterpolatingFunction[$\{\{0.0110753, 1.\}\}, <>]$

A.4 Solve For Y

cd = Block[{ϵ = $MachineEpsilon},

NDSolve $\left[\left\{x*P'[x] + P[x]*(P[x]-1) - 6*\left(1 - \frac{\rho[x]}{\rho m2[x]}\right)*(P[x]+2) == l*(l+1),\right.\right.$

$P[\epsilon] == l + 1\}, P[x], \{x, \epsilon, 1.0\}$, Method $\rightarrow$ "ImplicitRungeKutta",

AccuracyGoal $\rightarrow$ 10, PrecisionGoal $\rightarrow$ 10, MaxSteps $\rightarrow \infty$,

MaxStepFraction $\rightarrow$ 0.00001]]

$\{\{P[x] \rightarrow$ InterpolatingFunction$[\{\{2.220446049250313*\^-16, 1.\}\}, <>][x]\}\}$

w[x_] = First[P[x]/.cd]

InterpolatingFunction$[\{\{2.220446049250313*\^-16, 1.\}\}, <>][x]$

Plot $\left[\text{Evaluate}[P[x]/.\text{cd}], \left\{x, 1*10^{-6}, 1.0\right\}, \text{PlotRange} \rightarrow \text{All}\right]$
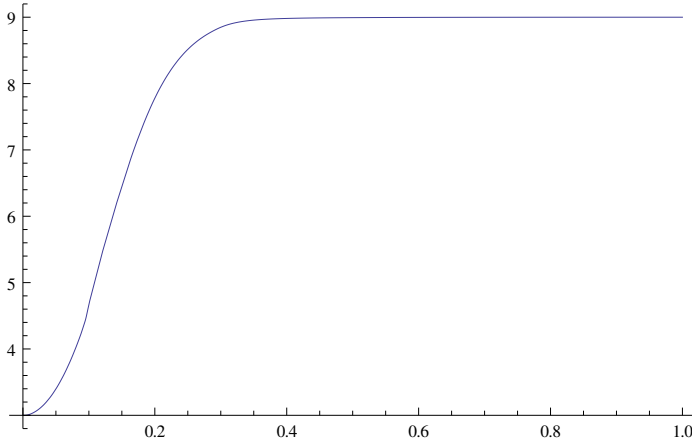
de = Block[{ϵ = $MachineEpsilon},

NDSolve $\left[\left\{x*Q'[x] == Q[x]*w[x], Q[\epsilon] == \epsilon^2*\epsilon/\text{gs}[\epsilon]\right\}, Q, \{x, \epsilon, 1.0\},\right.$

Method $\rightarrow$ "ImplicitRungeKutta", AccuracyGoal $\rightarrow$ 10, PrecisionGoal $\rightarrow$ 10,

MaxSteps $\rightarrow \infty$, MaxStepFraction $\rightarrow$ 0.00001]]

InterpolatingFunction::dmval : Input value $\{2.220446049250313*\^-16\}$ lies outside the range of data in the int

$\{\{Q \rightarrow$ InterpolatingFunction$[\{\{2.220446049250313*\^-16, 1.\}\}, <>]\}\}$

Plot $\left[\text{Evaluate}[Q[x]/.\text{de}], \left\{x, 1*10^{-6}, 1.0\right\}, \text{PlotRange} \rightarrow \text{All}\right]$
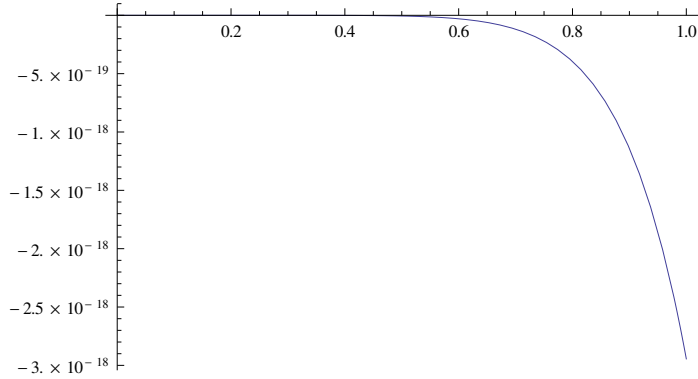
$Y[\text{x\_}] = \text{First}[Q[x]/.\text{de}]$

$\text{InterpolatingFunction}[\{\{2.220446049250313\times10^{-16}, 1.\}\}, <>][x]$

A.5   Finding E_2

$\text{hi} = \text{Block}[\{\epsilon = \text{\$MachineEpsilon}\},$

$\text{NIntegrate}\left[\left(Y''[x] - l*(l+1)*\frac{Y[x]}{x^2}\right)*\text{X2}[x], \{x, \epsilon, \text{rc}\}, \text{AccuracyGoal} \to 10,\right.$

$\text{PrecisionGoal} \to 10]]$

$-5.090035482957661\times10^{-27}$

$\text{H2} = \frac{(2*l+1)}{(l-3)*Y[1]*\text{X2[rc]}} * \text{hi}$

$-3.338139985292342\times10^{-7}$

$\text{d1} = D\left[\frac{\text{BV2}[x]}{x^2}, x\right]/.x \to \text{rc}$

23.5189

$\text{E2} = \frac{\left(3^{\frac{8}{3}}*(\text{Gamma}[4/3])^2\right)}{(2*l+1)*(l*(l+1))^{\frac{4}{3}}} \frac{\left(\rho[\text{rc}]*\text{R1}^3\right)}{\text{M1}} * \left(\frac{\text{R1}}{\text{gs}[1.0]}*\text{d1}\right)^{\frac{1}{3}}\text{H2}^2$

$3.8165580487112043\times^{-10}$

BIBLIOGRAPHY

Aerts, C., Christens-Dalsgaard, J., Kurtz, D.W. (2010). *Asteroseismology.* Dordrecht Netherlands: Springer

Behr, B. (2003). Chemical Abundances and Rotation Velocities of Blue Horizontal-Branch Stars in Six Globular Clusters. *Astrophysical Journal Supplement Series 149*(1), 67–99.

Behr, B. (2003). Rotation Velocities of Red and Blue Field Horizontal-Branch Stars. *Astrophysical Journal Supplement Series 149*(1), 101–121.

Billres, M., Fontaine, G., Brassard, P., Charpinet, S., Liebert, James, Saffer, R. A.(2000). Detection of p-Mode Pulsations and Possible Ellipsoidal Luminosity Variations in the Hot Subdwarf B Star KPD. *Astrophysical Journal,*

Birney, D.S., Gonzalez, G., & Oesper D. (2006). *Observational Astronomy* 2^{ed} *Edition.* Cambridge: Cambridge University Press.

Bloemen, et al.(2010). Kepler Observations of the Beaming Binary KPD 1946+4340. *Monthly Notices of the Royal Astronomical Society, 410*(3), 1787–1796.

Bochkarev, N. G.; Karitskaia, E. A.; Shakura, N. I.(1979). Calculation of the ellipsoidality effect in close binary systems with one optical component. *Astronomicheskii Zhurnal, 56*(1), 16–29.

Borucki, W. J., et al.(2010). Kepler Planet-Detection Mission: Introduction and First Results. *Science, 327*(5698), 977–980.

Borucki, W. J., et al. (2008). *IAU Symposium Proceedings, 249*(1), 17–24.

Carroll, B.W. and Ostlie D.A. (2007). *An Introduction to Modern Astrophysics*. San Francisco: Pearson Addison Wesley

Charpinet, S., Fontaine, G., Brassard, P., Dorman, B. (1996). The Potential of Asteroseismology for Hot, Subdwarf B Stars: A New Class of Pulsating Stars? *Astrophysical Journal Letters 471*, L103–L106.

Charpinet, S., Fontaine, G., Brassard, P., Dorman, B. (2000). Adiabatic Survey of Subdwarf B Star Oscillations. I. Pulsation Properties of a Representative Evolutionary Model. *Astrophysical Journal Supplement Series 131*(1), 223–247.

Charpinet, S., Fontaine, G., Brassard, P., Chayer, P. (2008). Radiative levitation and opacity driving: The potential of hot subdwarf pulsators for testing diffusion and other competing processes in stars. *Communications in Asteroseismology 157*(1), 168–176.

Charpinet, S., van Grootel, V., Reese, D., Fontaine, G., Green, E.M., Brassard, P., Chayer, P. (2008). Testing the forward modeling approach in asteroseismology. II. Structure and internal dynamics of the hot B subdwarf component in the close eclipsing binary system PG 1336-018. *Astronomy and Astrophysics 489*(1), 377–394.

Charpinet, S., van Grootel, V., Fontaine, G., Green, E.M., Brassard, P., Randall, S.K., Silvotti, R., Østensen, R.H., Kjeldsen, H., Christensen-Dalsgaard, J., Kawaler, S.D., Clarke, B.D., Li, J., Wohler, B.(2011). Deep asteroseismic sounding of the compact hot B subdwarf pulsator KIC02697388 from Kepler time series photometry. *Astronomy and Astrophysics 530*(1), 377–394.

Claret, A.; Gimenez, A.; Cunha, N. C. S. (1995). Circularization and Synchronization Times in the Main Sequence of Detached Eclipsing Binaries.I. Using the formalism by Tassoul. *Astronomy & Astrophysics 299*, 724–730.

Claret, A. & Cunha, N.C.S. (1997). Circularization and synchronization times in Main-Sequence of detached eclipsing binaries II. Using the formalisms by Zahn. *Astronomy & Astrophysics 318*, 187–197.

Claret, A. (2004). New grids of stellar models including tidal-evolution constants up to carbon burning. I. From 0.8 to 125 M_{sun} at . *Astronomy & Astrophysics 424*, 919–925.

Cowling, T.G. (1941). The Non-Radial Oscillations of Polytropic Stars. *Monthly Notices of the Royal Astronomical Society*, *101*(1), 367–375.

Cox, J.P. (1980). *The theory of stellar pulsation.* New Jersey: Princeton University Press

D'Cruz, N. L.; Dorman, B.; Rood, R. T.; O'Connell, R. W. (1996). The Origin of Extreme Horizontal Branch Stars. *Astrophysical Journal 466*(1), 359–371.

de Marchi, F.; Poretti, E.; Montalto, M.; Piotto, G.; Desidera, S.; Bedin, L. R.; Claudi, R.; Arellano Ferro, A.; Bruntt, H.; Stetson, P. B. (2007). Variable stars in the open cluster NGC 6791 and its surrounding field. *Astronomy and Astrophysics 471*(2), 515–526.

Dorman, B., Rood, R. T., O'Connell, R. W. (1993). On the Evolution of 'Ultra-violet' Horizontal Branch Stars and the UV Flux From Stellar Populations. *The globular clusters-galaxy connection*, *Astronomical Society of the Pacific Conference Series 48*(1), 553–556.

Downes, R.A. (1941). The KPD Survey for Galactic Plane Ultraviolet-excess Objects Space Densities of White Dwarfs and Subdwarfs . *Astrophysical Journal*, *307*(1), 170,171,173–177.

Eddington, A.S. (1890). The Reflection Effect in Eclipsing Variables. *Monthly Notices of the Royal Astronomical Society*, *130*(1), 323–332.

Gautschy, A. & Saio H. (1996). Stellar Pulsations Across the HR Diagram: Part 2. *Annual Review of Astronomy and Astrophysics*, *34*(1), 551–606.

Geier, S., Nesslinger, S., Heber, U., Przybilla, N., Napiwotzki, R., Kudritzki, R.-P. (2007). The hot subdwarf B + white dwarf binary KPD 1930+2752. A supernova type Ia progenitor candidate. *Astronomy and Astrophysics*, *464*(1), 299–307.

Geier, S., Nesslinger, S., Heber, U., Randall, S. K., Edelmann, H., Green, E. M. (2008). Tidal synchronisation of the subdwarf B binary PG 0101+039. *Astronomy and Astrophysics* *477*(2), L13-L16.

Geier, S., Heber, U., Podsiadlowski, Ph., Edelmann, H , Napiwotzki, R., Kupfer, T., Mller, S. (2010). Hot subdwarf stars in close-up view. I. Rotational properties of subdwarf B stars in close binary systems and nature of their unseen companions. *Astronomy and Astrophysics*, *519*(1), A25.

Gilliland et al. (2010). Kepler Asteroseismology Program: Introduction and First Results. Hot subdwarf stars in close-up view. *Publications of the Astronomical Society of the Pacific*, *122*(888), 131–143.

Gilliland, R., Jenkins, J., Borucki, W., Bryson, S., Caldwell, D., Clarke, B., Dotson, J. L., Haas, M., Hall, J., Klaus, T., Koch, D., McCauliff, S., Quintana, E., Twicken, J., van Cleve, J. (2010). Initial Characteristics of Kepler Short Cadence Data. *Astrophysical Journal Letters* *713*(2), L160-L163.

Giuricin, G., Marirossian, F., Mezzetti, M. (1984). Synchronization in Eclipsing Binary Stars. *Astronomy and Astrophysics*, *131*(1), 152–158.

Giuricin, G., Marirossian, F., Mezzetti, M. (1984b). Orbital Circularization in Early-Type Detached Close Binaries. *Astronomy and Astrophysics*, *134*(1), 365–367.

Goldreich, P., Nicholson, P. D. (1989). Tidal friction in early-type stars. *Astrophysical Journal*, *342*(1), 1079–1084.

Green, E. M.; Fontaine, G.; Reed, M. D.; Callerame, K.; Seitenzahl, I. R.; White, B. A.; Hyde, E. A.; stensen, R.; Cordes, O.; Brassard, P.; Falter, S.; Jeffery, E. J.; Dreizler, S.; Schuh, S. L.; Giovanni, M.; Edelmann, H.; Rigby, J.; Bronowska, A.(2003). Discovery of A New Class of Pulsating Stars: Gravity-Mode Pulsators among Subdwarf B Stars. *The Astrophysical Journal, 583*(1), L31–L34.

Green, E. M., For, B., Hyde, E. A., Seitenzahl, I. R.; Callerame, K.; White, B. A.; Young, C. N.; Huff, C. S.; Mills, J.; Steinfadt, J. (2004). Companions of Post-Common Envelope sdB Binaries. *Astrophysics and Space Science*, *291*(1), 267–274.

Han, Z., Podsiadlowski, Ph., Maxted, P. F. L., Marsh, T. R., Ivanova, N. (2002). The Origin of Subdwarf B Stars– I. The Formation Channels *Monthly Notices of the Royal Astronomical Society*, *336*(1), 449–466.

Han, Z., Podsiadlowski, Ph., Maxted, P. F. L., Marsh, T. R. (2003). The Origin of Subdwarf B Stars– II. *Monthly Notices of the Royal Astronomical Society*, *341*(1), 669–691.

Hansen, C.J., Kawaler, S.D., & Trimble, V. (2004). *Stellar Interiors Physical Principles, Structure, and Evolution.* 2^{ed} *Edition* New York: Springer

Heber, U., Hunger, K., Jonas, G., Kudtritzki, R. P. (1984). The Atmosphere of Subluminous B Stars. *Astronomy and Astrophysics*, *331*(1), 966–971.

Heber, U., Hunger, K., Jonas, G., Kudtritzki, R. P. (1984). Hot Subdwarf Stars. *Annual Review of Astronomy & Astrophysics*, *47*(1), 211–251.

Hu, Haili, Glebbeek, E., Thoul, A. A., Dupret, M.-A., Stancliffe, R. J., Nelemans, G., Aerts, C. (2010). Gravitational Settling in Pulsating Subdwarf B Stars and their Progenitors. *Astronomy and Astrophysics*, *511*(1), A87.

Hutchings, J. B. (1974). The synthesis of close-binary light curves. VI. X-ray and collapse binaries. *Astrophysical Journal 188*(1), 341–348.

Jenkins et al. (2010). Overview of the Kepler Science Processing Pipeline. *Astrophysical Journal Letters 713*(2), L87-L91.

Kallrath, J., & Milone, E. (2009). *Eclipsing Binary Stars: Modeling and Analysis.* New York: Springer.

Kaluzny, J., & Udalski, A. (1992). Photometric study of the old open cluster NGC 6791. *42*(1), 29–47.

Karl, C. A., Heber, U., Drechsel, H., Napiwotzki, R., Altmann, M., stensen, R., Folkes, S., Solheim, J. E., Cordes, O., Voss, B., Koester, D. (2004). HS 2333 + 3927: a new sdB binary with a large reflection effect. *291*(3), 283–289.

Kawaler, S.D., & Hostler, S.(2005). Internal Rotation of Subdwarf B Stars: Limiting Cases and Asteroseismological Consequences. *Astrophysical Journal 621* 432–444.

Kawaler, S.D.(2010). Structure and evolution of pulsating hot subdwarfs. *Astronomische Nachrichten 331* 1020–1025.

Kawaler, S. D., Reed, M. D., stensen, R. H., Bloemen, S., Kurtz, D. W., Quint, A. C., Silvotti, R., Baran, A. S., Green, E. M., Charpinet, S., Telting, J., Aerts, C., Handler, G., Kjeldsen, H., Christensen-Dalsgaard, J., Borucki, W. J., Koch, D. G. (2010). First Kepler results on compact pulsators - V. Slowly pulsating subdwarf B stars in short-period binaries. *Monthly Notices of the Royal Astronomical Society 409*(4), 1509–1517.

Kilkenny, D. (2007). Pulsating Hot Subdwarfs – An Observational Review. *Communications in Astroseismology 150*, 234–240.

Kjeldsen, H., Christensen-Dalsgaard, J., Handberg, R., Brown, T. M., Gilliland, R. L., Borucki, W. J., Koch, D. (2010). The*Kepler* Asteroseismic Investigation: Scientific Goals and First Results. *Astronomische Nachrichten*, *331*(1), 966–971.

Klaus, T. C., McCauliff, S., Cote, M. T., Girouard, F. R., Wohler, B., Allen, C., Middour, C., Caldwell, D. A., Jenkins, J. M. (2010). *Kepler* Science Operations Center pipeline framework. *Software and Cyberinfrastructure for Astronomy, Proceedings of the SPIE 7740*(1), 774017-774017-12.

Klaus, Todd C., Cote, Miles T., McCauliff, S., Girouard, F. R., Wohler, B., Allen, C., Chandrasekaran, H., Middour, C., Caldwell, D. A., Jenkins, J. M. (2010). *Kepler* Science Operations Center pipeline framework extensions. *Software and Cyberinfrastructure for Astronomy, Proceedings of the SPIE 7740*(1), 774018–774018–11.

Koch, D., et al. (2010). *Kepler Mission* Design, Realized Photometric Performance, and Early Science. *The Astrophysical Journal Letters*, *713*(1), L79–L86.

Kopal, Z. (1939). The Reflection Effect in Eclipsing Binary Systems. *Astrophysical Journal*, *89*(1), 323–332.

Kopal, Z. (1978). *Dynamics of Close Binary Systems. Astrophysics and Space Science Library*, *68* Holland/Boston: D. Reidel

Kopal, Z. (1989). *The Roche Problem.* Netherlands: Kluwer Academic Publishers

Laplace, P. S., Young, T. (1832). *Elementary illustrations of the celestial mechanics of Laplace.* London: J.Murray

Ledoux, P. (1951). The Nonradial Oscillations of Gaseous Stars and the Problem of Beta Canis Majoris. *Astrophysical Journal*, *114*, 373–384.

Lenz, P., Breger, M. (2005). Period04 User Guide. *Communications in Asteroseismology*, *146*, 53–136.

Loeb,A. and Gaudi, S.B. (2003). Periodic Flux Variability of Stars due to the Reflex Doppler Effect Induced by Planetary Companions. *Astrophysical Journal*, *588*(2), L117–L120.

Maxted, P.f. L., Marsh, T. R., North, R. C. (2001). KPD 1930+2752: a candidate Type Ia supernova progenitor. *Monthly Notices of the Royal Astronomical Society*, *317*(3), L41–L44.

Maxted, P.f. L., Heber, U., Marsh, T. R., North, R. C. (2001). The Binary Fraction of Extreme Horizontal Branch Stars. *Monthly Notices of the Royal Astronomical Society*, *326*(1), 1391–1402.

McCauliff, S., Cote, M. T., Girouard, F. R., Middour, C., Klaus, T. C., Wohler, B. (2010). The *Kepler* DB: a Database Management System for Arrays, Sparse Arrays, and Binary Data . *Software and Cyberinfrastructure for Astronomy*, *Proceedings of the SPIE 7740*(1), 77400M–77400M–12.

Middour et al. (2010). *Kepler* Science Operations Center Architecture. *Software and Cyberinfrastructure for Astronomy, Proceedings of the SPIE 7740* (1), 77401A–77401A–12.

Milne, E.A. (1926). The Reflection in Eclipsing Binaries. *Monthly Notices of the Royal Astronomical Society, 87* (1), 43–55.

Mochejska, B. J., Stanek, K. Z., Kaluzny, J. (2003). Long-Term Variability Survey of the Old Open Cluster NGC 6791. *Astronomical Journal 125* (6) 3175–3184.

Montgomery, M. H., & Odonoghue, D. (1999). A Derivation of the Errors for Least Squares Fitting to Time Series Data. *Delta Scuti Star Newsletter 13*, 28–32.

Morales-Rueda, L., Maxted, P. F. L., Marsh, T. R., North, R. C., Heber, U. Orbital periods of 22 subdwarf B stars. *338* (3), 752–764.

Nather, R. E., Winget, D. E., Clemens, J. C., Hansen, C. J., Hine, B. P.(1990). The Whole Earth Telescope - A New Astronomical Instrument. *Astrophysical Journal, 361* (1), 309–317.

O'Donoghue, D.; Lynas-Gray, A. E.; Kilkenny, D.; Stobie, R. S.; Koen, C. (1997).A new class of rapidly pulsating star - IV. Oscillations in EC 20117-4014 and atmospheric analyses . *Monthly Notices of the Royal Astronomical Society, 285* (3), 657–672.

Østensen, R.H.Green, E. M., Bloemen, S., Marsh, T. R., Laird, J. B., Morris, M., Moriyama, E., Oreiro, R., Reed, M. D., Kawaler, S. D., Aerts, C., Vukovi, M., Degroote, P., Telting, J. H., Kjeldsen, H., Gilliland, R. L., Christensen-Dalsgaard, J., Borucki, W. J., Koch, D. (2010). 2M1938+4603: a Rich, Multimode Pulsating sdB Star with an Eclipsing dM Companion Observed with Kepler. *Monthly Notices of the Royal Astronomical Society: Letters, 408* (1), L51–L55.

Silvotti R., Charpinet S., Oreiro, R., Handler, G., Green E.M., Bloemen, S., Heber, U., Gansicke, B.T., Marsh, T.R., Kurtz, D.W., Telting J.H., Reed, M.D., Kawaler S.D., Aerts, C., Rodriguez-Lopez, C., Vuckovic, M., Ottosen, T.A., Liimets, T., Quint, A.C., van Grootel, V., Randall, S.K., Gilliland, R.L., Kjeldsen, H., Christensen-Dalsgaard, J., Borucki, W.J., Koch, D., Quintana, E.V. (2010). First Kepler results on compact pulsators I. Survey Target Selection and the First Pulsators. *Monthly Notices of the Royal Astronomical Society: Letters 409*, 1470–1486.

Østensen, R.H.(2010). Observational asteroseismology of hot subdwarf stars . *Astronomische Nachrichten, 331*(1), 1026–1033.

Østensen et al. (2011). First Kepler results on compact pulsators - VI. Targets in the final half of the survey phase. *Monthly Notices of the Royal Astronomical Society 414*(4), 2860–2870.

Pablo, H., Kawaler S.D., and Green E.M. (2011). Exploring B4: A Pulsating sdB Star, in a Binary, in the Open Cluster NGC 6791. *Astrophysical Journal Letters, 740*(2), L47–L53.

Paxton, B. Bildsten, L., Dotter, A., Herwig, F., Lesaffre, P., Timmes, F. (2011). Modules for Experiments in Stellar Astrophysics (MESA). *Astrophysical Journal Supplement 192*(1), id. 3.

Pickering (1890). A New Class of Binary Stars. *Monthly Notices of the Royal Astronomical Society, 50*(1), 296–299.

Plavec, M.J. (1968). Mass Exchange and Evolution of Close Binaries. *Advances in Astronomy and Astrophysics, 6*(1), 201–278.

Press, W. H., Rybicki, G.B. (1989). Fast Algorithm for Spectral Analysis of Unevenly Sampled Data *Astrophysical Journal. 338*, 277–280.

Prsa, et al. (2011). Kepler Eclipsing Binary Stars. I. Catalog and Principal Characterization of 1879 Eclipsing Binaries in the First Data Release. *Astrophysical Journal, 141*(1), 83–99.

Prsa, A., (2012). Eclipsing Binaries with the *Kepler Mission American Astronomical Society*, *220*(1), 406.01.

Reed, M. et al. (2000). Preliminary Results from XCOV 17: PG 1336-018. *Baltic Astronomy*, *9*(1), 183-195.

Reed, et al.(2011). Observations of the Pulsating Subdwarf B Star Feige 48: Constraints on Evolution and Companions. *Monthly Notices of the Royal Astronomical Society*, *412*(1), 371–390.

Reed, M. D., Terndrup, D. M., Zhou, A.-Y., Unterborn, C. T., An, D., Eggen, J. R. (2007). Resolving the pulsations of subdwarf B stars: HS 0039+4302, HS 0444+0458 and an examination of the group properties of resolved pulsators. *Monthly Notices of the Royal Astronomical Society 378*(3), 1049–1063.

Reed, M. D., Kawaler, S. D., Ostensen, R. H., Bloemen, S., Baran, A., Telting, J. H.,Silvotti, R., Charpinet, S., Quint, A. C., Handler, G., Gilliland, R. L., Borucki, W. J., Koch, D. G., Kjeldsen, H., Christensen-Dalsgaard, J. (2010). First Kepler results on compact pulsators - III. Subdwarf B stars with V1093 Her and Hybrid (DW Lyn) Type Pulsations. *Monthly Notices of the Royal Astronomical Society 409*(4), 1496–1508.

Reed, et al. (2011). Whole Earth Telescope observations of the subdwarf B star KPD 1930+2752: a rich, short-period pulsator in a close binary. *Monthly Notices of the Royal Astronomical Society*, *348*(4), 1164–1174.

Reed, M. D., Baran, A., Quint, A. C., Kawaler, S. D., O'Toole, S. J., Telting, J., Charpinet, S., Rodrguez-Lpez, C., stensen, R. H., Provencal, J. L., Johnson, E. S., Thompson, S. E., Allen, C., Middour, C. K., Kjeldsen, H., Christensen-Dalsgaard, J. (2011). First Kepler Results on Compact Pulsators - VIII. Mode Identifications via Period Spacings in g-mode Pulsating Subdwarf B Stars. *Monthly Notices of the Royal Astronomical Society*, *414*(4), 2885–2892.

Roberts, A.W. (1895). Close Binary Systems and Their Relation to Short Period Variations. *Astrophysical Journal*, *2*(1), 283–292.

Russell, H.N. (1914). Relations Between the Spectra and Other Characteristics of the Stars. *Popular Astronomy, 22*(1), 275–294.

Saffer, R. A., Bergeron, P., Koester, D., Liebert, J. (1994). Atmospheric Parameters of Field Subdwarf B Stars. *Astrophysical Journal, 432*(1), 351–366.

Shankar, A., Livio, Mario, Truran, James W. (1991). The Common Envelope Phase in Classical Novae - One-dimensional models. *Astrophysical Journal 374*(1), 623–630.

Shibahashi, H., & Kurtz, D. (2012). FM stars: a Fourier view of pulsating binary stars, a new technique for measuring radial velocities photometrically. *Monthly Notices of the Royal Astronomical Society, 412*(1), 738–752.

Tassoul, M. (1980). Asymptotic Approximations for Stellar Nonradial Pulsations. *Astrophysical Journal Supplement Series, 43*(1), 469–490.

Tassoul, J.-L., & Tassoul M. (1982). Meridional Circulation in Rotating Stars. I - A Boundary Layer Analysis of Mean Steady Motions in Early-Type Stars. *Astrophysical Journal Supplement Series, 49*(1), 317–350.

Tassoul, J.-L. (1987). On Synchronization in Early-Type Binaries. *Astrophysical Journal, 322*(1), 856–861.

Tassoul, J.–L. (1988).On orbital circularization in detached close binaries . *Astrophysical Journal, 324*(1), L71–L73.

Tassoul, M., & Tassoul, J.-L. (1992). On the Efficiency of Ekman Pumping for Synchronization in Close Binaries. *Astrophysical Journal, 322*(1), 856–861.

Tassoul, M., & Tassoul, J.-L. (1997). On Synchronization in Detached Close Binaries: Reply to Rieutord and Zahn. *Astrophysical Journal, 481*(1), 363–368.

Telting, J., Østensen, R.H., Oreiro, R., Reed M., Farris L., O'Toole S., Aerts C. (2011). *Fifth meeting on hot subdwarf stars and related objects Astronomical Society of the Pacific* in press

Unno, W., Osaki, Y., Ando, H., Shibahashi, H. (1979). *Nonradial oscillations of stars.* Tokyo: University of Tokyo Press

van Grootel, V., Charpinet, S., Fontaine, G., Brassard, P. (2008). Asteroseismology in action: a test of spin-orbit synchronism in the close binary system Feige 48. *Astronomy and Astrophysics*, *483*(3), 875–885.

Van Grootel, V., Charpinet, S., Fontaine, G., Brassard, P., Green, E. M., Randall, S. K., Silvotti, R., stensen, R. H., Kjeldsen, H., Christensen-Dalsgaard, J., Borucki, W. J., Koch, D. (2010). Early Asteroseismic Results from Kepler: Structural and Core Parameters of the Hot B Subdwarf KPD 1943+4058 as Inferred from g-mode Oscillations. *718*(2), L97-L101.

van Kerkwijk, Marten H., Rappaport, Saul A., Breton, R. P., Justham, S., Podsiadlowski, P., Han, Z. (2010). Observations of Doppler Boosting in Kepler Light Curves. *Astrophysical Journal*, *715*(1), 51–58.

Willems, B. and Aerts, C. (2002). Tidally Induced Oscillations in Close Binaries. *Astronomical Society of the Pacific, IAU Colloquium 185*(1), 76–79.

Wilson, R. E., & Sofia, S. (1976). Effects of Tidal Distortion on Binary–Star Velocity Curves and Ellipsoidal Variation. *Astrophysical Journal 203*, 182–186.

Winget, D. et al. (1991). Asteroseismology of the DOV star PG 1159–035 with the Whole Earth Telescope. *Astrophysical Journal 378*, 326–346.

Winget, D. et al. (1994).Whole earth telescope observations of the DBV white dwarf GD 358. *Astrophysical Journal 430*, 839–849.

Zahn, J.-P. (1966). Les Mares Dans une toile Double Serre (suite) *Annales d'Astrophysique*, *29*(1), 489–506.

Zahn, J.-P. (1970). Forced Oscillations in Close Binaries. The Adiabatic Approximation *Astronomy and Astrophysics*, *4*(1), 452–461.

Zahn, J.-P. (1975). Dynamical Tides in Close Binaries. *Astronomy and Astrophysics*, *41*(1), 329–344.

Zahn, J.-P. (1977). *Astronomy and Astrophysics*, *57*(1), 383–394.

Zucker, Shay, Mazeh, Tsevi, and Alexander, Tal (2007). Beaming Binaries: A New Observational Category of Photometric Binary Stars *Astrophysical Journal*, *670*(2), 1326–1330.